AEDC-TR-71-274

EFFECTS OF WALL COOLING AND LEADING-EDGE BLUNTING ON RAMP-INDUCED, LAMINAR FLOW SEPARATIONS AT MACH NUMBERS FROM 3 THROUGH 6

J. Don Gray and R. W. Rhudy
ARO, Inc.

March 1972

VON KÁRMÁN GAS DYNAMICS FACILITY
ARNOLD ENGINEERING DEVELOPMENT CENTER
AIR FORCE SYSTEMS COMMAND
ARNOLD AIR FORCE STATION, TENNESSEE

NOTICES

When U. S. Government drawings specifications, or other data are used for any purpose other than a definitely related Government procurement operation, the Government thereby incurs no responsibility nor any obligation whatsoever, and the fact that the Government may have formulated, furnished, or in any way supplied the said drawings, specifications, or other data, is not to be regarded by implication or otherwise, or in any manner licensing the holder or any other person or corporation, or conveying any rights or permission to manufacture, use, or sell any patented invention that may in any way be related thereto.

Qualified users may obtain copies of this report from the Defense Documentation Center.

References to named commercial products in this report are not to be considered in any sense as an endorsement of the product by the United States Air Force or the Government.

EFFECTS OF WALL COOLING AND LEADING-EDGE BLUNTING ON RAMP-INDUCED, LAMINAR FLOW SEPARATIONS AT MACH NUMBERS FROM 3 THROUGH 6

J. Don Gray and R. W. Rhudy
ARO, Inc.

FOREWORD

The work reported herein was done at the request of the Air Force Flight Dynamics Laboratory (AFFDL), Flight Dynamics Control Criteria Division, Air Force Systems Command (AFSC), under Program Element 62201F.

The results of the tests presented were obtained by ARO, Inc. (a subsidiary of Sverdrup & Parcel and Associates, Inc.), contract operator of the Arnold Engineering Development Center (AEDC), AFSC, Arnold Air Force Station, Tennessee, under Contract F40600-72-C-0003. The tests were conducted from November 30, 1970, to April 16, 1971, under ARO Project No. VT0036, the data reduction was completed on June 4, 1971, and the manuscript was submitted for publication on October 22, 1971.

The authors gratefully acknowledge the assistance of E. O. Marchand and A. W. Mayne, Aerodynamics Project Branch of the von Kármán Gas Dynamics Facility (VKF), AEDC, who provided, respectively, the numerical solutions for the inviscid flow field about the plate-ramp configurations and the boundary-layer development on the plate alone. The authors also acknowledge and appreciate the generous support given to this investigation by Mr. E. L. Fleeman of AFFDL.

This technical report has been reviewed and is approved.

Emmett A. Niblack, Jr.
Lt Colonel, USAF
AF Representative, VKF
Directorate of Test

Duncan W. Rabey, Jr.
Colonel, USAF
Director of Test

ABSTRACT

The effects of wall cooling and nose bluntness on laminar and transitional reattaching flows induced by a 9.5-degree ramp were investigated at Mach numbers from 3 through 6 by measuring the longitudinal surface pressure and heat-transfer rate distributions, as well as the flow-field pressures, at several longitudinal stations. Reynolds number based on flat-plate length was varied from 0.25 to 1.0 million. Although transitional reattachment generally prevailed at all but the minimum Reynolds number at $M_\infty = 3$, an increase in leading-edge radius was found to delay transition onset at $M_\infty \geqq 4.5$. When transition was well downstream of reattachment, increased cooling delayed the onset; however, the opposite was true when transition was near reattachment. The trend in the change in interaction length with Reynolds number increase indicated laminar reattachment at all test Reynolds numbers at $M_\infty = 6$ and transitional at the two higher Reynolds numbers at $M_\infty = 3.0$. The change in interaction length with a Reynolds number increase at $M_\infty = 4.5$ indicated that the reattachment was probably transitional at the highest test Reynolds number. A maximum upstream interaction extent was found with an intermediate nose radius, regardless of the proximity of transition to reattachment. A modification of the integral-moment theory was shown to correctly predict this reversal in interaction extent caused by nose blunting, as well as the general characteristics of the overall interaction for the adiabatic wall condition with laminar reattachment. Wall cooling always reduced the interaction extents. Peak heating rates generally were dominated by transition onset and were reasonably close to predicted turbulent levels. Tabulated surface pressure and heat-transfer data at minimum Reynolds number are also presented.

CONTENTS

ILLUSTRATIONS

Figure | Page

NOMENCLATURE

b	Model semispan, in.
C	Chapman-Rubesin viscosity factor, $(T/\mu) \div (T/\mu)_{wall}$
C_p'	Maximum gradient of ramp pressure coefficient, $D_p\ S_c/q_c$
D_p	Maximum gradient of ramp pressure, $(dp/dS)_{max}$, psi/in.
H	Enthalpy, Btu/lbm
h	Heat-transfer rate, Btu/ft^2-sec-°R
M	Mach number
P	Chapman-Curle pressure parameter, $1.75 \left(\frac{p - p_{\bar{o}}}{p_{\bar{o}}}\right) \left(\frac{Re_{\bar{o}}}{CM_w^{3/2}}\right)^{1/4}$
p	Static pressure, psia
p_t	Total pressure, psia

p_t' Pitot pressure, psia

q Dynamic pressure, psia

R_N Nose radius, in.

Re Reynolds number based on free-stream conditions and length, S

S Wetted axial distance from stagnation point, in. (see Fig. 2b)

St Stanton number, $h(T_{ad}-T_{wall})/[\rho_\infty U_\infty(H_t-H_{wall})]$

T Temperature, °R

T_t Total temperature, °R

u Velocity, ft/sec

u/ν Unit Reynolds number, $in.^{-1}$

X Chapman-Curle length parameter, $0.47\left(\frac{S-S_\delta}{S_\delta}\right)\frac{M_w^{1/2}\ Re_\delta^{1/4}\ T_w}{C^{1/4}\ T_{wall}}$

y Distance perpendicular to surface, in.

z Lateral distance from centerline, in.

β $\sqrt{M^2-1}$

γ Ratio of specific heats, 1.40

δ Estimated boundary-layer thickness, in.

θ Ramp angle, deg

ρ Density, lb_m/ft^3

$\bar{\chi}$ Viscous interaction parameter, $M^3\sqrt{C/Re}$

ν Kinematic viscosity, μ/ρ, ft^2/sec

μ Dynamic viscosity, $lb_m/ft\text{-}sec$

SUBSCRIPTS

ad Adiabatic

c Corner or hinge line

d	Disk probe
FP	Flat plate
f	Peak value on ramp
max	Maximum
$\bar{o}$	Value at beginning of interaction (see Fig. 26)
p	Plateau or peak value on plate
r	Reattachment
s	Separation
t	Total
to	Transition onset
TT	Theoretical turbulent value
w	Local inviscid value
wo	Local inviscid value at beginning of interaction
∞	Free-stream value
δ	Value at boundary-layer edge

SECTION I
INTRODUCTION

Despite the practical significance of leading-edge bluntness and nonadiabatic wall conditions, relatively few investigations of the influence of these factors on shock-induced flow separations have been made, particularly at moderate Mach numbers.

The effect of leading-edge radius on the pressure distribution for a ramp-induced laminar flow separation was investigated first by Townsend (Ref. 1) at a Mach number of 10 for an equilibrium wall temperature. Because the ramp was less than 15 percent of the flat-plate length, these tests should not necessarily be considered representative of results for which reattachment is unrestrained by the ramp length. In a comprehensive investigation of the heat transfer in separated flows induced in a variety of ways, the effect of blunting was also examined by Holloway, Sterrett, and Creekmore in Ref. 2 at a Mach number of 6 and a wall temperature of approximately 55 percent of the stagnation value. Although this investigation was also conducted with a short ramp, the plate length was varied significantly to allow the ramp length to change from 14 to 51 percent of the distance to the hinge line. Tests with a ramp model at cold wall, hypersonic conditions for which there were no apparent model geometry limitations were reported by Holden in Ref. 3. In these tests, conducted at $M_\infty \geq 14$, it was found that the size of the separated region increased for small bluntness increases, whereas if bluntness were increased sufficiently the size finally decreased. The decrease in the interaction extent observed in Ref. 3 for plane flow when the bluntness is large was also found by Harvey in tests at similar cold wall conditions (Ref. 4). On the other hand, pressure tests at similar conditions with a flared cone model (Ref. 5) showed that the size of the interaction only increased with bluntness increase. However, the appreciable reduction in net pressure rise observed in plane flow tests with large bluntnesses was not found in these tests.

The first experimental investigation of boundary-layer separation with heat transfer was that reported by Gadd (Ref. 6). These results, at Mach number 3, indicated that for moderate cooling there was no definable influence of wall temperature on the separation of a laminar boundary layer which was transitional at reattachment. The tests, moreover, were conducted with a very narrow plate (aspect ratio less than 1.0) which spanned the test section; thus the results must have been affected by the aspect ratio limitations delineated in Ref. 7. On the other hand, Lewis (Ref. 8) found at Mach number 6 that with a high degree of cooling and for plane laminar reattaching flow there was a significant reduction in the size of the interaction over that for adiabatic wall conditions. Similar effects on the pressure distributions with axisymmetric (flared) configurations were obtained for a transitional reattachment by Ferguson and Schaeffer (Ref. 9), and for laminar reattachment in Ref. 10 for a systematic wall temperature range.

Most of the literature concerning flow separation deals with surface pressure measurements, and there is a shortage of data dealing with heat-transfer-rate measurements. This is primarily because most tests have been run in conventional supersonic wind tunnels where heat-transfer-rate measurements are not practical without special procedures. Cold wall tests conducted in an impulse-type tunnel at Mach number 10 by Holden (Ref. 11) and Needham (Ref. 12) showed that for laminar flow reattachment the maximum or peak

heat-transfer rate occurred near the peak pressure location, which was coincident with the neck or minimum thickness of the reattached boundary layer. Available hypersonic ($M_\infty \geq 10$), cold wall, peak heating data for ramps were correlated by Bushnell and Weinstein (Ref. 13) on the basis of local flow conditions and the estimated neck thickness. Data such as those of Ref. 2 were excluded presumably because the ramp was not long enough to allow reattachment unrestrained by geometry or because transition during flow reattachment was indicated. It is noted that essentially none of these data (Ref. 2) exhibit the extreme peaks observed in Ref. 12, for example. The only other data available, at low supersonic speeds and higher wall temperature, are those of Ginoux (Ref. 14). His results, which were obtained at a Mach number of 2 with constant heat transfer to the stream, were judged transitional during reattachment on the ramp for moderate deflections; but they did agree with Gadd's result in that no measurable effect on the pressure distribution was found for the small heating imposed. Data have also been obtained on flared cone-cylinder models (Ref. 9) at a Mach number of 5, but comparisons with theoretical estimates indicated that the flow was transitional during reattachment and also that there were no extreme peaks.

Because of the lack of data showing the effects of wall cooling and nose blunting on ramp-induced, laminar boundary-layer interactions at moderate supersonic speeds, the present experimental investigation was made. The basic model geometry used to study aspect ratio criteria with laminar flow reattachment (Ref. 7) was retained, but a new model was built having internal coolant passages and a removable leading-edge section. Asymptotic calorimeter gages were added to this model so that both pressure and heat-transfer data could be obtained simultaneously. In addition, boundary-layer and flow-field surveys were made to supplement flow-field photographs and to verify the state of the boundary layer in the vicinity of reattachment. The fast-response measurement technique utilized first in Ref. 10 to approximate isothermal wall temperature conditions was also used in this test program.

SECTION II
APPARATUS

2.1 MODEL AND SUPPORTS

The model, designed and fabricated at AEDC, consisted of a 2.5-in.-chord flat plate with a fixed-angle ramp of 9.5 deg and a chord of 5.0 in. (Fig. 1). The span of the model was 26.0 in., giving an aspect ratio ($2b/S_c$) of 10.4 which is large enough (Ref. 7) to give a large span of two-dimensional flow on each side of the model centerline. Three removable leading-edge sections were provided with nose radii (R_N) of 0.001, 0.023, and 0.105 in. These leading edges were designed so that the horizontal distance from the stagnation point to the plate-ramp hinge line was the same (2.5 in.) for all three leading edges. The leading edges were designed to be flush with and parallel to the instrumented surface of the flat plate; however, a slight mismatch (of the order of 0.002 to 0.004 in.) and a small windward angle on the leading edge were observed at times during the test as a result of the compound applied to seal the joint. Lower surface skirts were an integral part of the model. Numerous internal passages were provided for the liquid nitrogen (LN_2) used to cool the model during the cold wall phases of the test.

A supply manifold was located at the base of the model to insure more uniform cooling, and an exhaust manifold was used to discharge the nitrogen well downstream of the model in order to eliminate any flow disturbance or freezing of the transducer package cooling water.

Altogether, 87 surface pressure taps, 11 Gardon heat gages, and 30 thermocouples were provided. The pressure taps were arranged in four chordwise rows, with 33 within at least 0.25 in. of the model centerline and 18 each at 6.5, 11.0, and 12.25 in. from the centerline (see Fig. 2a). In general, because of instrumentation limitations, only the centerline and the first row off centerline were used. The taps being used could be changed by a quick disconnect manifold just downstream of the ramp trailing edge. The Gardon gages were located in a chordwise row, four on the flat plate and seven on the ramp, 2.75 in. off the model centerline. The 30 thermocouples were imbedded in and distributed over the entire model surface and were used only to monitor the uniformity of the model surface temperature.

The survey probe mechanism was supported by a sting which was attached to the main model support bracket by means of an offset strut (Fig. 2b). The probe drive mechanism was attached to a shaft which allowed manual positioning of the probe in the axial direction while the probe pitch and vertical position were set by a remotely controlled motor drive. Two probes, a disk probe for static pressure and an impact probe for pitot pressure, were mounted 3 in. on either side of the model centerline. Details of these probes are included in Fig. 2b.

The entire model and probe mechanism was attached to the forward face of the wafer gage transducer package, the external shell of which acted as the sting (Fig. 2b). The transducer package was mounted to a 12-deg bent sting which in turn was attached to the tunnel roll mechanism. This combination allowed for alignment of the model in pitch and roll and positioning of the model above the tunnel centerline to obtain clearance between the survey probe mechanism and the tunnel wall.

During some phases of the tests, "orifice dams" (Ref. 15) were installed on the model in an attempt to define more closely the flow separation and reattachment points. These "dams" were 20-deg wedges, either 0.030 or 0.045 in. high and 0.1 in. wide. They were glued to the surface of the model (with clear cement) either just upstream of a pressure orifice with the leading edge of the ramp windward or just downstream of an orifice with the trailing edge of the ramp windward. The orifice dams were used either separately or a series of them were placed on a row of orifices. The results from this investigation are presented in Appendix I.

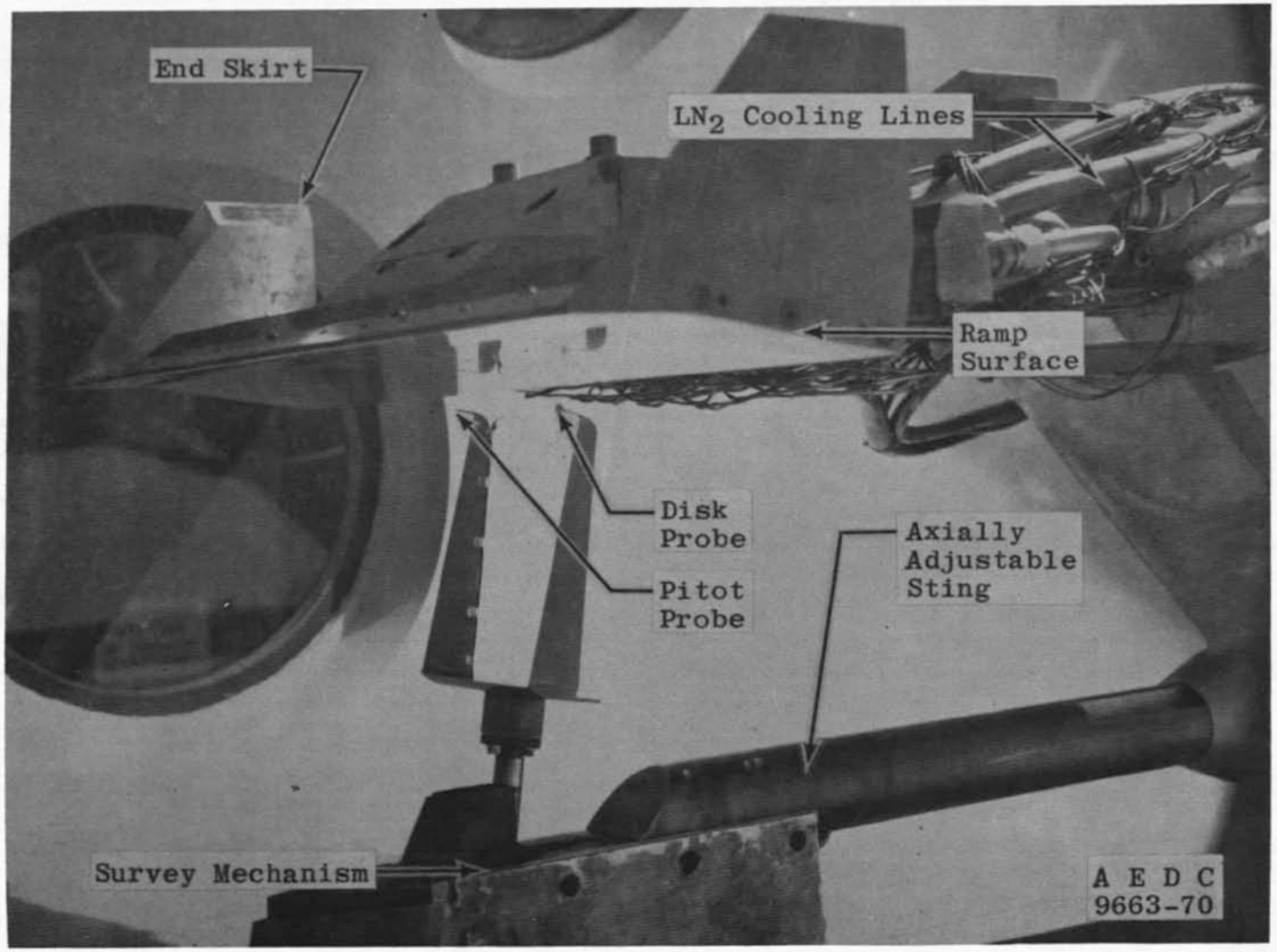

Fig. 1 Sharp-Leading-Edge Ramp Model and Survey System Installed (Inverted) in Tunnel B

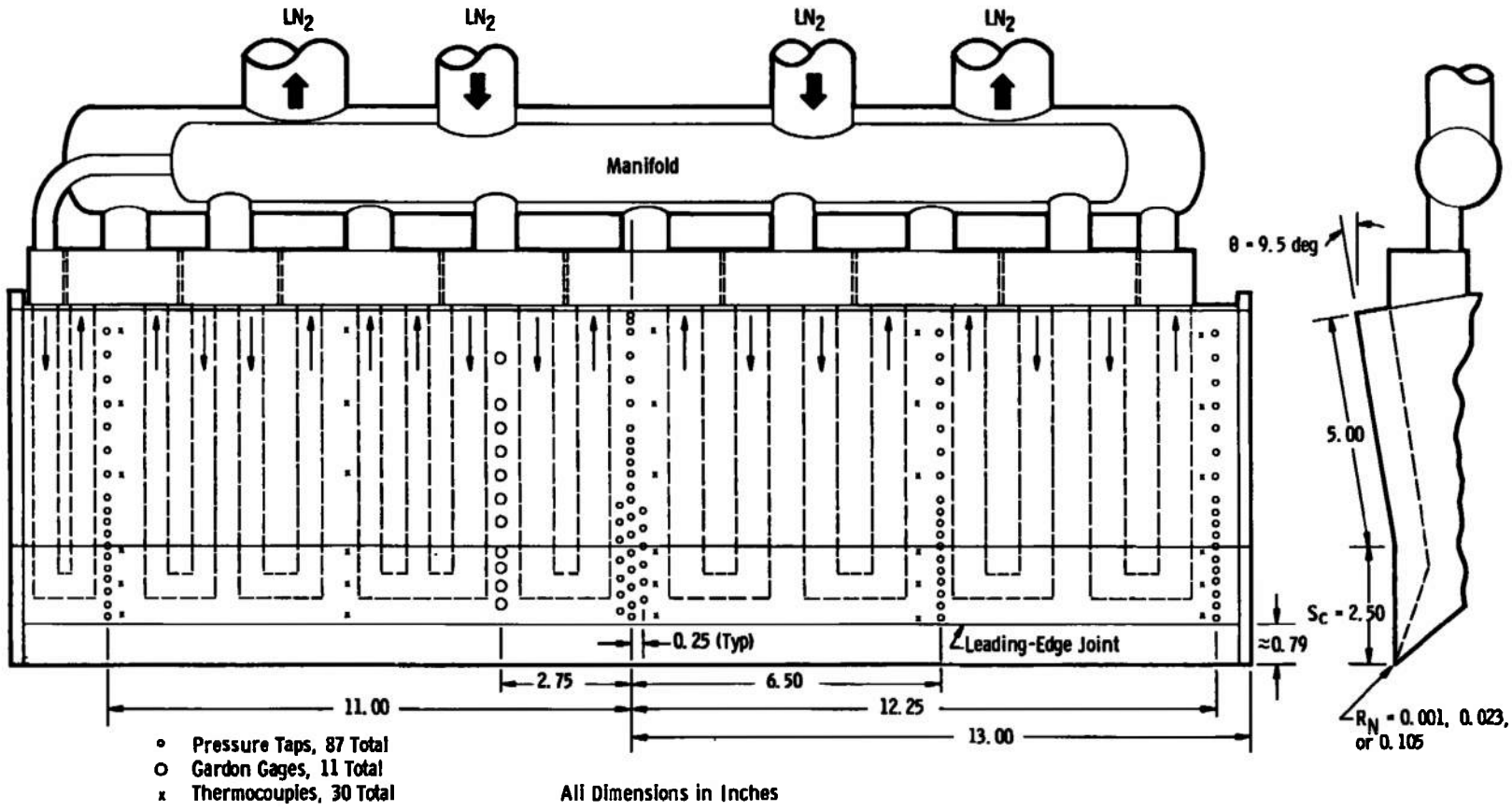

a. Instrumentation and Cooling

Fig. 2 Model Geometry Details

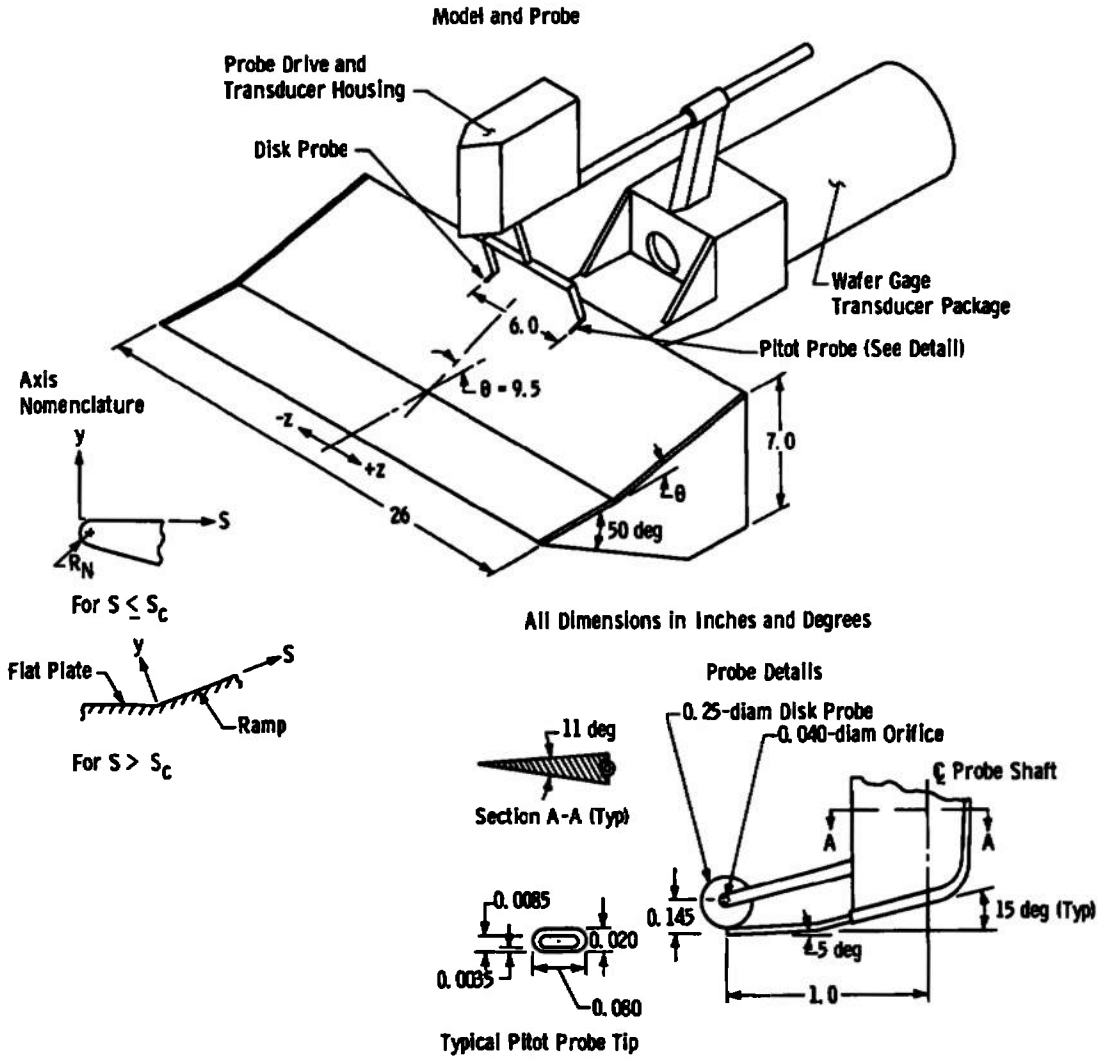

b. Model and Probe dimensions

Fig. 2 Concluded

2.2 INSTRUMENTATION

Model surface pressures were measured on 42 variable-reluctance (wafer gage) transducers rated at 3.0 psid for the Mach number 3.0 and 6.0 test entries and 0.5 psid for the Mach number 4.5 entry. Eleven carrier amplifiers (each with four channels) were used for excitation and signal conditioning. The d-c output of the carrier amplifiers was attenuated, digitized, and recorded on magnetic tape by a Beckman® 210 Data System. The wafer gage transducers were referenced to the tunnel tank pressure which was trapped (by suitable valving) in the transducer package before the model was injected into the tunnel. This pressure ranged from 1 to 3 times free-stream static pressure and was measured with a 20-psid Baratron® transducer which was calibrated at 3.0, 1.0, or 0.3 psid full scale. The Baratron transducer was referenced to near vacuum. The wafer gage transducers were calibrated in two ranges. In general, these were 1.0 and 0.5 psid full scale for the 3.0-psid transducers and 0.5 and 0.25 psid full scale for the 0.5-psid transducers. Six calibration loads were applied from zero to the full-scale pressure being calibrated, and scale factors were calculated for each loading. A linear interpolation of the scale factor between the two loadings closest to the measured pressure was used for the data reduction thereby accounting for any nonlinearity in the transducers. The transducers were operated on the calibrated range closest to the expected pressure; i.e., in general, the taps on the flat plate were on the lower and the taps on the ramp were on the higher of the two calibrated ranges. Based on examination of the repeat data, the estimated precision of the 3.0-psid wafer gage transducers was ±0.005 psia or ±2 percent of the calibrated pressure, whichever was larger, and the estimated precision for the 0.5 psid wafer gage transducers was ±0.002 psia. The reference pressure was measured to an estimated precision of ±1.0 percent of the operating range.

The pitot pressure measurements were made with a 15-psid transducer calibrated over four ranges. The disk static pressure measurements were made with a 5-psid transducer calibrated on two ranges. These transducers were also referenced to the trapped pressure in the wafer gage transducer package. From repeat calibrations, the estimated precision of the pitot pressure measurements was ±0.01 psia or ±1.0 percent, whichever was greater, and for the static probe measurements was ±1.0 percent of the calibrated range. The data reduction procedure for the disk static probe is given in Appendix II.

The probe drive and mechanical positioning mechanism allowed the probe to be positioned axially with an estimated precision of ±0.010 in. and in the y direction within ±0.003 in.

2.3 WIND TUNNELS

The tunnels (Supersonic Wind Tunnel (A) and Hypersonic Wind Tunnel (B)) are continuous, closed-circuit, variable density wind tunnels. Tunnel A has an automatically driven, flexible-plate-type nozzle and a 40- by 40-in. test section. The tunnel was operated at Mach numbers 3.0 and 4.5 at stagnation pressures from 9 to 37 psia and from 20 to 78 psia, respectively, and at a stagnation temperature of 600°R. Tunnel B has an axisymmetric contoured nozzle and a 50-in.-diam test section. The tunnel was operated at a nominal Mach number of 6 at stagnation pressures from 66 to 265 psia, at a stagnation

temperature of 850°R. The model may be injected into the tunnels for a test run and then retracted for model cooling or model changes without interrupting the tunnel flow. In the Tunnel A tests, the model was always in the most forward position for injection so that the elapsed time was a minumum from the start of the vertical travel (injection) to closure of the fairing doors.

The heat-transfer-rate measurements were made with asymptotic-type heat-transfer (Gardon) gages. The gages in the lower heating areas (flat plate and lower portion of the ramp) had a disk thickness of 0.002 in., while in the higher heating area (ramp) the gage disks were 0.005 in. thick. The gages were calibrated at three temperatures: room temperature (80°F), dry ice temperature (-90°F), and liquid-nitrogen temperature (-320°F). A linear interpolation of these scale factors was used to obtain a scale factor at different values of wall temperature. At room temperature, the estimated precision of the Gardon gage measurements was ±5 percent of the reading or ±0.02 Btu/ft^2-sec for the 0.002-in. gages and ±0.05 Btu/ft^2-sec for the 0.005-in. gages, whichever was larger. The precision of the model wall temperature measurements, using Chromel®-Alumel® thermocouples, was ±2°F or ±0.5 percent, whichever was greater.

SECTION III
PROCEDURE

3.1 TEST CONDITIONS AND METHODS

The tests were conducted at nominal Mach numbers of 3, 4.5, and 6 with Reynolds numbers based on the length to the hinge line (Re_c) of 0.25, 0.5, and 1.0 million. Data were obtained at nominal model wall to tunnel total temperature ratios (T_{wall}/T_{t_∞}) of 0.9, 0.6, and 0.3 at all Mach numbers, with an additional series at $T_{wall}/T_{t_\infty} \approx 0.1$ at Mach number 6. Boundary-layer and flow-field survey data were obtained at several model locations for selected configurations and test conditions. A complete summary of the test matrix is given in Appendix III.

Before a particular test series, the model was adjusted to a roll angle within ±0.1 deg of zero using an inclinometer, and the survey probe was set at the desired model location and proper pitch angle (either 0 or 9.5 deg) to survey perpendicular to the surface. Model leading-edge yaw was checked on each installation and found to be within ±0.1 deg. In general, the model was aligned in pitch, to within ±0.05 deg, by injecting the model into the tunnel, allowing the model to reach equilibrium wall temperature, then adjusting to zero angle of attack by use of an optical level and a scribe mark on the model.

During a typical data group, the model was first cooled to the desired wall temperature by use of liquid nitrogen in the internal passages while gaseous nitrogen was blown over the surface to prevent frost accumulation. After the desired level was reached, the liquid and gaseous nitrogen were cut off, transducer zeros were taken, and the reference pressure trapped in the transducer package. The model was then injected into the airflow and,

as soon as steady flow was established (approximately 5 to 10 sec),[1] the probe vertical drive was started. Model surface data were taken continuously at the rate of 20 scans per second from the time the injection cycle started until the probe survey (30 to 45 sec) was completed. By comparing several sets of data reduced at various times it was determined that the surface pressures reached a steady value no later than 7 sec after the model reached the tunnel centerline. The surface data contained in this report were obtained from the earliest possible time in order to have the most uniform wall temperature. The monitor thermocouples indicated that at the worst conditions the wall temperature was uniform to within ±30°F and was usually much more uniform (±18°F). Checks were also made early in the test to determine the speed at which the probe could be driven and still agree with the conventional finite point method of taking data. A vertical drive speed of 1 in. per minute was shown to give reliable data at even the lowest Reynolds number.

3.2 UNCERTAINTIES OF THE DATA

An evaluation of the influence of random measurement errors is presented in this section to provide a partial measure of the precision of the results contained in this report. No evaluation of the systematic measurement error (bias) is included here. Therefore, the precision of the test results was estimated using the estimated instrumentation precisions quoted in Section II, and the uncertainties in free-stream conditions given below, considering that the propagation of these independent measurement errors is closely approximated by a Taylor's series expansion.

The estimated uncertainties in free-stream Mach number (based on repeat calibrations) and stagnation pressure are presented below along with the corresponding estimates of the precision of pertinent free-stream conditions:

PERCENTAGE (±) OF UNCERTAINTIES IN FREE-STREAM CONDITIONS

Nominal Mach Number	M_∞	p_{t_∞}	p_∞	q_∞	$(u/\nu)_\infty$
6	0.5	0.5	3.1	2.1	2.1
4.5	0.3	0.5	1.8	1.2	1.4
3	0.3	0.5	1.4	0.9	1.2

The estimated random errors in the surface pressure measurements are presented below in terms of the ratio p/p_∞ for both the flat plate ($p/p_\infty \approx 1$) and the ramp (p/p_∞ = maximum measured value) because of the significant differences in pressure at all test conditions. The ranges quoted correspond to those at maximum and minimum free-stream stagnation

[1]This unsteady tunnel flow was caused by a temporary "choking" of the tunnel when the model was injected with the instrumented surface down (Fig. 1). The tunnel "restarted" as soon as the injection tank fairing doors were closed. All tests were conducted with the model in this attitude because, at some tunnel conditions, the flow would not "restart" with the model instrumented surface up.

pressure for the sharp leading-edge configuration and are considered to be representative of all the data. The uncertainties in pressure ratio at $p_{t_\infty,min}$ were dominated by the reference pressure uncertainty.

PERCENTAGE (±) OF UNCERTAINTIES IN SURFACE PRESSURE RATIO, p/p_∞

Nominal Mach Number	$0 < S/S_c \leq 1.0$		$1 < S/S_c < 3$	
	$p_{t_\infty,max}$	$p_{t_\infty,min}$	$p_{t_\infty,max}$	$p_{t_\infty,min}$
6	7.4	24.0	3.9	7.9
4.5	4.1	12.8	2.3	5.4
3.0	3.5	11.8	2.4	5.8

The uncertainties associated with the pressure surveys were estimated for the condition of minimum stagnation pressure, the sharp-leading-edge configuration, and the most downstream survey station. The values listed for p_t'/p_{t_∞}' and p_d/p_∞ are for the maximum and minimum measured pressures, while those quoted for the Rayleigh Mach number, M, are based on the measured surface pressure and the values of p_t' at the surface and at the boundary-layer edge. These values are considered to be representative of all the survey data.

UNCERTAINTIES IN SURVEY DATA

Nominal Mach Number	Percentage (±) of Uncertainty					Absolute (±) Uncertainty
	p_t'/p_{t_∞}'		p_d/p_∞		M_δ	M_{wall}
	$p_{t'max}$	$p_{t'min}$	$p_{d_{max}}$	$p_{d_{min}}$		
6	2.4	2.9	5.8	11.0	4.0	0.09
4.5	1.2	3.1	5.4	5.9	3.7	0.10
3.0	1.3	2.1	3.8	3.8	1.3	0.05

The estimated uncertainties in the heat-transfer coefficient (St) are based only on the error in measured heat flux, and do not include a propagation of the uncertainties in the tunnel conditions. This uncertainty in Stanton number at minimum plate Reynolds number was ±5 percent of the value with a minimum absolute uncertainty for the two sizes of gages and at the calibration temperatures listed below.

MINIMUM ABSOLUTE (±) UNCERTAINTIES IN STANTON NUMBER, St x 10^3 AT Re_c = 0.25 x 10^6

Nominal Mach Number	Disk Thickness = 0.002 in.			Disk Thickness = 0.005 in.		
	80°F	-90°F	-320°F	80°F	-90°F	-320°F
6	0.09	0.06	0.08	0.22	0.15	0.18
4.5	—	0.10	0.10	—	0.24	0.23
3.0	—	0.06	0.06	—	0.14	0.13

SECTION IV
EXPERIMENTAL RESULTS

4.1 BOUNDARY-LAYER TRANSITION

Because of the important influence which boundary-layer transition onset has on ramp-induced laminar flow separations, shadowgraphs for M_∞ = 6 are presented to illustrate the variations in transition caused by changes in wall temperature (Fig. 3) and nose radius (Fig. 4) for the Reynolds number range investigated. Where possible, the boundary layer itself was used to determine the location of transition onset. However, when the boundary layer was not clear, the point at which the boundary between the model and the flow became ill-defined was chosen as the onset of transition. No photographs of satisfactory quality were obtained in Tunnel A, presumably because of the combined effects of the wide model and the double-pass schlieren system used. A disturbance wave produced by the leading-edge joint became most evident for the sharp leading edge at wall maximum cooling (Fig. 3c), whereas it was plainly evident with blunt leading edges for the adiabatic wall condition (Fig. 4). These pictures mainly show that transition was moved upstream by an increase in Reynolds number and that the boundary layer appeared the thickest with the moderate nose radius, cf. Figs. 3a, 4a, and 4b. It should be noted, however, that these data (Fig. 4) indicate transition did not begin on the ramp at even the highest Reynolds number when the leading edge was blunted at M_∞ = 6 (adiabatic). The shadowgraphs for the two blunt leading-edge configurations at T_{wall}/T_{t_∞} = 0.65 and 0.12 were of poorer quality; however, they also indicated that transition did not begin on the ramp at even the highest Reynolds number.

There are few references dealing with the effects of significant leading-edge blunting on transition, although most have dealt with slight blunting (e.g., Ref. 16). The reference most applicable to the conditions investigated here is that of Brinich and Sands (Ref. 17). Their results for adiabatic flow on hollow cylinders at $(u/\nu)_\infty$ = 0.35 million indicate that the onset of transition was essentially independent of nose radius for $0.001 \leq R_N \leq 0.125$, a result which is at odds with the results shown in Figs. 3 and 4 for reattaching flows.

An estimate of the transition onset location for adiabatic wall condition in the Tunnel A tests may be made by utilizing the correlation (of data from Refs. 7 and 18) shown in Fig. 5. These results in effect relate the influence of the reattachment pressure gradient on the transition location on the ramp to the location of transition onset on a flat plate. That is, increasing the flat-plate length, S_c, causes the relative location of transition (S_{to}/S_c) to move forward toward reattachment. This correlation is effectively the same as was used by Roberts (Ref. 19), in the form of the estimated length of the mixing layer, ℓ_{sep}, and the length of the transition zone, Δx_{tr}, to correlate transitional separation data obtained on different length models. Once the transition location on the flat plate is known (assuming that $(S_{to}/S_c)_{FP} > 1$), the transition location on a 9.5-deg ramp is obtained from Fig. 5 at the appropriate Mach number. This figure shows quite clearly the benefits to be gained by testing at the highest possible Mach number if one desires laminar flow reattachment. The influence of plate Reynolds number, Re_c, on the relative transition location for adiabatic conditions (sharp plate) presented in Fig. 6a indicates that transitional flow reattachment should be expected at $M_\infty = 4.5$ and $Re_c > 0.5 \times 10^6$, and at $M_\infty = 3.0$ and $Re_c > 0.3 \times 10^6$ if reattachment takes place in the vicinity of $S/S_c \approx 1.5$. The variation of transition onset with wall temperature is shown in Fig. 6b to have been significantly affected by the value of the plate Reynolds number at $M_\infty = 6$, but this trend is probably only a result of the interaction being studied.

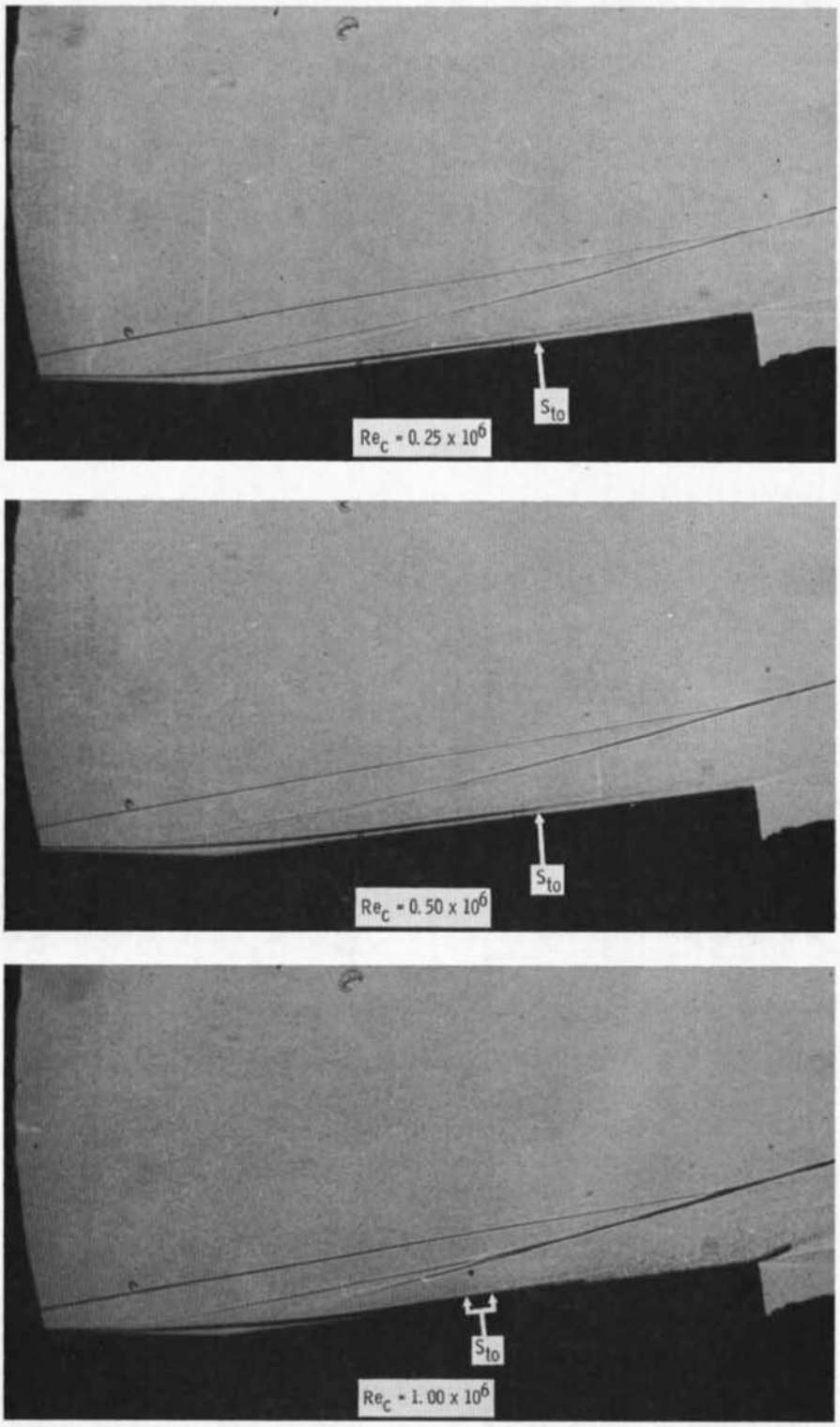

a. $T_{wall}/T_{t_\infty} = 0.9$

Fig. 3 Effects of Reynolds Number on Flow-Field Photographs at $M_\infty = 6.0$, $R_N = 0.001$

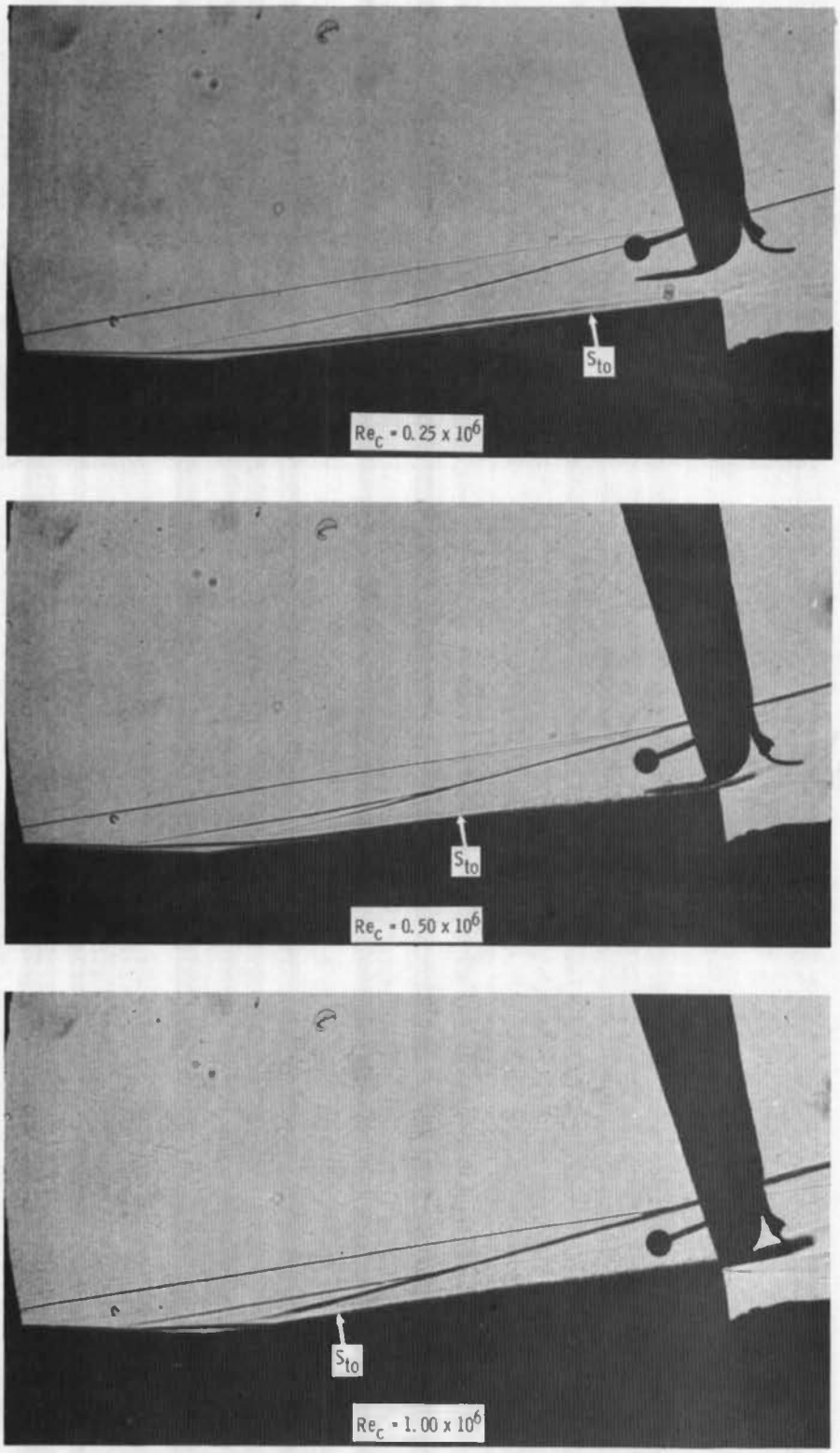

b. $T_{wall}/T_{t_\infty} = 0.65$

Fig. 3 Continued

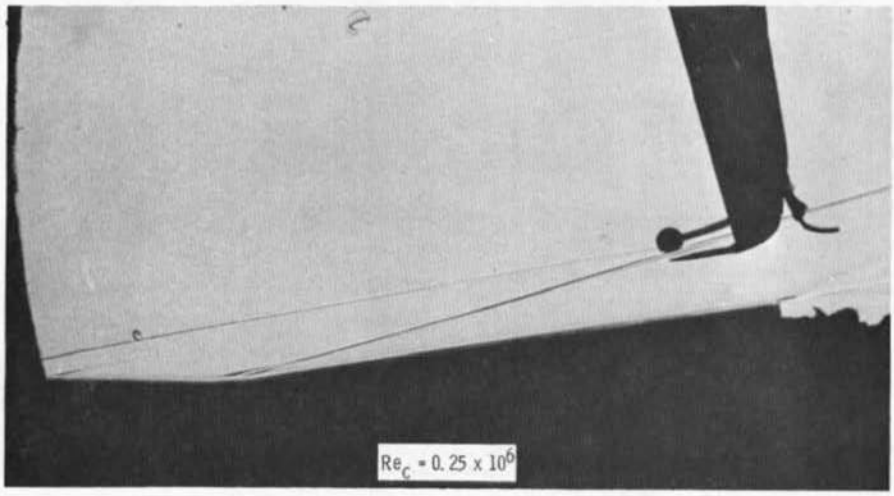

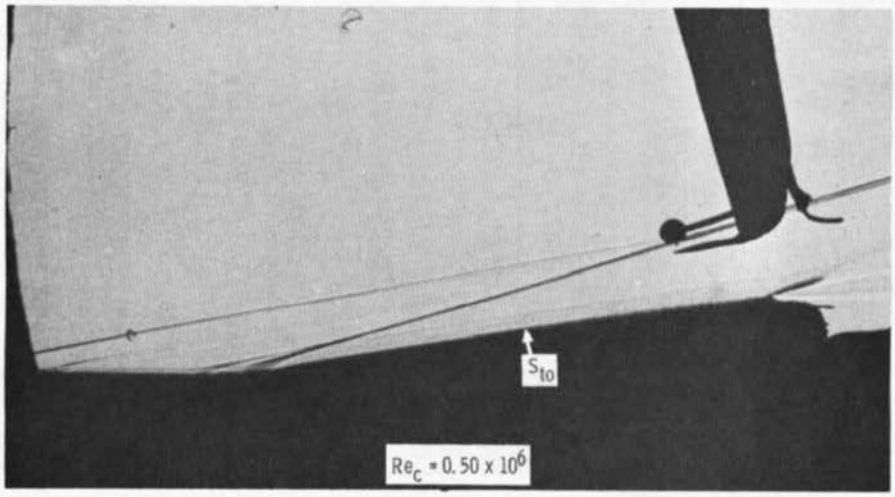

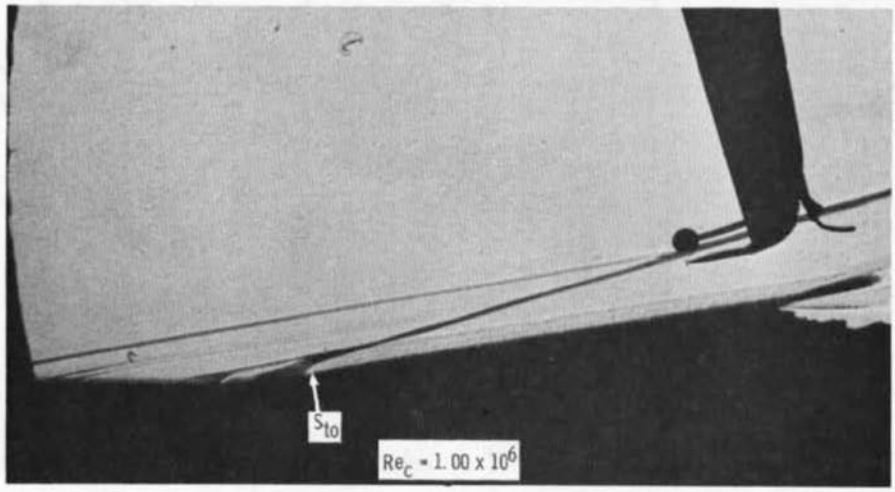

c. $T_{wall}/T_{t_\infty} = 0.12$
Fig. 3 Concluded

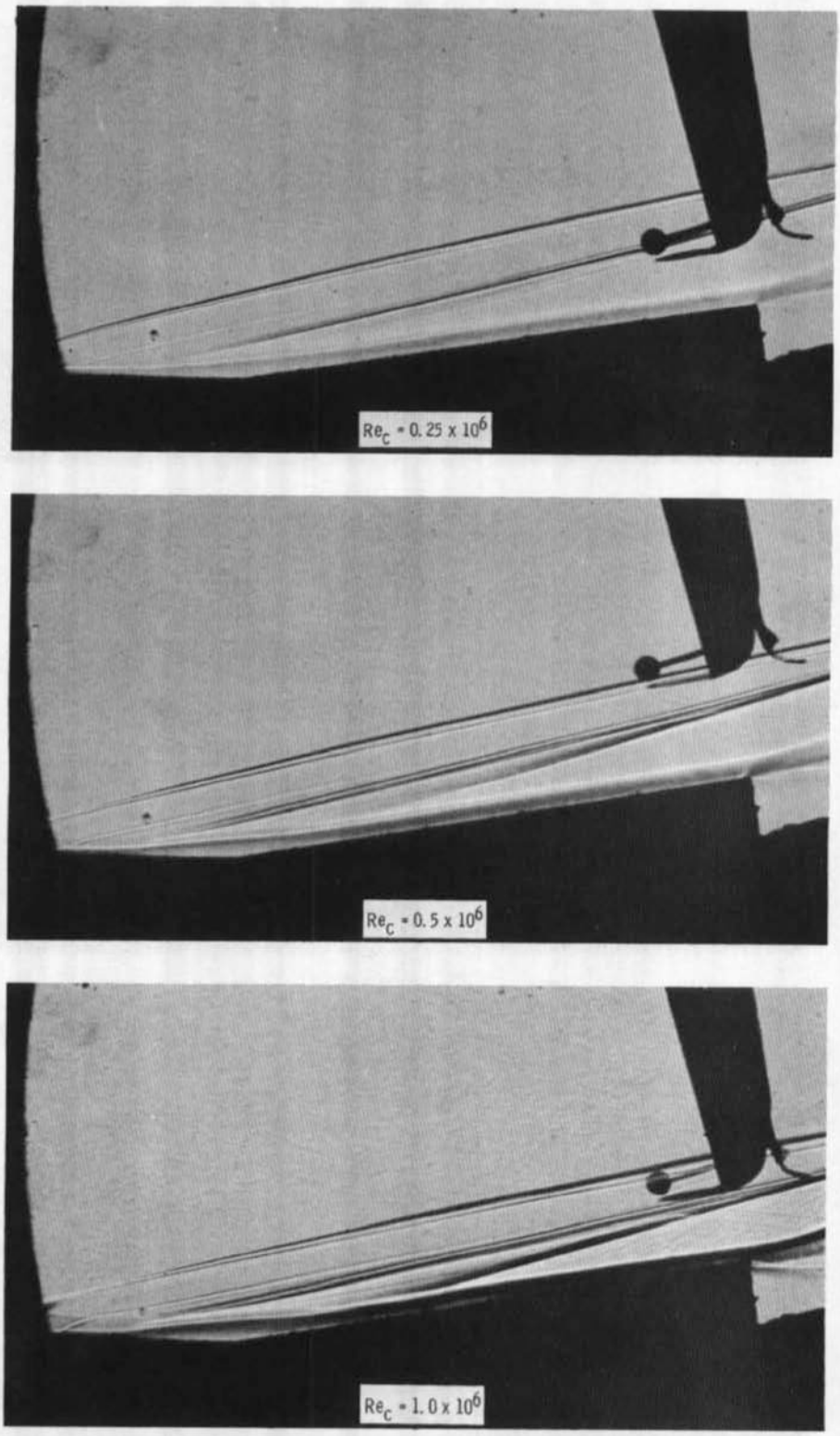

a. R_N = 0.023 in.

Fig. 4 Effects of Reynolds Number on Flow-Field Photographs at M_∞ = 6, Adiabatic Wall

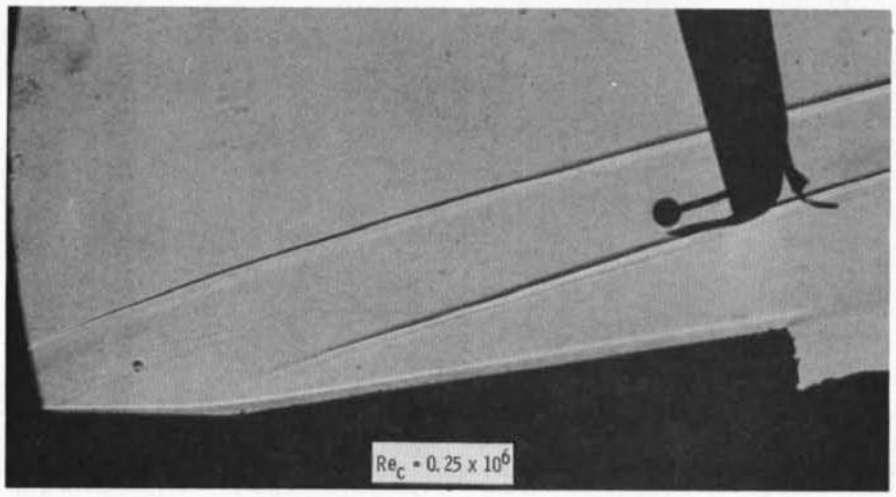

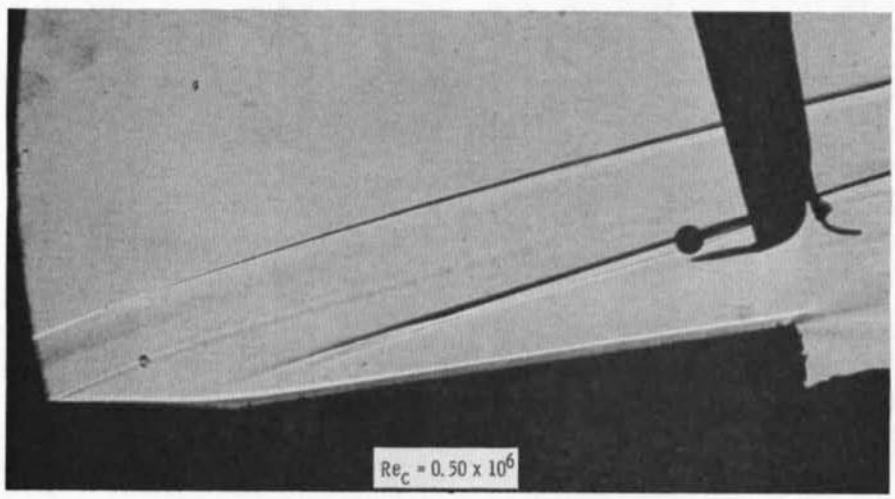

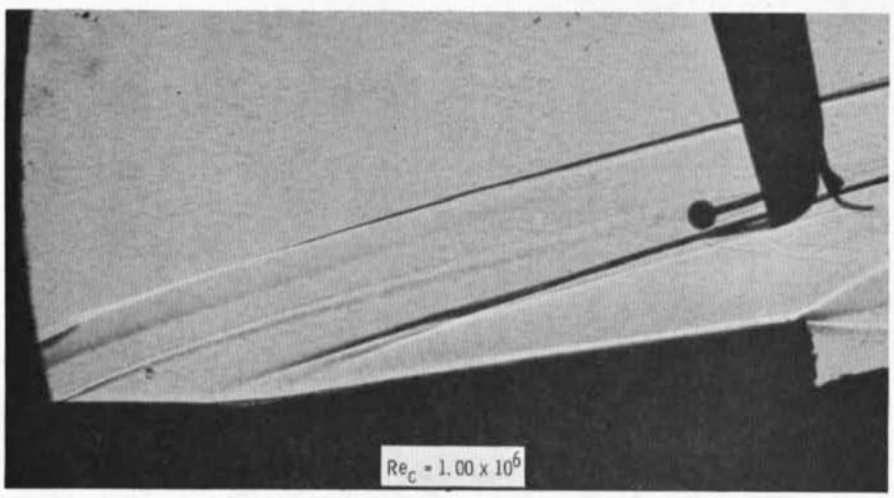

b. R_N = 0.105 in.
Fig. 4 Concluded

Sym	S_c	Source
○	1.9	Unpublished Data
◇	2.5	Ref. 7
□	3.8	Unpublished Data and Ref. 18
△	7.6	Unpublished Data

Sym	M_∞	$(u/\nu)_\infty \times 10^{-6}$
Solid	3.0	0.05 to 0.20
Half Solid	4.5	0.03 to 0.25
Open	6.0	0.10 to 0.40

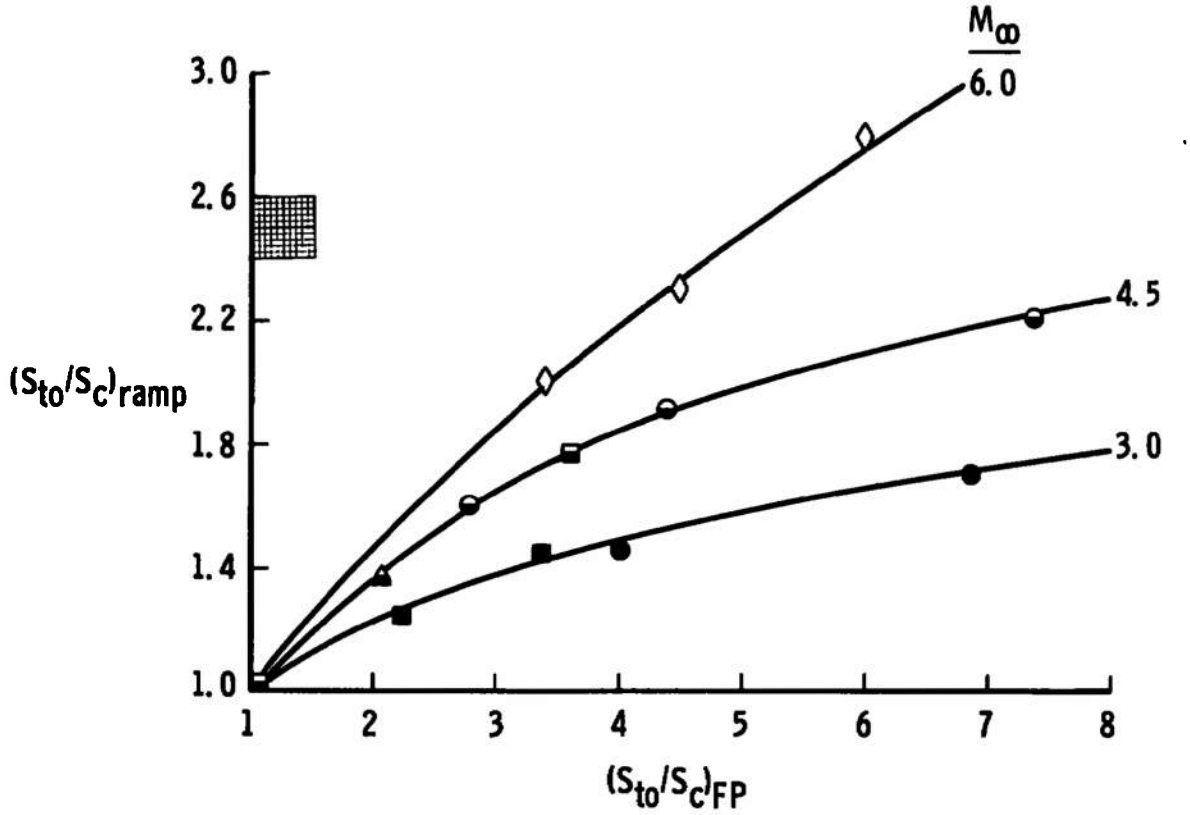

Fig. 5 Effect of Mach Number on the Relation between Transition Onset on a Flat Plate and a Flat-Plate-Ramp Combination, θ = 9.5 and $R_N \leq 0.001$ (Adiabatic Wall)

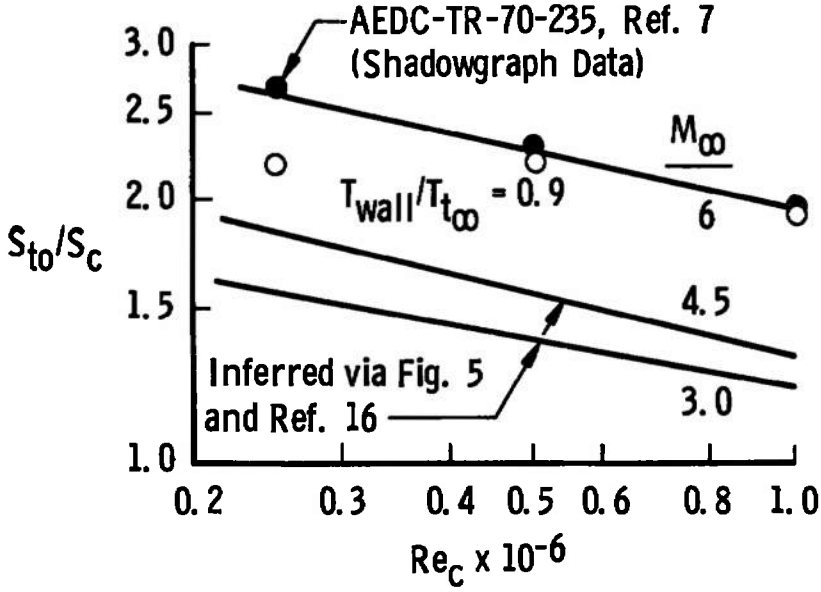

a. Variation with Flat Plate Reynolds Number

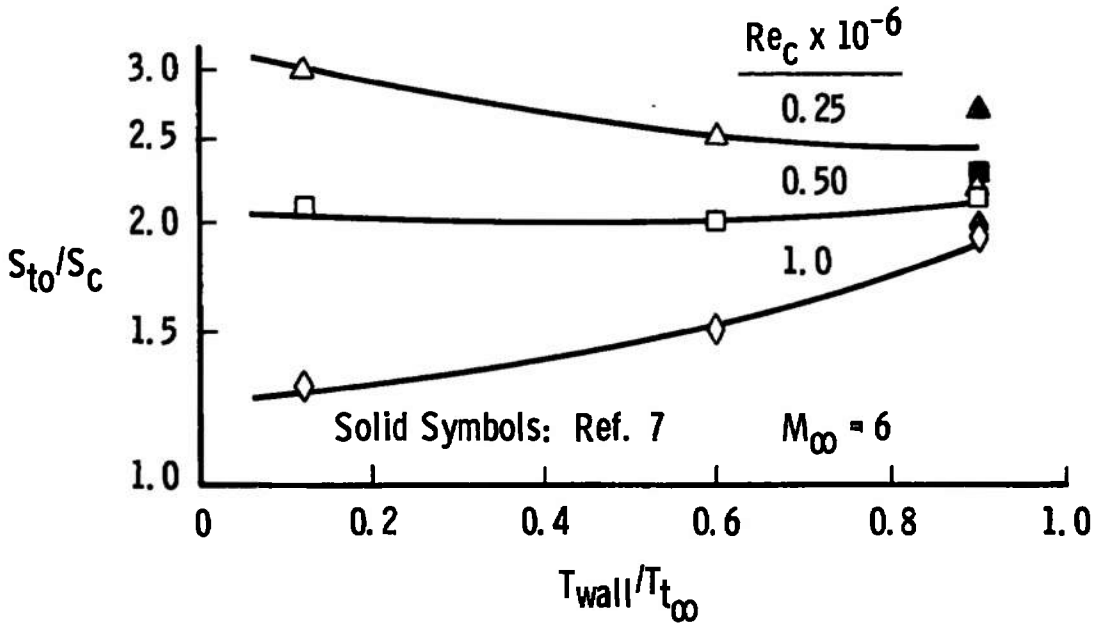

b. Variation with Wall Temperature

Fig. 6 Effects of Reynolds Number and Wall Temperature on the Relative Transition Location, θ = 9.5 and R_N = 0.001

4.2 SURFACE PRESSURE DISTRIBUTIONS

Longitudinal surface pressure distributions are presented in Figs. 7 and 8 to show the influence of leading-edge bluntness at the three test Mach numbers and at the maximum and minimum Reynolds numbers and wall temperatures. The adiabatic wall, low Reynolds number data, Fig. 7a, show that the most notable effect of an increase in nose bluntness was the increase in the flat-plate pressure level, especially at the higher Mach numbers. This amplification of the nose bluntness effect with an increase in Mach number was also shown by the ramp pressure distribution, $S/S_c > 1$. While it was not evident at $M_\infty = 3$, a very pronounced base "bleed" (i.e., sharp drop in pressure near the trailing edge of the ramp) was obtained as the Mach number was increased to 6. Upstream of this "bleed," however, the ramp pressure levels for two blunt leading edges approached closely that for the sharp leading edge. The ramp-induced upstream interaction extent was usually reduced as Mach number was increased, but at a given Mach number there appears to have been a reversal in the effect of nose radius on this interaction. While the interaction appears to have increased slightly from the 0.001-in. leading edge to the 0.023-in. leading edge, a sharp decrease was obtained for the 0.105-in. leading edge. This effect of nose radius on the interaction length will be dealt with in more detail in Section 4.3. The present results agree quite well with previous data (solid symbols, Ref. 7) taken at $M_w = M_\infty = 6$; however, when the present $M_\infty = 4.5$ data are compared to that taken previously with the model pitched ($M_w = 4.5$, $M_\infty = 8$), there is a small discrepancy. This disagreement was caused by the intersection of the bow wave and ramp shock when the model was pitched and is explained in more detail in Ref. 7 (see Fig. 17 in Ref. 7).

The effects of wall cooling on the pressure distribution, at the same free-stream conditions, can be seen by comparing Fig. 7a with Fig. 7b. The major effect of the wall cooling was to reduce the overall pressure level on the plate and ramp at all test conditions and to reduce the extent of the ramp-induced interaction. Besides a reduction in the interaction extent, wall cooling caused a much steeper ramp pressure rise, especially at $M_\infty = 6$. It is also noted that with wall cooling the base bleed was absent. The most surprising result of nose blunting is the significant increase in the length required for the pressure to reach the asymptotic level for the ramp, especially for $R_N = 0.023$. These distances are much greater than the size of the interaction on the flat plate.

Pressure distributions for the same wall temperatures and Mach numbers are shown in Figs. 8a and b for $Re_c = 1.0$ million, but the reattachment was probably transitional at this Reynolds number (see Fig. 6a). The relative change in the pressure distribution with an increase in leading-edge radius at a given Mach number was very nearly the same as at the low Reynolds number. It is interesting to note, however, that, although the extent of the ramp-induced interaction was decreased when Reynolds number was increased for a given wall temperature at $M_\infty = 3$, there was very little change at $M_\infty = 4.5$ and even a slight increase at $M_\infty = 6$. Although this increase at $M_\infty = 6$ is an indication of the existence of a laminar reattaching flow, the rate of change of this increase must also be considered to determine if transition was sufficiently far downstream of reattachment that the overall interaction (Ref. 7) was not affected.

Theoretical inviscid pressure distributions for M_∞ = 4.5 and 6 are compared in Fig. 9 with data for the blunt leading edges at the lowest plate Reynolds number. Inviscid calculations at M_∞ = 3 are not available because blunt body solutions to provide the initial data for the characteristics part could not be obtained with the existing program. The adiabatic wall data, Fig. 9a, show an unexpectedly large difference in level for both nose radii at both Mach numbers outside of the ramp-induced interaction region. Although the levels of the cold wall data (Fig. 9b) appear to agree quite well with the inviscid theory, except in the separation region, this agreement is seen to be rather fortuitous when the plate data are examined in terms of weak-interaction coordinates.

The pressure ratio measured near the leading edge (S = 1.0) for all three radii and all test conditions is presented as a function of the hypersonic weak-interaction parameter, $\bar{\chi}_\infty$, in Fig. 10. This pressure tap was sufficiently far upstream to be free of the ramp-induced interaction in all cases. These data at M_∞ = 6 (Fig. 10a) clearly show that, while a uniform trend was established for all leading-edge radii at all wall temperatures as Reynolds number was increased, the extrapolated value of p/p_∞ at $\bar{\chi}_\infty$ = 0 was well below that of the inviscid prediction. As pointed out earlier, a slight mismatch between the leading edge and the flat plate was observed at times during the test; in fact, measurements taken at the conclusion of the test indicated that, even when extreme care was used in installing the leading edge, an equivalent expansion angle of 0.3 deg existed. It is interesting to note that the intercept of the data fairing for all three leading edges at all temperatures was nearly a constant 14 percent below the inviscid value, which is approximately equivalent to a 1-deg expansion at M_∞ = 6. The data obtained at M_∞ = 3 and 4.5 (Fig. 10b) give extrapolated inviscid values which are closer to the predicted value, but which are still about 10 percent off at M_∞ = 3. It should be pointed out that the testing sequence was M_∞ = 6 first and M_∞ = 4.5 last, but as the investigation progressed the significance of a very slight misalignment became more and more obvious so that more care was exercised to minimize steps in the joint. These data illustrate that the viscous interaction influence expressed as a rate of change, $d(p/p_\infty)/d\bar{\chi}_\infty$, for the blunt leading edges at M_∞ = 6 was as large as, if not larger than, that for the sharp (R_N = 0.001) flat plate, and the effects were still appreciable at M_∞ = 4.5. Maximum wall cooling, as expected, reduced the viscous interaction effects, particularly when $M_\infty \geq 4.5$.

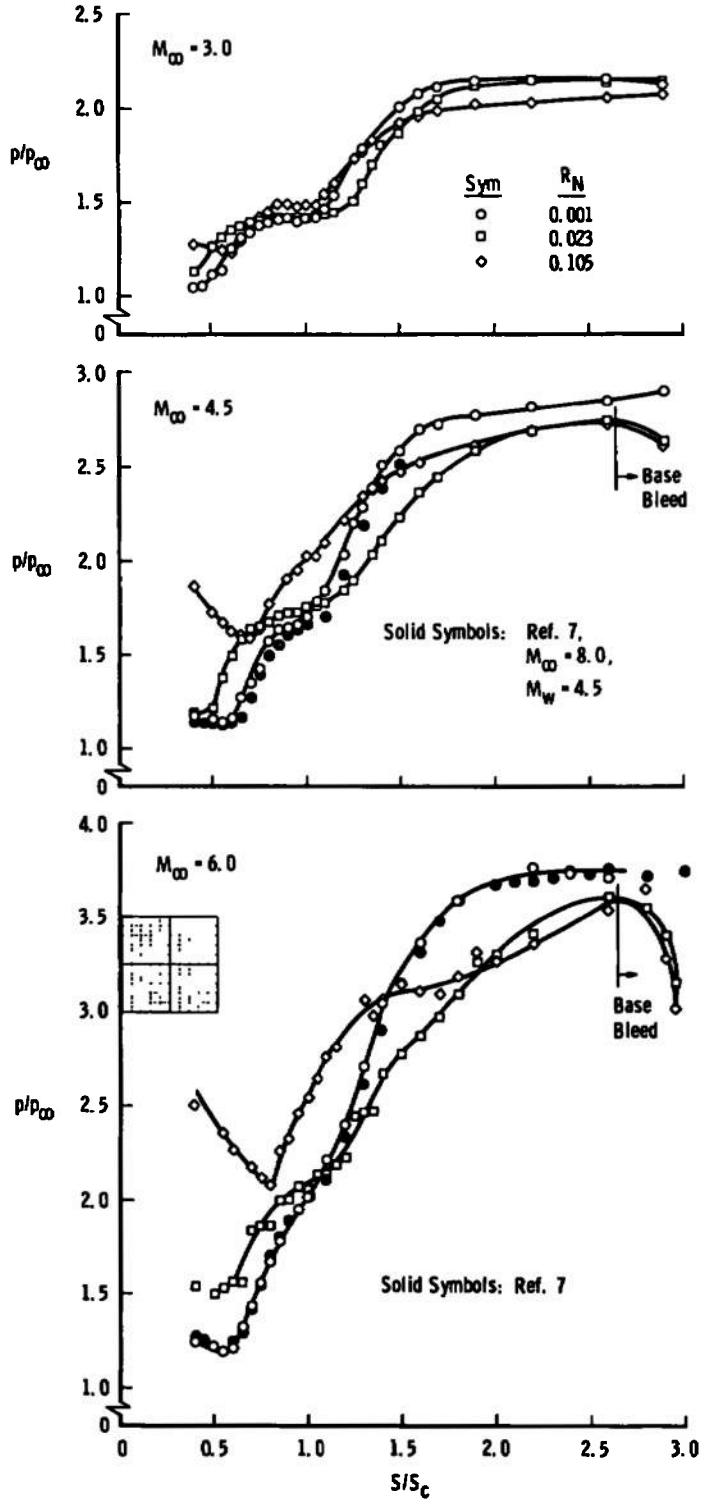

a. $T_{wall}/T_{t_\infty} \approx 0.9$

Fig. 7 Effects of Nose Radius on Surface Pressure Distribution, $Re_c = 0.25 \times 10^6$

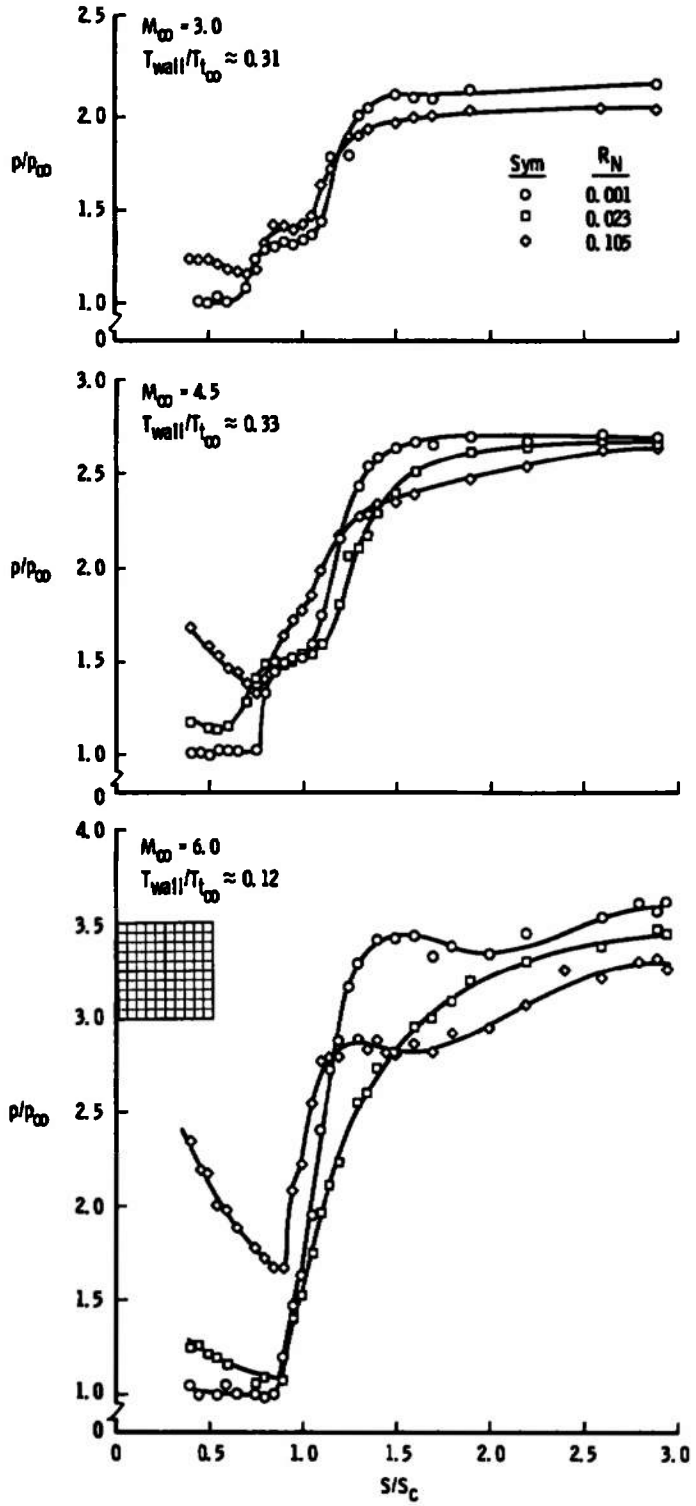

b. Cold Wall
Fig. 7 Concluded

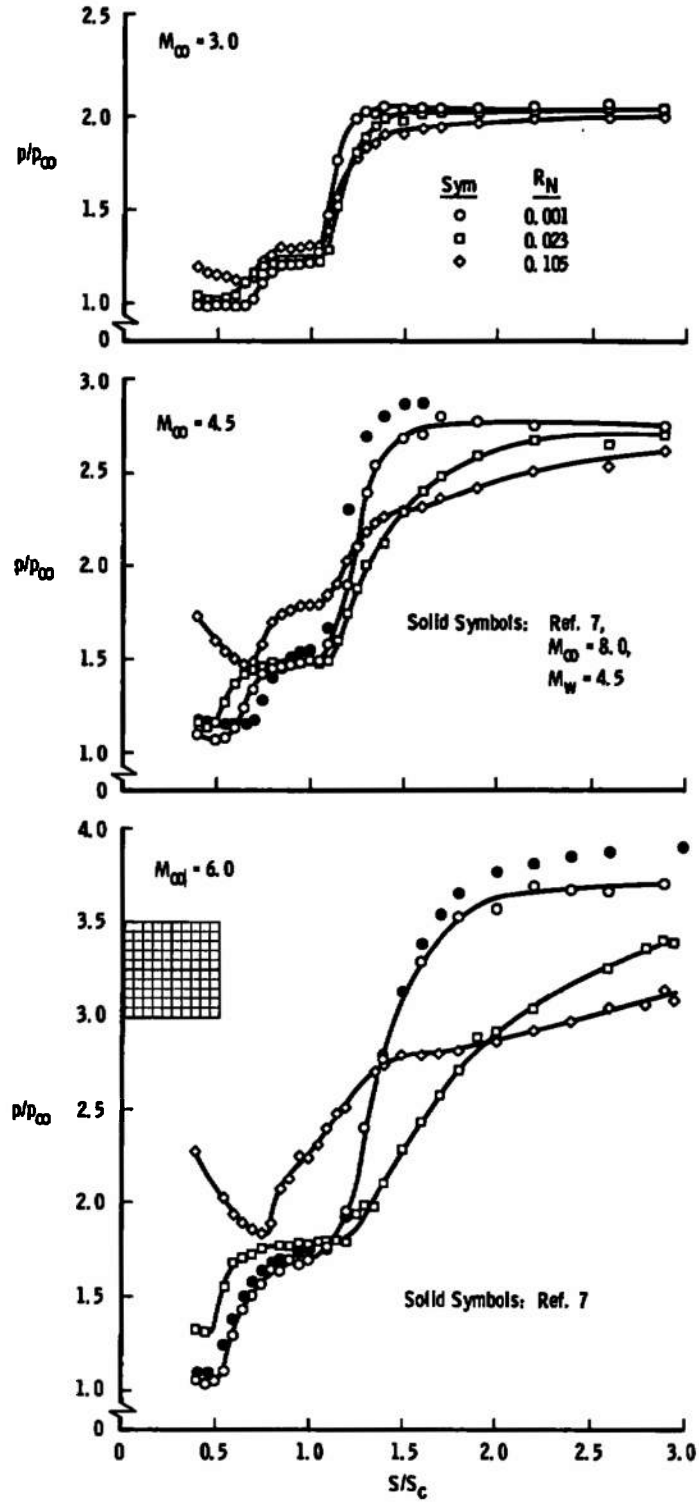

a. $T_{wall}/T_{t_\infty} \approx 0.9$

Fig. 8 Effects of Nose Radius on Surface Pressure Distribution, $Re_c = 1.00 \times 10^6$

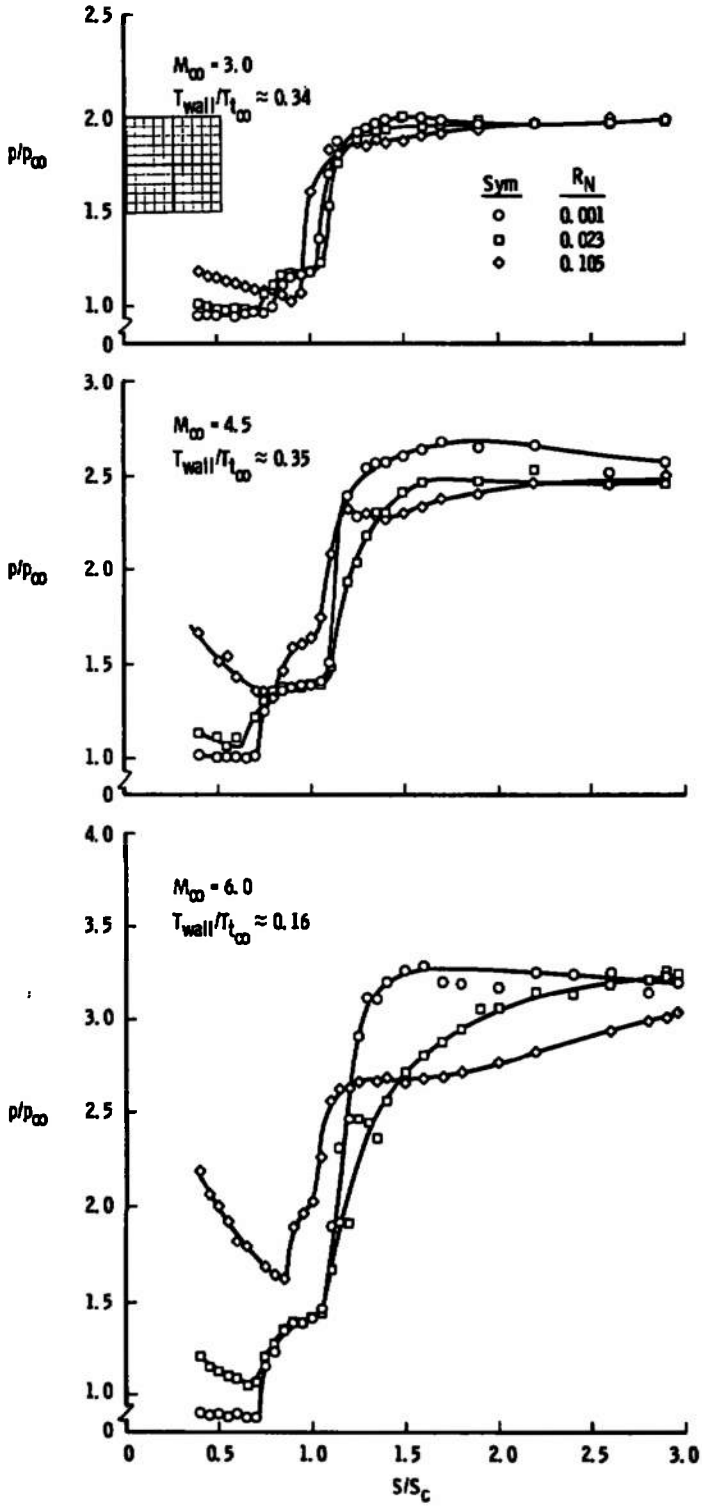

b. Cold Wall

Fig. 8 Concluded

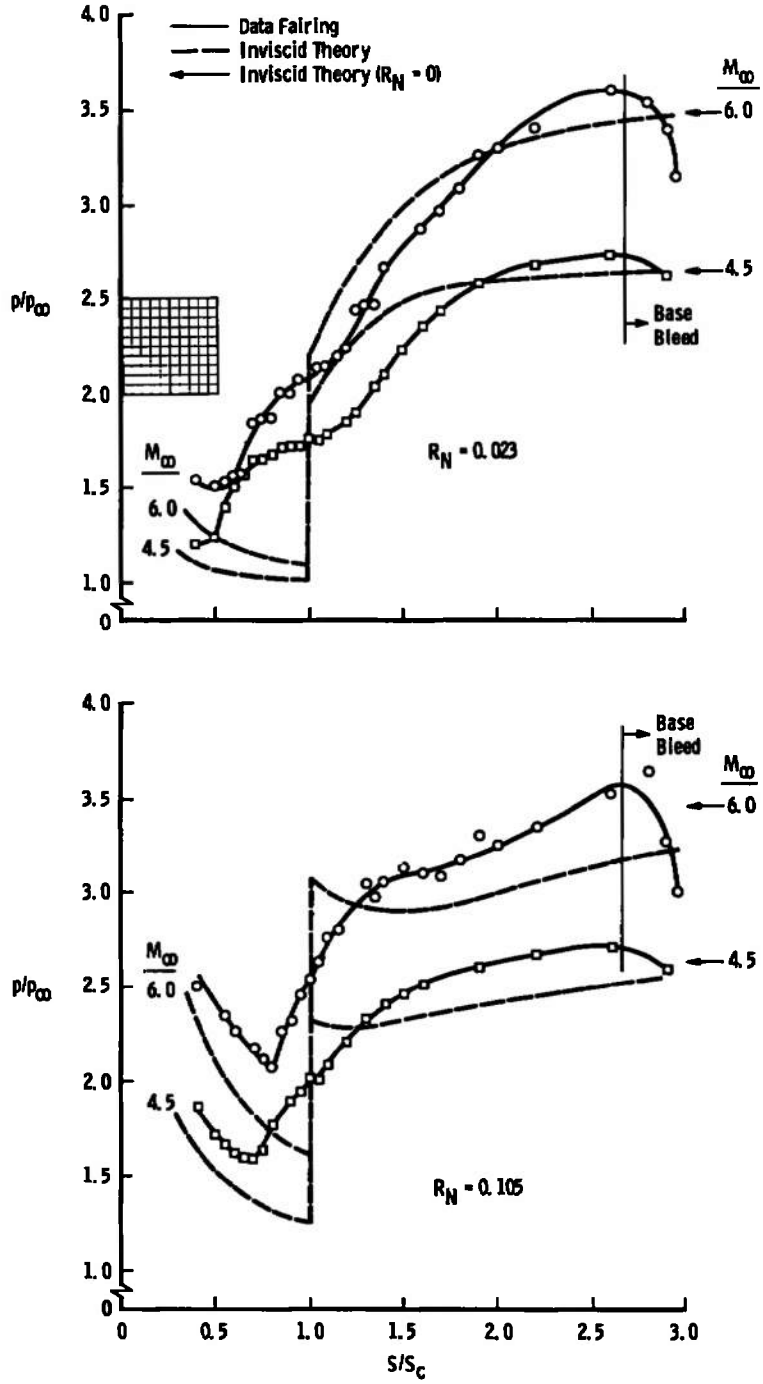

a. $T_{wall}/T_{t_\infty} \approx 0.9$

Fig. 9 Comparison of Inviscid and Experimental Surface Pressure Distributions on 9.5-deg Ramp Model with Blunt Leading Edges, $Re_c = 0.25 \times 10^6$

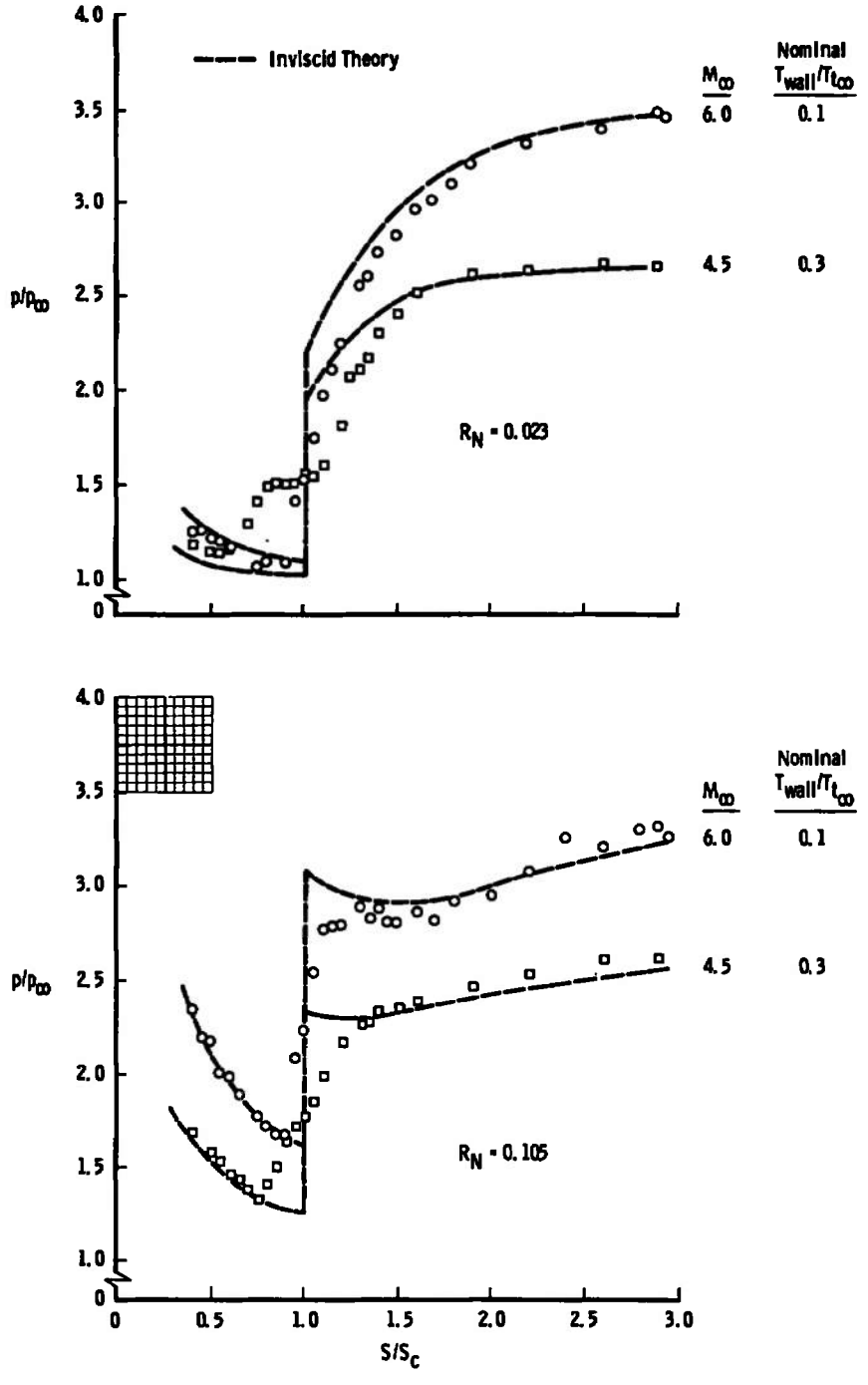

b. Cold Wall

Fig. 9 Concluded

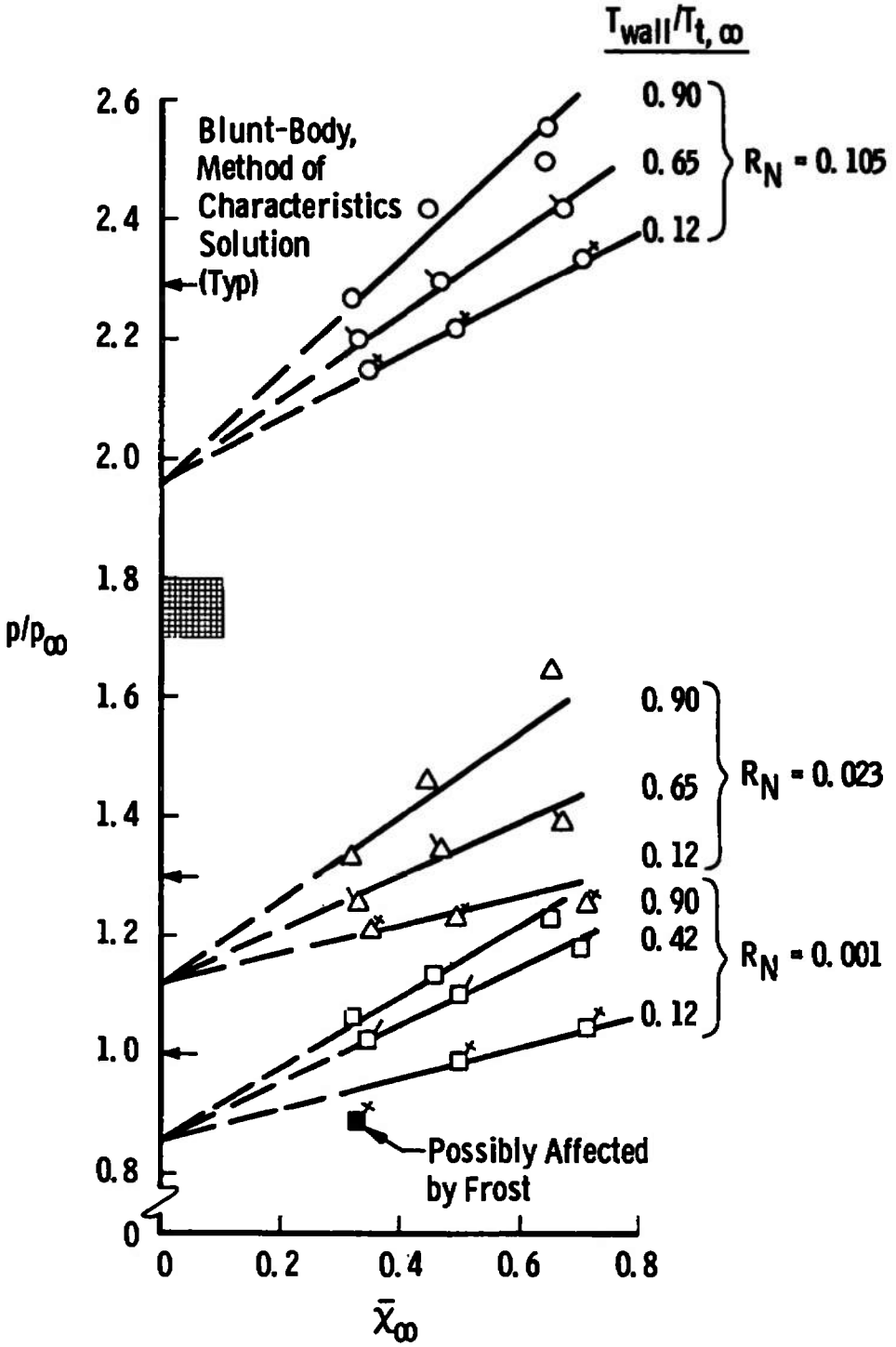

a. M_∞ = 6.0

Fig. 10 Effects of Wall Temperature and Nose Bluntness for Weak Interaction on Flat Plate at S = 1.0

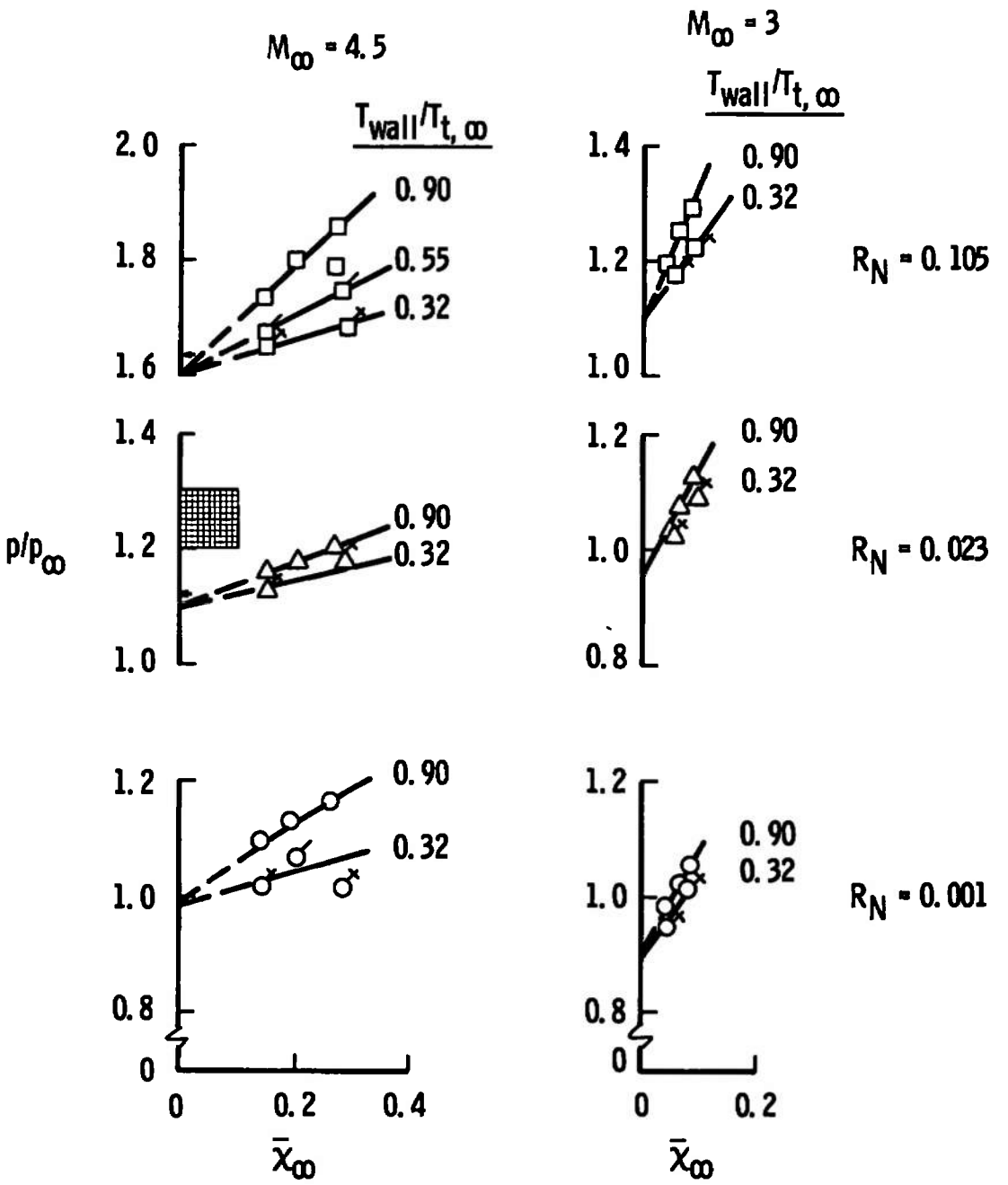

b. M_∞ = 3.0 and 4.5
Fig. 10 Concluded

4.3 UPSTREAM INTERACTION EXTENT

A summary of the effect of Reynolds number on the relative upstream extent of the ramp-induced interaction, which is useful for identifying transitional reattachment, is shown in Fig. 11. For both wall temperature ratios shown, the $M_\infty = 6$ results exhibit the laminar trend, i.e., increasing interaction length with increasing Reynolds number, whereas the $M_\infty = 3$ trend is the opposite, indicating transitional reattachment at least at the two higher Reynolds numbers. The $M_\infty = 4.5$ data show only slight increases in interaction length with an increase in Reynolds number, thus indicating that—at least at the highest Reynolds number—transition occurred near enough to reattachment to reduce the relative size of the interaction. The sharp-leading-edge results at $M_\infty = 6$ agree reasonably well with those of Ref. 7.

It is quite clear from Fig. 12 that, as in Ref. 3 for the cold wall case, an increase in the interaction length was obtained with a small increase in bluntness for both an adiabatic and a cold wall, while a decrease occurred when the bluntness was relatively large ($R_N = 0.105$). This trend was obtained both when the reattaching flow was most certainly laminar ($M_\infty = 6$, $Re_c = 0.25$ million) and when the reattaching was most likely transitional ($M_\infty = 3$, $Re_c = 1.0$ million). It thus appears that this reversal with increasing nose radius is not restricted to laminar flow reattachment conditions alone.

The influence of wall temperature on the interaction length is shown in Fig. 13. At $Re_c = 0.25$ million, Fig. 13a, a reduction in wall temperature or an increase in Mach number produced a reduction in the interaction length for all three leading edges. At $Re_c = 1.0$ million, Fig. 13b, the decrease in upstream interaction length with a decrease in wall temperature is again evident; however, the trend with a change in Mach number was reversed at this Reynolds number, in most cases. This reversal in the trend of the length of the interaction as a function of Mach number and Reynolds number is clearly shown in Fig. 14. It is interesting to note that an increase in Mach number caused a decrease in the interaction at low Reynolds number and an increase at high Reynolds number, except for the bluntest leading edge at adiabatic wall conditions. For these latter conditions, the increase in Mach number produced a decrease in the interaction at all Reynolds numbers.

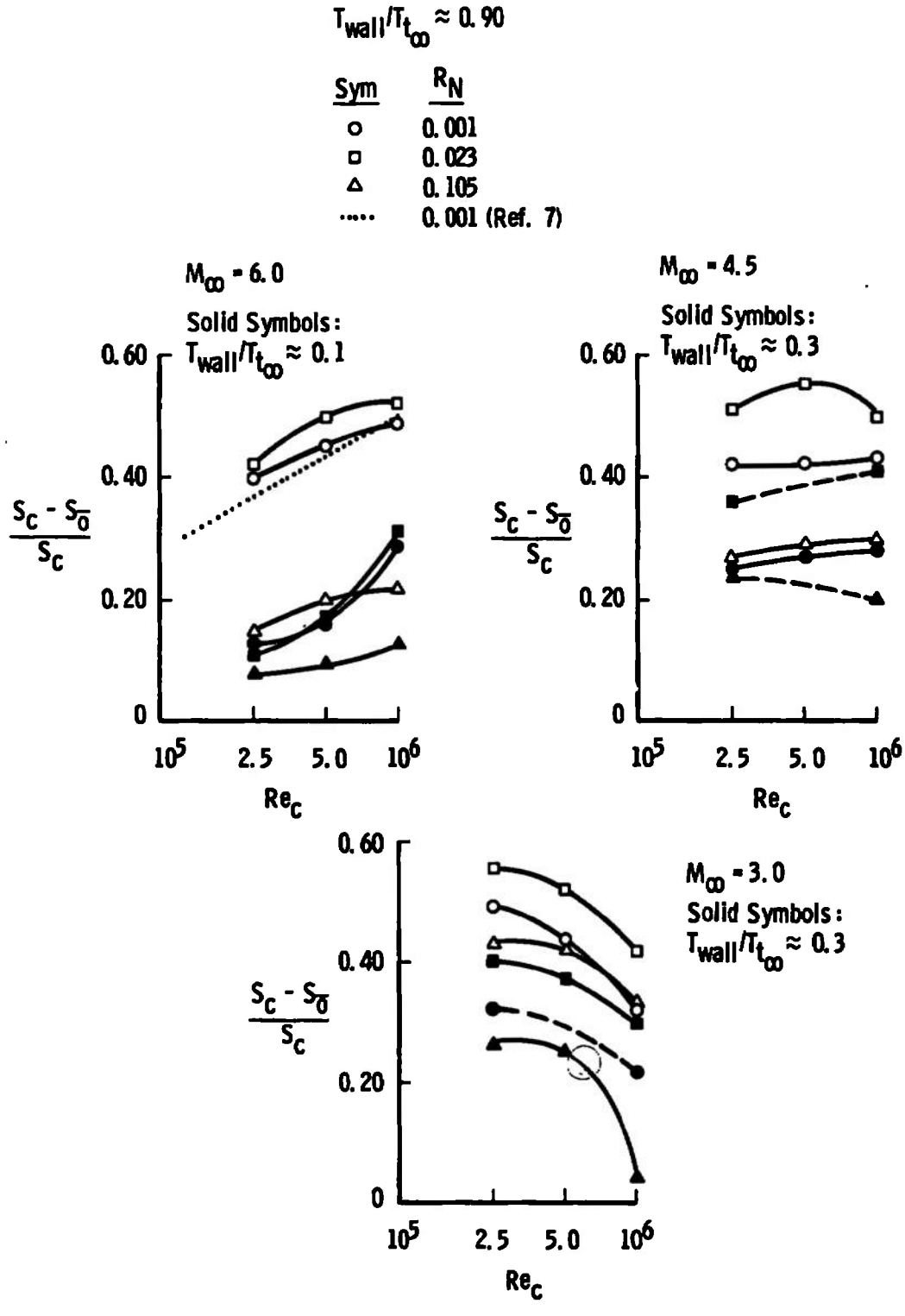

Fig. 11 Effects of Plate Reynolds Number on the Upstream Interaction Extent

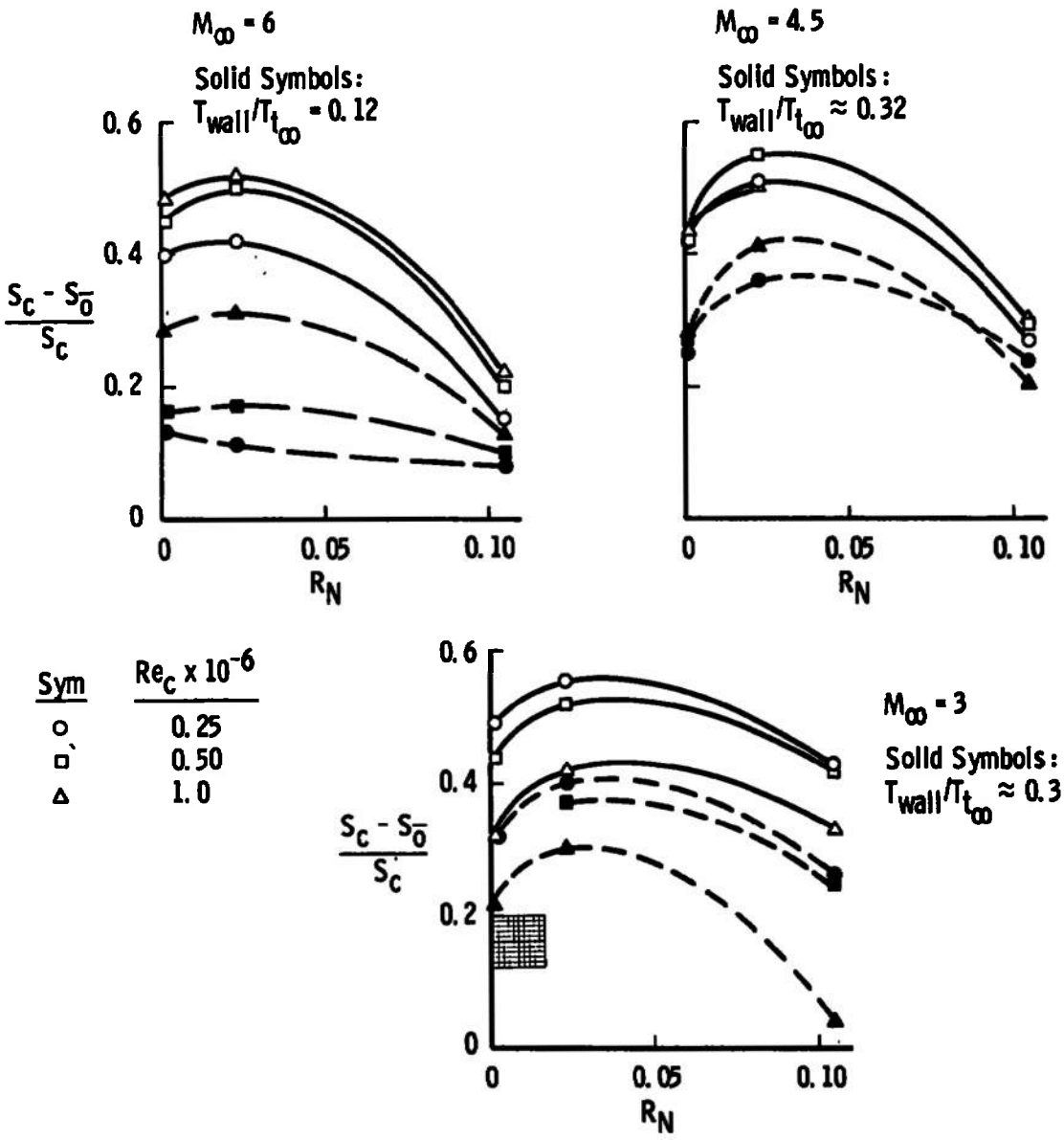

Fig. 12 Effects of Nose Radius on the Upstream Interaction Extent for Adiabatic and Cold Wall Conditions

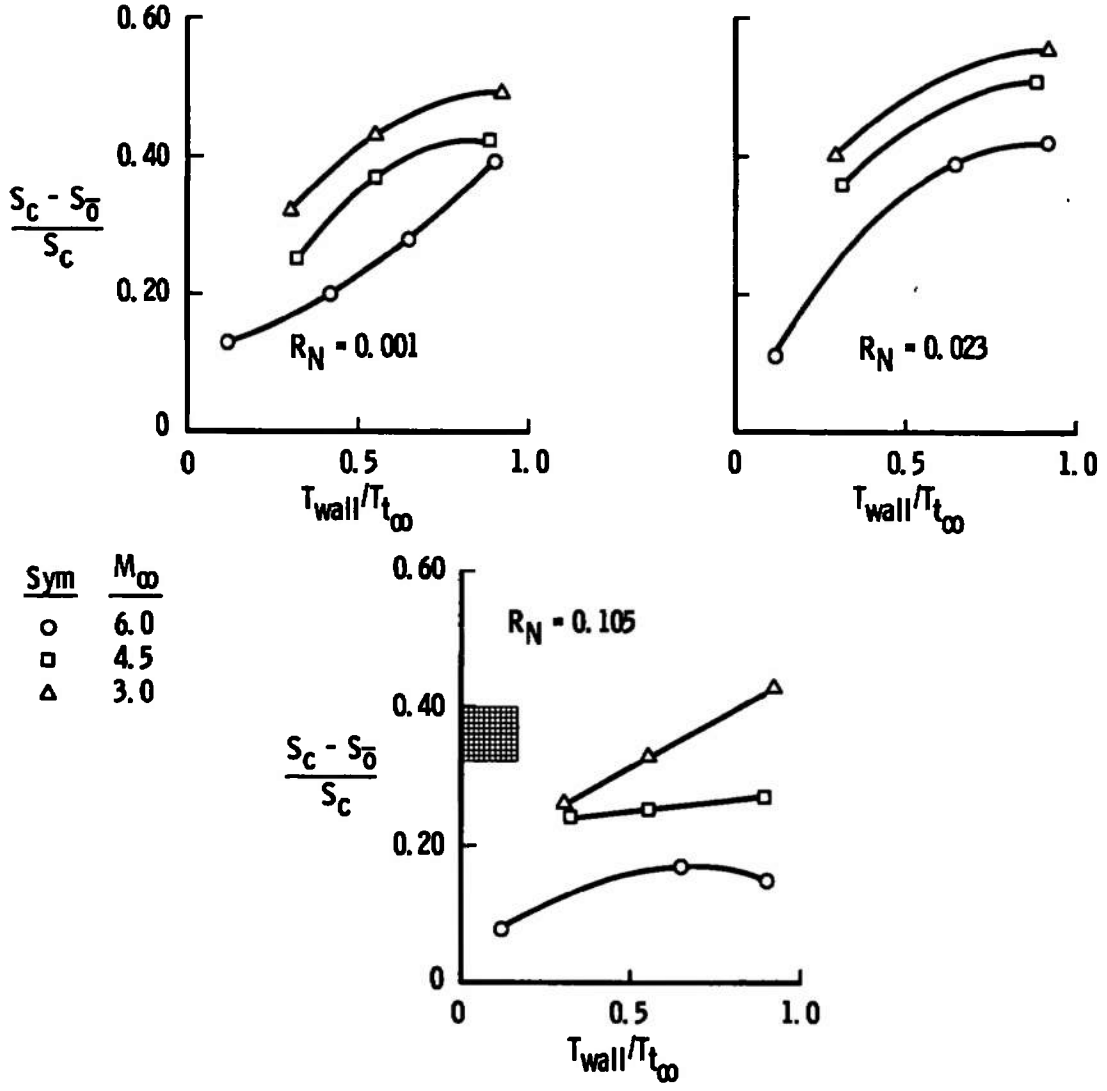

a. $Re_c = 0.25 \times 10^6$

Fig. 13 Effects of Wall Temperature on the Upstream Interaction Extent

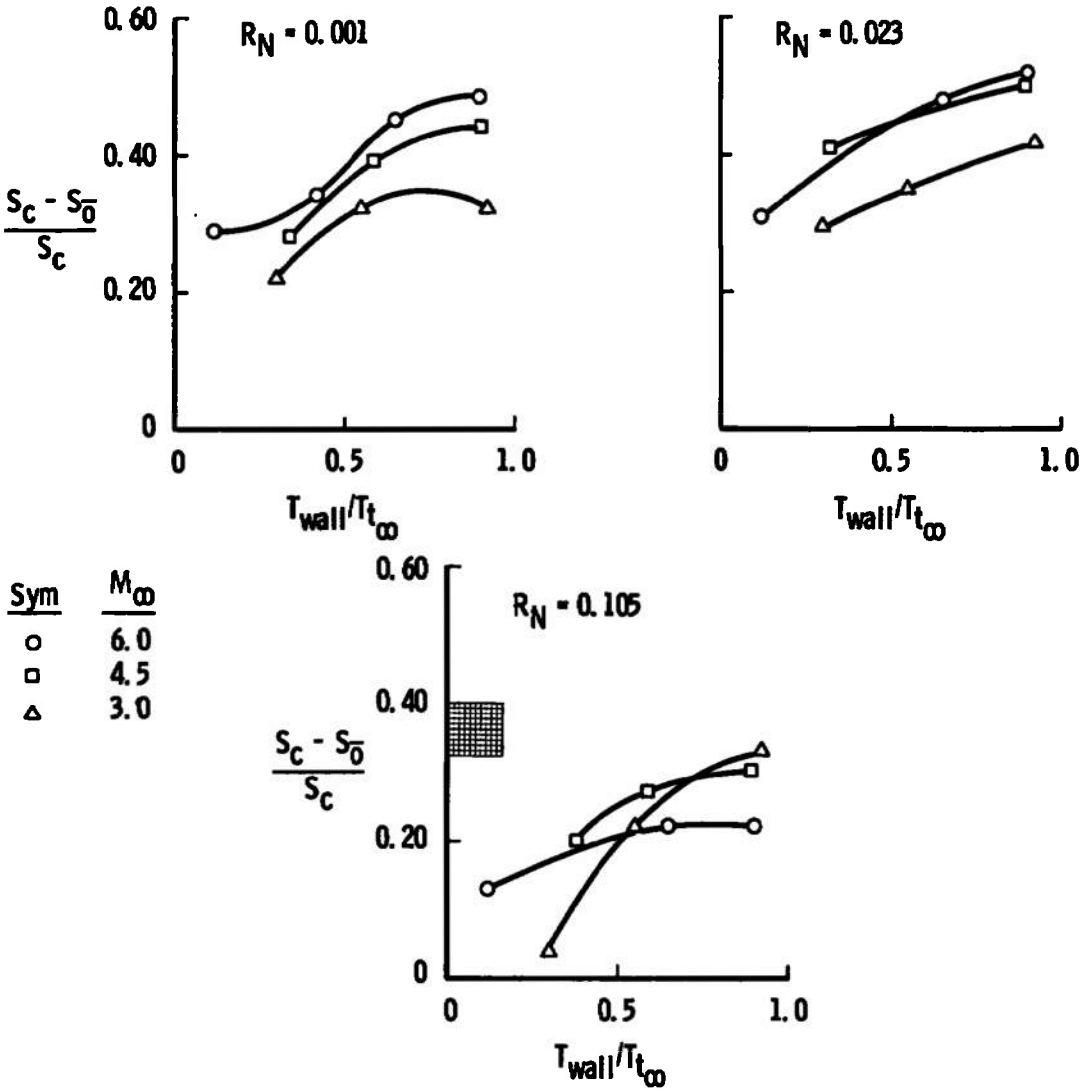

b. $Re_c = 1.0 \times 10^6$

Fig. 13 Concluded

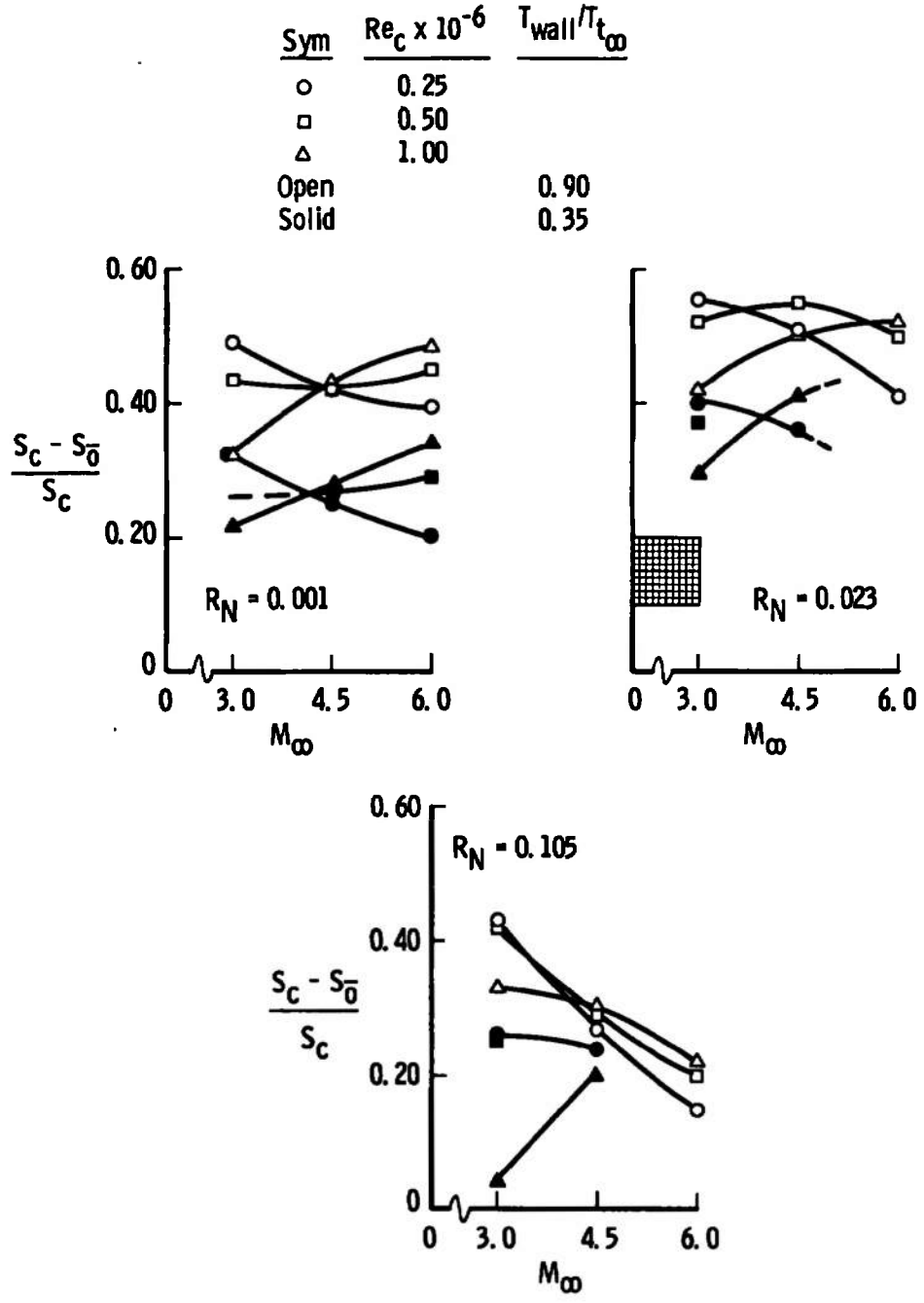

Fig. 14 Effects of Mach Number on the Upstream Interaction Extent for Adiabatic and Cooled Wall Conditions

4.4 HEAT-TRANSFER-RATE DISTRIBUTIONS

Longitudinal heat-transfer-rate data in Stanton number form are presented in Fig. 15 to show the influence of nose radius at the three test Mach numbers, two wall temperatures, and the maximum and minimum test Reynolds numbers. Since several of the gages failed during the different phases of the investigation, it is impossible to present data at the same values of S/S_c for all the test conditions. These gage failures, in general, occurred near the model hinge line on the flat plate, thus making it difficult to establish the flat-plate separation heating trend.

Data are presented in Fig. 15a to show that an increase in leading-edge radius had very little effect on the level of the heat-transfer coefficient, St, on the flat plate ahead of the ramp-induced interaction at moderate wall temperature ($T_{wall}/T_{t_\infty} \approx 0.6$) and Re_c = 0.25 million. This level was relatively independent of free-stream Mach number. The sharp-leading-edge data at M_∞ = 3.0 and 4.5 show a pronounced drop in the heat-transfer-rate just ahead of the hinge line which is characteristic of the separated region (Refs. 3, 11, and 12). The ramp heating rates were, in general, higher on the sharp leading-edge configuration than on the blunt configuration, except just downstream of the hinge line at M_∞ = 3 and 4.5. Although the trends in the ramp heating at M_∞ = 3 and 6 were similar, the M_∞ = 4.5 distributions were quite different.

Data at a lower wall temperature ratio presented in Fig. 15b, also at the low Reynolds number, show very little change in the value of the Stanton number, whereas the character of the ramp distribution was changed and the consistency of the results was significantly improved over that of Fig. 15a, particularly at M_∞ = 6. It is noted these M_∞ = 6 data show the same trends on the ramp as Holden's data (Ref. 11) at comparable ramp angles.

Data for a plate Reynolds number of 1.0 million with moderate wall cooling are shown in Fig. 16a and, as expected, show an appreciable decrease in the value of the Stanton number on the flat plate relative to Fig. 15a. At M_∞ = 3 and $\overline{Re}_c$ = 1.0 million, the three leading edges produced fairly uniform heating over the entire ramp, whereas at M_∞ = 4.5 and 6.0 the results from the various bluntnesses were much different.

Reducing the wall temperature again produced important changes at M_∞ = 4.5 and improved the data consistency in general (Fig. 16b). The major effect of a reduction in wall temperature at M_∞ = 6 was, as before at low Reynolds number, an overall increase in the level of the heat-transfer distributions for all nose radii.

In contrast to the usual situation with attached flows, it is difficult to deduce from these data any information regarding transition onset. Although the results of Holden (Ref. 11) and Needham (Ref. 12) indicate that a definite peak exists (near the pressure peak on the ramp) for laminar flow reattachment at high Mach number, one was not necessarily found in the present tests when the flow was most likely laminar during reattachment (e.g., Figs. 8b and 16b). However, this may be because of the sparsity of the heat-transfer instrumentation on the present model. Thus, it is evident that these heat-transfer data presented versus S/S_c provided no additional information regarding the location of transition. Nevertheless, this presentation does show that the peak heat transfer can be situated much farther than one flat-plate length downstream of the hinge line. Hence, laminar reattachment heat-transfer data with short flaps ($<S_c$) could be dominated by flap length effects on reattachment.

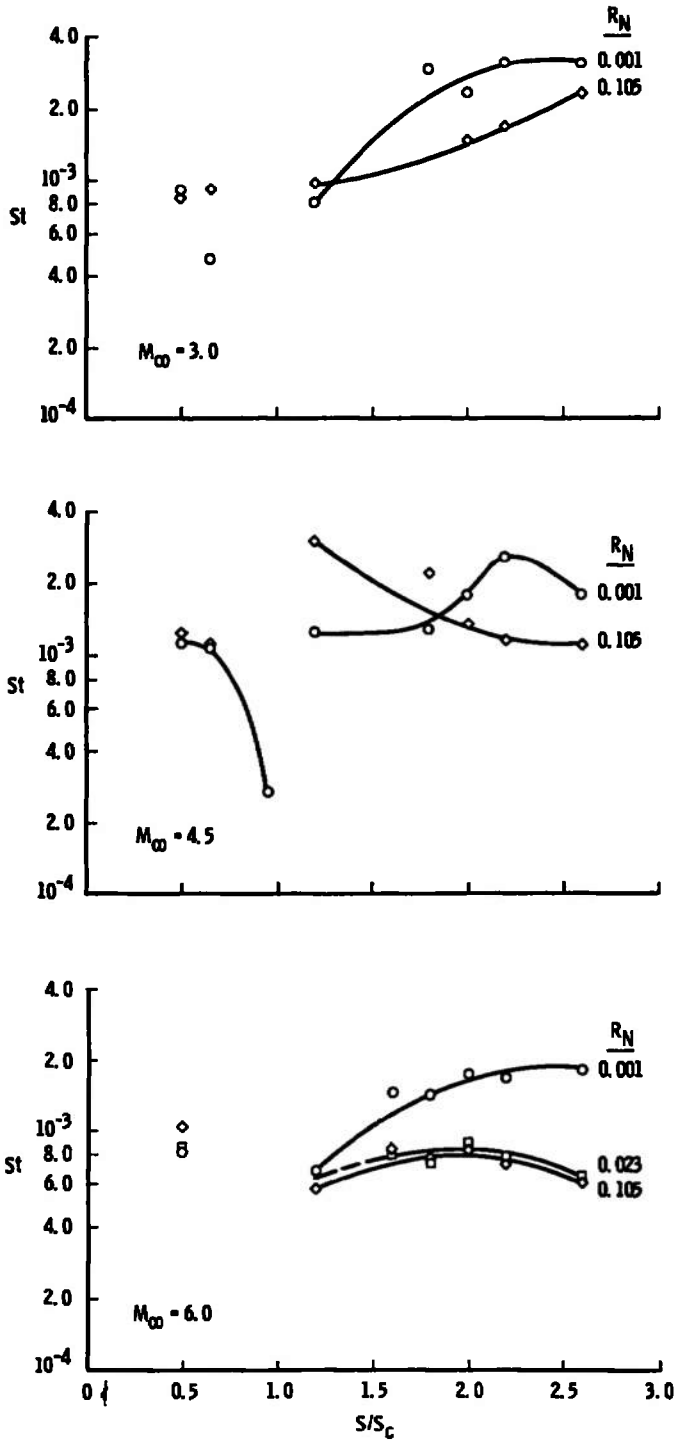

a. $T_{wall}/T_{t_\infty} \approx 0.6$

Fig. 15 Effects of Nose Radius on Stanton Number Distribution at $Re_c = 0.25 \times 10^6$

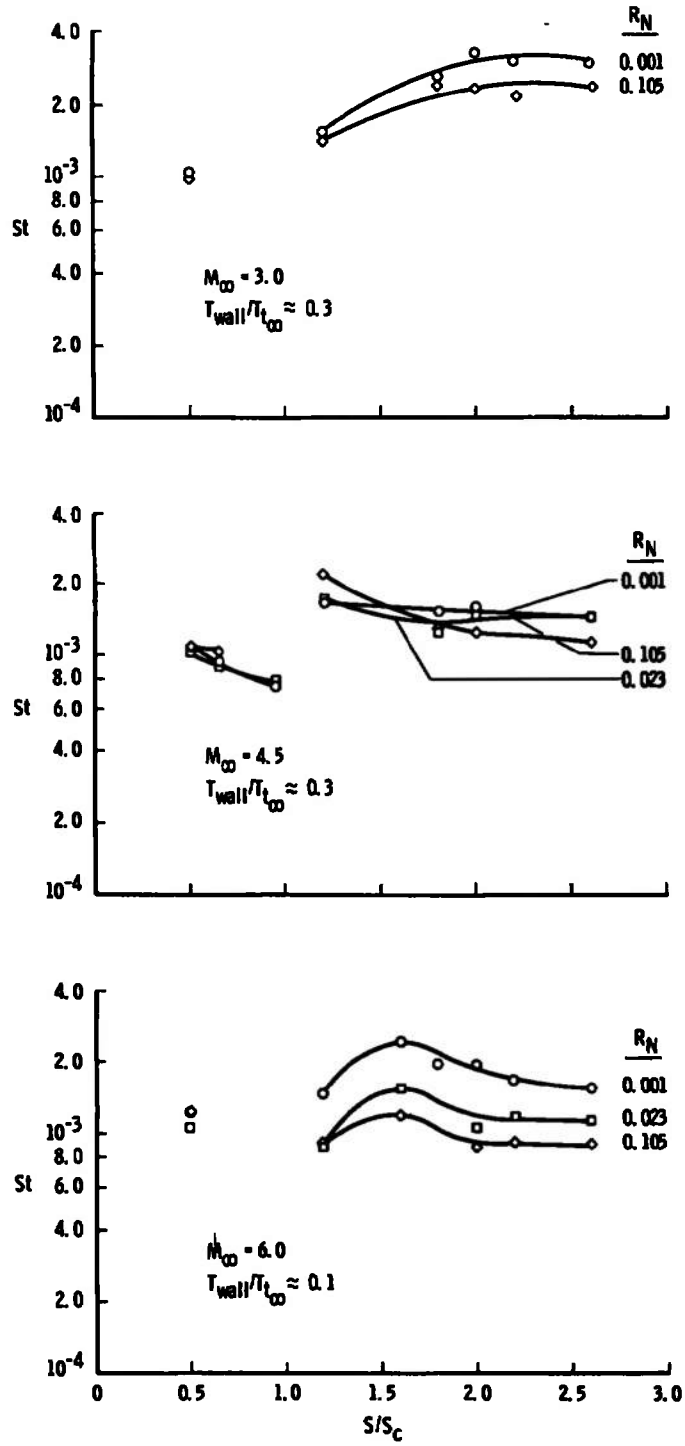

b. Cold Wall

Fig. 15 Concluded

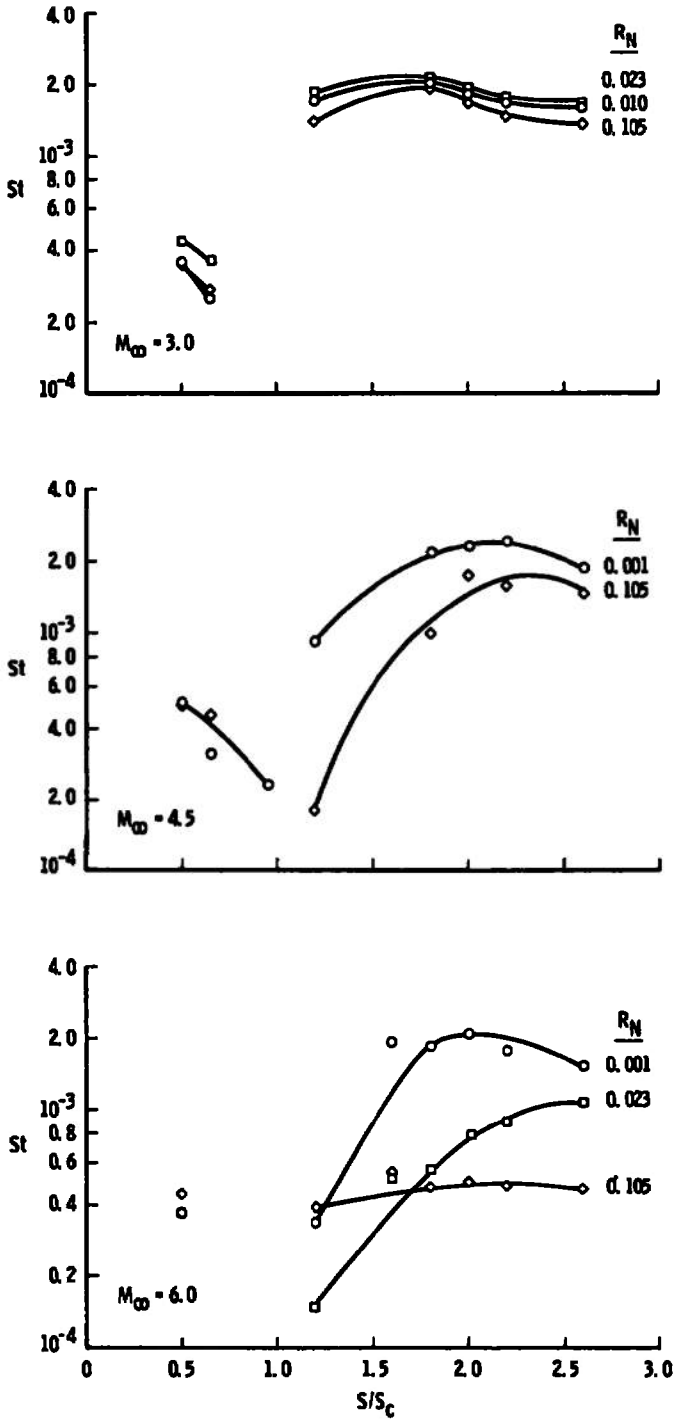

a. $T_{wall}/T_{t_\infty} \approx 0.6$

Fig. 16 Effects of Nose Radius on Stanton Number Distribution at $Re_c = 1.00 \times 10^6$

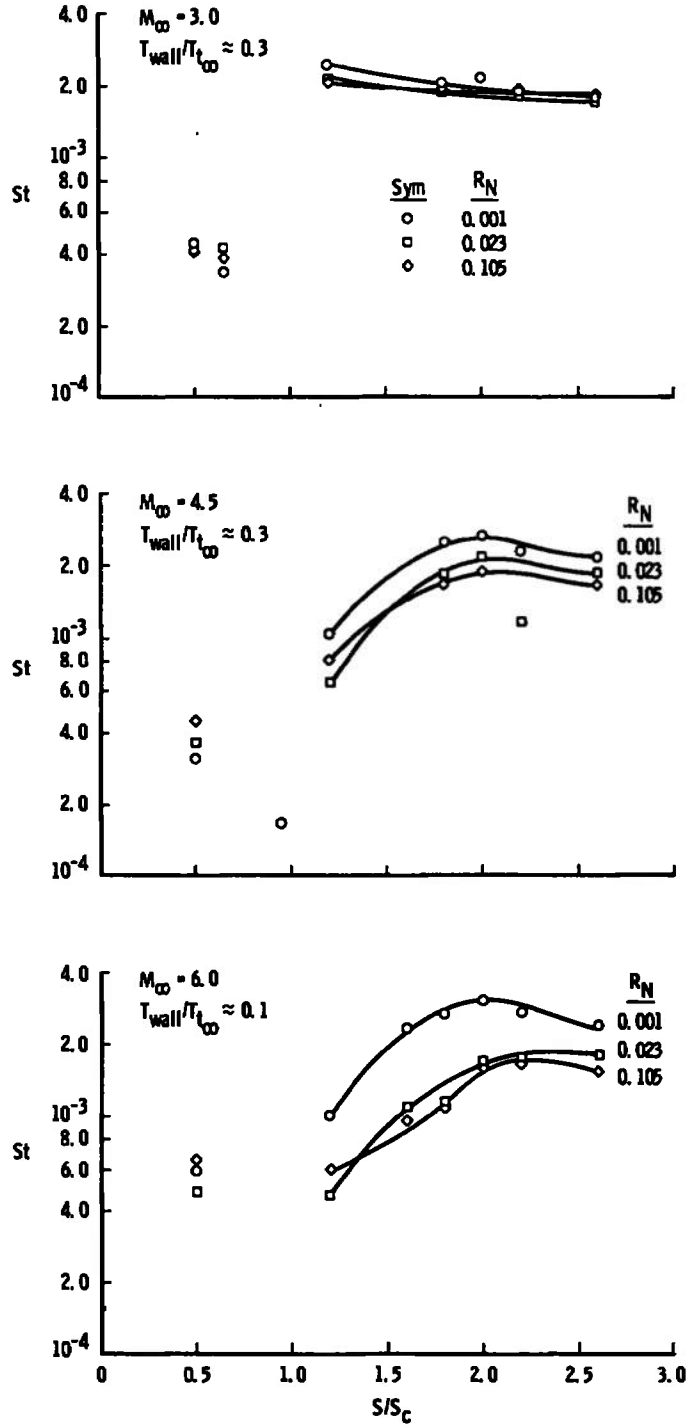

b. Cold Wall

Fig. 16 Concluded

4.5 BOUNDARY-LAYER AND FLOW-FIELD SURVEYS

Typical pitot and disk probe data are presented in Fig. 17 to show the effects of leading-edge radius on the flat plate (S/S_c = 0.5) boundary layer and external flow at M_∞ = 4.5 with an adiabatic wall. As was shown in Fig. 11a, this survey station was sufficiently far upstream of the start of the interaction, except for R_N = 0.023. The measured pitot pressure profiles shown in Fig. 17 outside of the boundary layer, at both Reynolds number for R_N = 0.023 and 0.105, agree well with the inviscid theory. The pronounced peak in the p'_t/p'_{t_∞} and M data at y ≈ 0.05 was probably a result of the pitot probe interference (Ref. 20). It is interesting to note that no peak was obtained for R_N = 0.023. The less pronounced, and yet measurable, offset in the above parameters at y ≈ 0.2 for R_N = 0.001 is evidence of the mismatch in the leading-edge joint, as described earlier. Note the gradual blending of the boundary layer into the external inviscid flow field for R_N = 0.023. As expected, neither the measured (p_d/p_∞) or the corrected (p/p_∞) disk pressure data agree with the inviscid levels, but the trend for the bluntest leading edge is very near to that predicted; however, the poor qualitative agreement for R_N = 0.023 was unexpected. Inasmuch as the measured disk pressure was corrected by use of the model surface pressure, as outlined in Appendix II, all of the corrected values must be higher than inviscid predictions because of the viscous interaction (Fig. 10) on the surface pressures. Note that the model surface pressures are indicated by a solid symbol at y = 0. These discrepancies in the static pressure combined with the minor disagreement between the measured pitot pressure and theory account for the differences in the Rayleigh Mach number calculated and the inviscid values shown. These flow-field data illustrate the large reduction in local Mach number caused by the nose radius increase which must be accounted for in any theoretical calculation of such ramp-induced interactions. The indicated free-stream Mach number for y > 0.45 and R_N = 0.001 was well below the correct value at this height because the inferred (corrected) static pressure was too high, probably as a result of an interaction between the model bow wave and the disk probe boundary layer.

Pitot and static pressure survey data obtained at M_∞ = 4.5 on the ramp at S/S_c = 1.8 (probably downstream of reattachment) with an adiabatic wall are shown in Fig. 18. The pitot pressure data, at both Reynolds numbers, generally have the same trend as the inviscid predictions, with the data at Re_c = 1.0 million (Fig. 18b) agreeing quite well. The "overshoot" in the pitot pressure at y ≈ 0.05 obtained with the sharp leading edge was probably caused primarily by the reattachment compression process, although it could also be probe interference. The disk probe data, along with a typical example of the inferred static pressure, exhibit the same general trends at both Reynolds numbers, except nearest the wall at the low value of Re_c. The large normal pressure gradient shown (Fig. 18a) is consistent with effects from a compression-wave fan. The Rayleigh Mach number profiles calculated from these data are presented in Fig. 18c. As on the plate, definition of the boundary-layer edge is noted to be vague when R_N = 0.023. The lower than predicted pitot pressures and higher than predicted static pressures at Re_c = 0.25 million resulted in the lower than predicted Mach number, whereas the profiles at Re_c = 1.0 million agree much better because the pressures were much closer to the inviscid values. The discontinuities shown in these profiles are a result of the reattachment and separation shock wave systems and the distortions caused by the disk probe data. A

characteristic deficiency of the disk probe is clearly shown in these results by the very broad region on both sides of the shock wave location over which the static pressure decreased with height. This was a result of the finite disk size and the shock wave interaction with the disk boundary layer.

A comparison of the ramp boundary-layer Mach number profiles at all free-stream Mach numbers investigated (at minimum and maximum Re_c) is shown for the adiabatic wall case in Figs. 19a and b. For the cold wall case, a complete set of data for all bluntnesses was obtained only at $M_\infty = 4.5$, and these data are compared with the adiabatic data (at $S/S_c = 1.8$) in Fig. 19c. These data, in Fig. 19, although they do indicate by the changes in the shape of the profile that either lowering the free-stream Mach number or increasing Re_c induced transition onset, they also illustrate that moderate bluntness produced effects on the profiles that are rather similar to the increase in boundary-layer thickness resulting from transition onset. Note the peculiar peaks shown at $y \approx 0.05$ at $M_\infty = 4.5$ for $R_N = 0.001$ at $Re_c = 1.0$ million in Figs. 19b and c. Because this result was not obtained with the blunter leading edges, it is believed that this was not caused by probe interference alone.

More complete flow-field data in terms of Mach number and static pressure ratio are presented for $M_\infty = 4.5$ at four longitudinal stations (adiabatic wall) in Figs. 20a and b and two stations (cold wall) in Figs. 20c and d for low and high Reynolds numbers, respectively.

The effects of free-stream Mach number on the ramp boundary-layer Mach number profiles for the sharp and blunt leading edges are shown in absolute as well as in relative coordinates in Fig. 21. It is particularly evident in the relative coordinate presentation (Fig. 21b) that transition was about to begin at $S/S_c = 1.8$ for $M_\infty = 3.0$ and 4.5 at even the lowest Reynolds number with $R_N = 0.001$; with the bluntest leading edge it was clearly indicated at the lowest Reynolds number only at $M_\infty = 3$. These results for $R_N = 0.001$ are consistent with the estimated locations of transition onset given in Fig. 6a, and they indicate that nose blunting may delay transition onset for reattaching flows at Mach numbers higher than 3. Because of the ambiguous definitions of the edge when $R_N = 0.023$, similar profiles could not be presented for this leading edge. It is evident in such cases as this that total-temperature surveys should also be made to define the edge location.

A comparison of the longitudinal variation of boundary-layer thickness on a flat plate (Ref. 21) with that measured on the ramp at $M_\infty = 4.5$ and 6 is made in Fig. 22a for $Re_c = 0.25$ million. The $M_\infty = 6$ results indicate thinning of the boundary layer relative to the flat-plate estimate when the profile was laminar (Fig. 22b); at $M_\infty = 4.5$, when the profile was indicated to be transitional at $S/S_c = 1.8$, there was negligible thinning. Evidence at $M_\infty = 4.5$ of the change in boundary-layer growth characteristic of transition onset with increased Reynolds number is shown by the data in Fig. 22b.

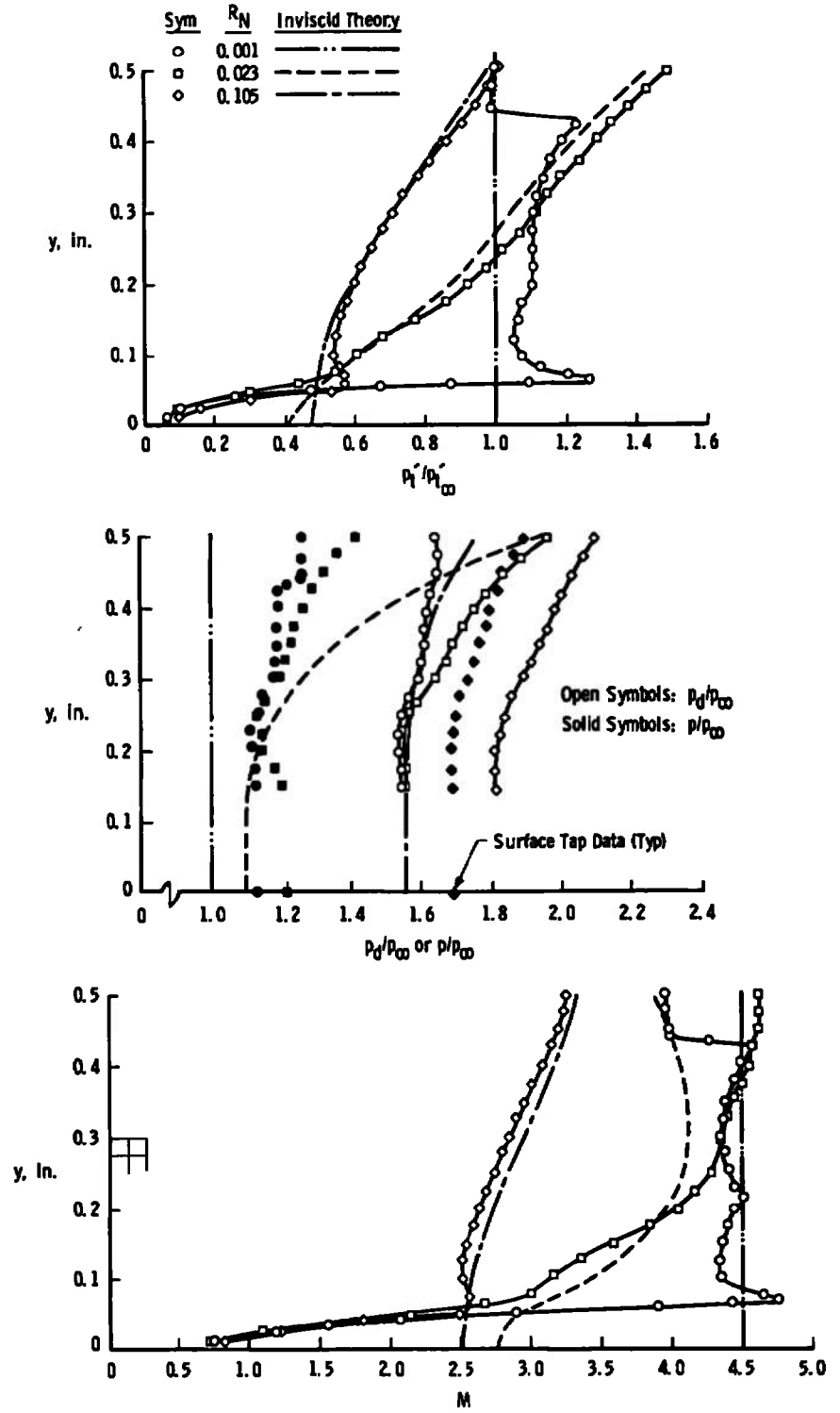

a. $Re_c = 0.25 \times 10^6$

Fig. 17 Effects of Nose Radius on Flat-Plate Flow Field at $M_\infty = 4.5$, Adiabatic Wall, and $S/S_c = 0.5$

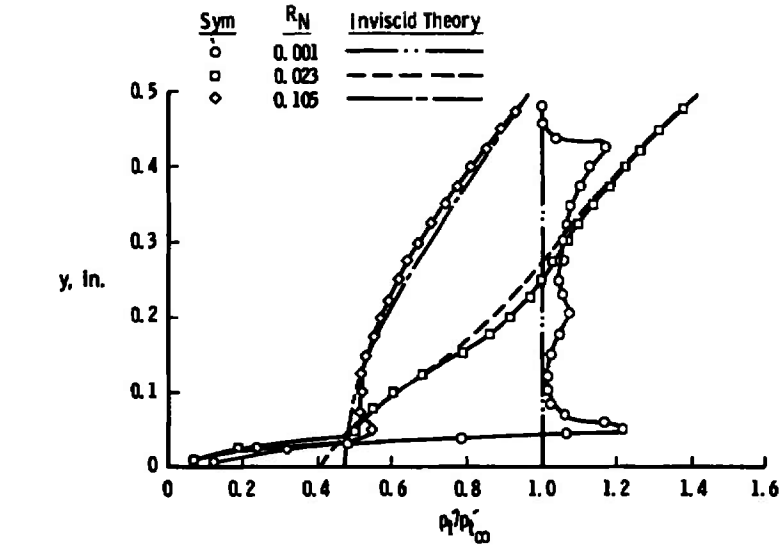

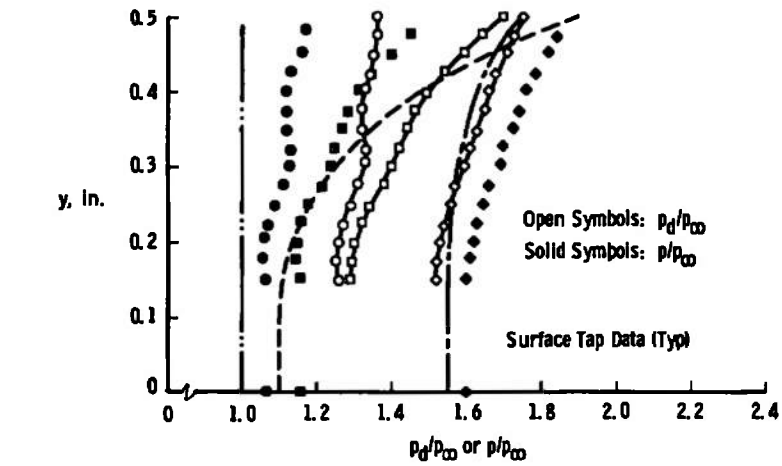

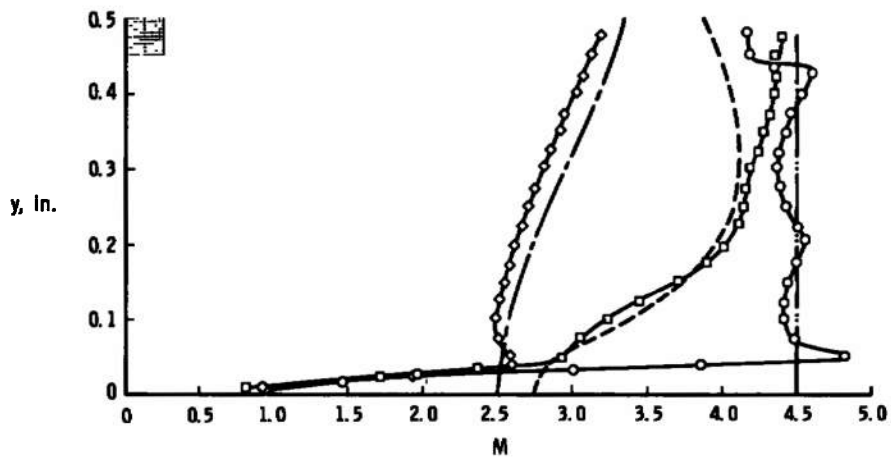

b. $Re_c = 1.00 \times 10^6$

Fig. 17 Concluded

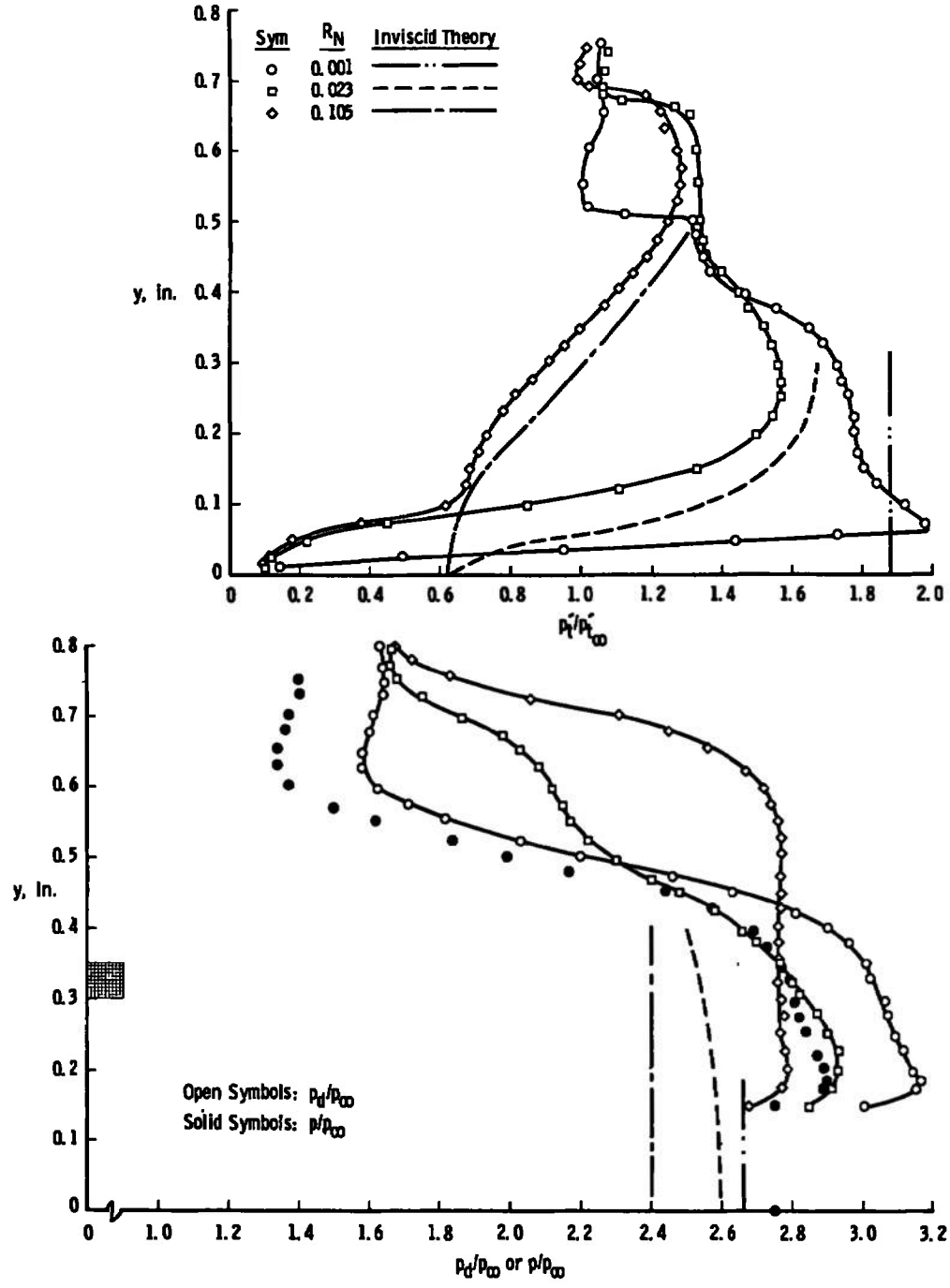

a. Pressure Profiles at $Re_c = 0.25 \times 10^6$

Fig. 18 Effects of Nose Radius on Ramp Flow Field at $M_\infty = 4.5$, Adiabatic Wall, and $S/S_c = 1.8$

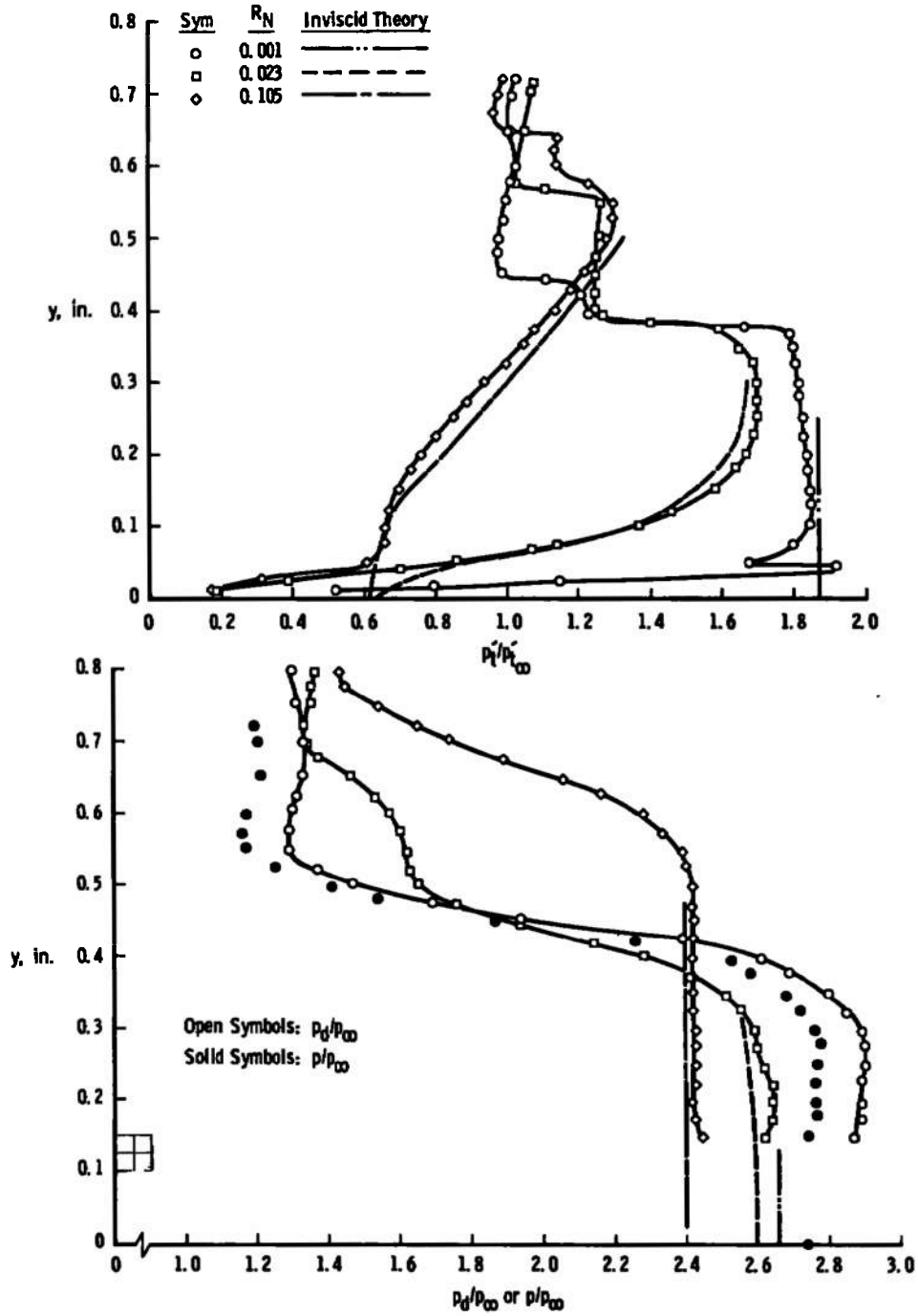

b. Pressure Profiles at $Re_c = 1.00 \times 10^6$
Fig. 18 Continued

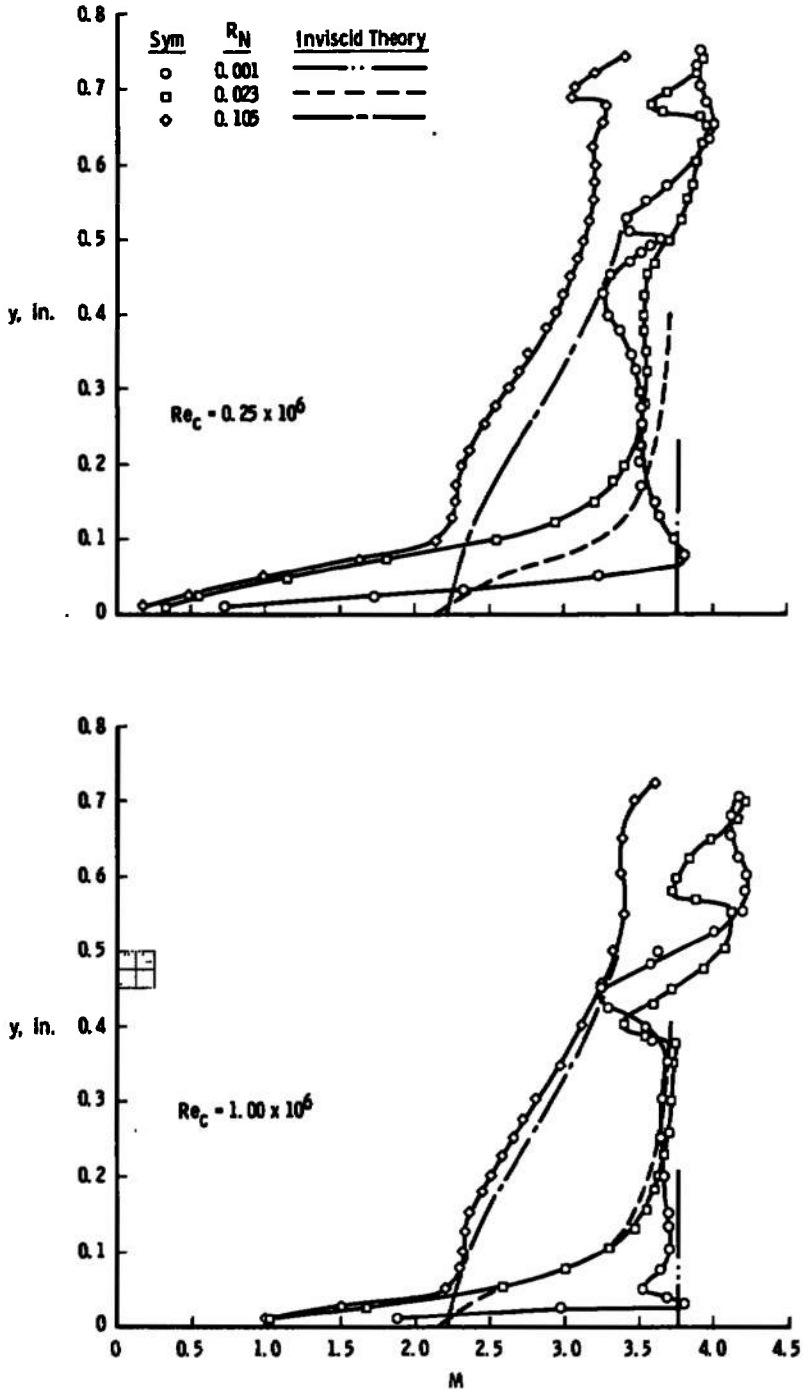

c. Mach Number Profiles
Fig. 18 Concluded

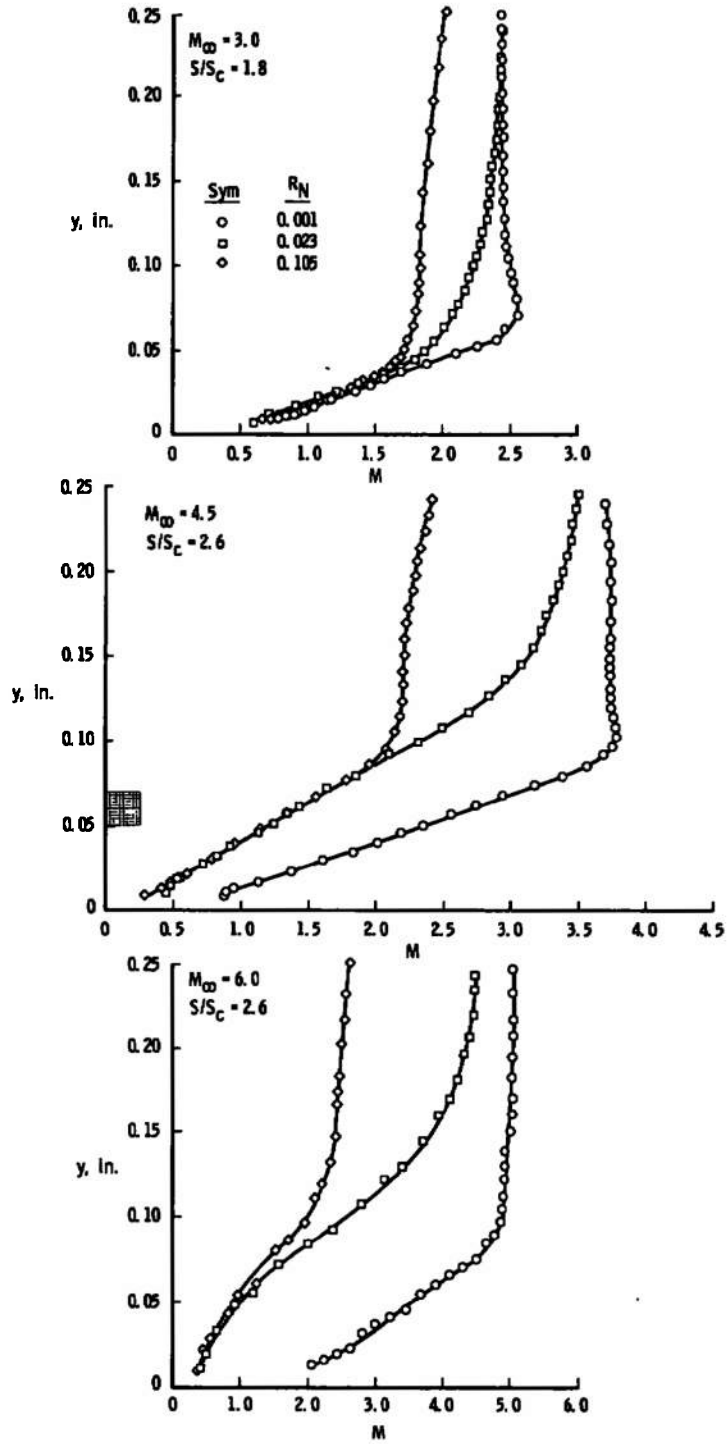

a. $Re_c = 0.25 \times 10^6$

Fig. 19 Effects of Nose Radius on the Ramp Boundary-Layer Profiles, Adiabatic Wall, and $1.8 \leqslant S/S_c \leqslant 2.6$

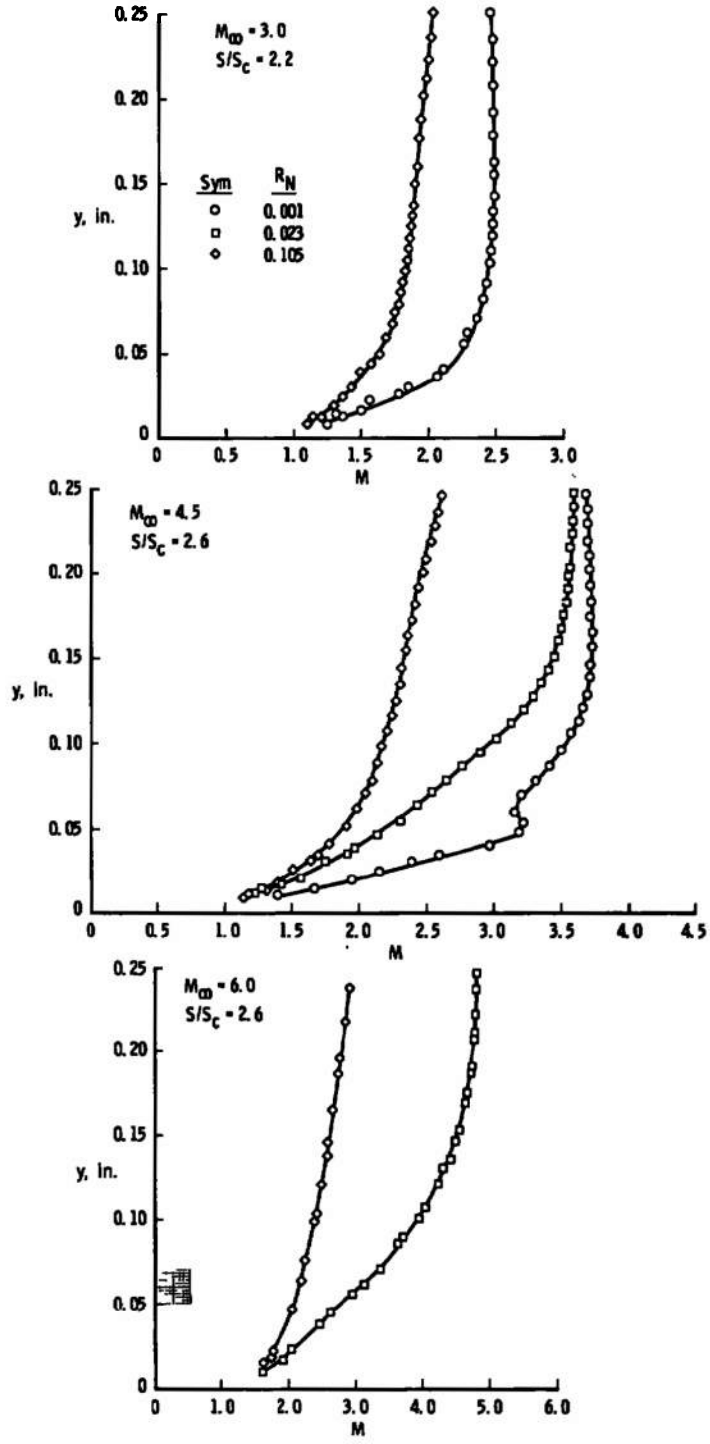

b. $Re_c = 1.00 \times 10^6$
Fig. 19 Continued

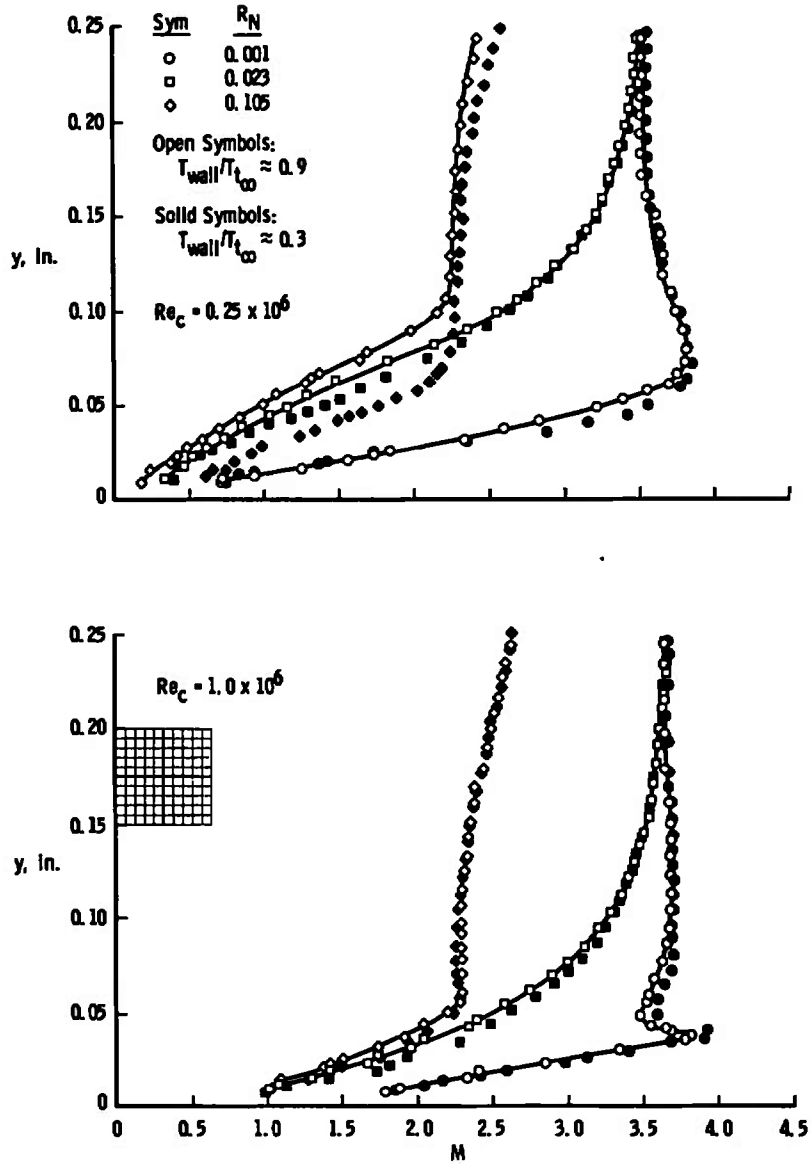

c. $M_\infty = 4.5$, $S/S_c = 1.8$

Fig. 19 Concluded

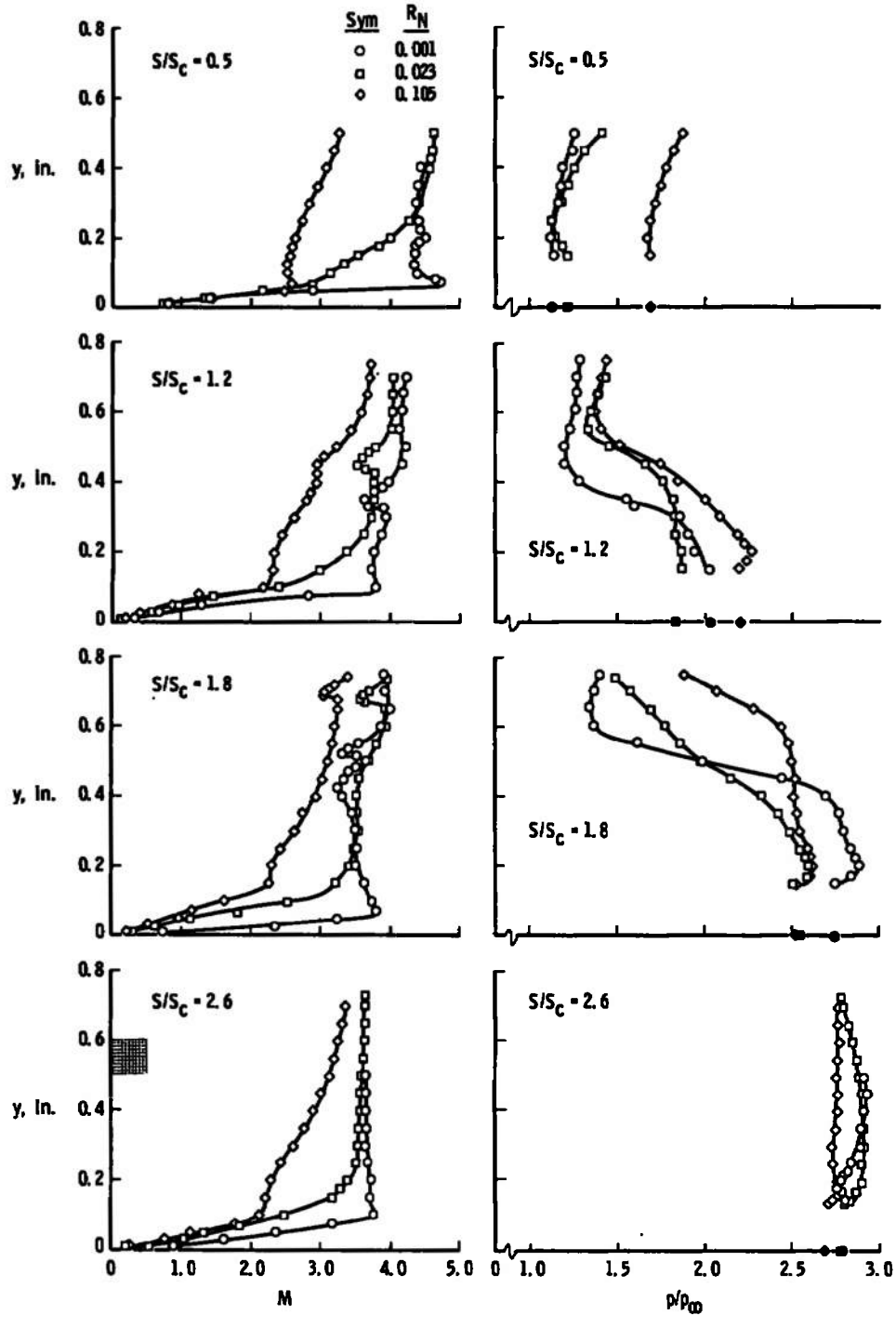

a. $Re_c = 0.25 \times 10^6$, $T_{wall}/T_{t_\infty} \approx 0.9$

Fig. 20 Effects of Nose Radius on Flow-Field Surveys at Different Longitudinal Stations for $M_\infty = 4.5$

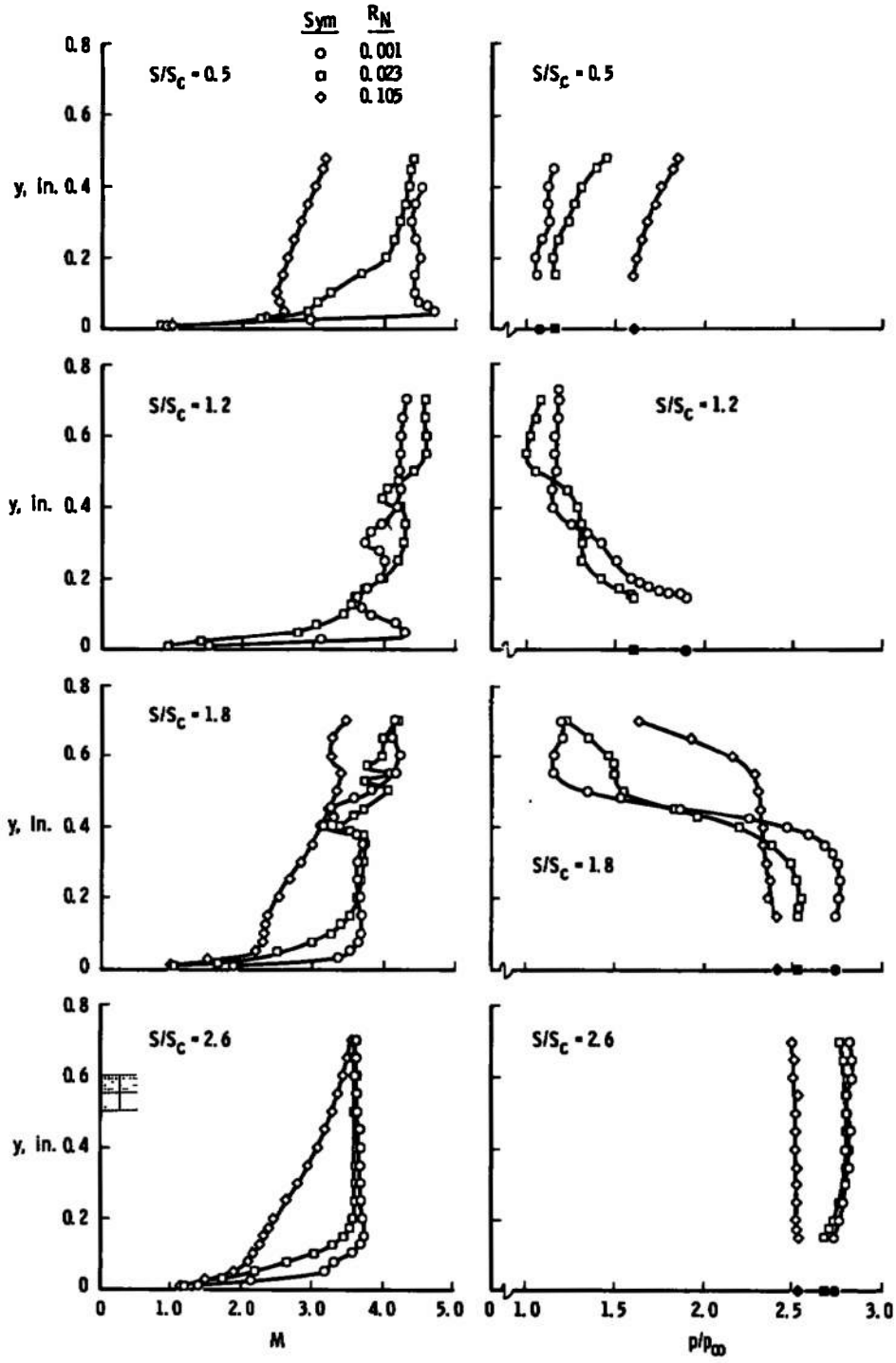

b. $Re_c = 1.00 \times 10^6$, $T_{wall}/T_{t_\infty} \approx 0.9$
Fig. 20 Continued

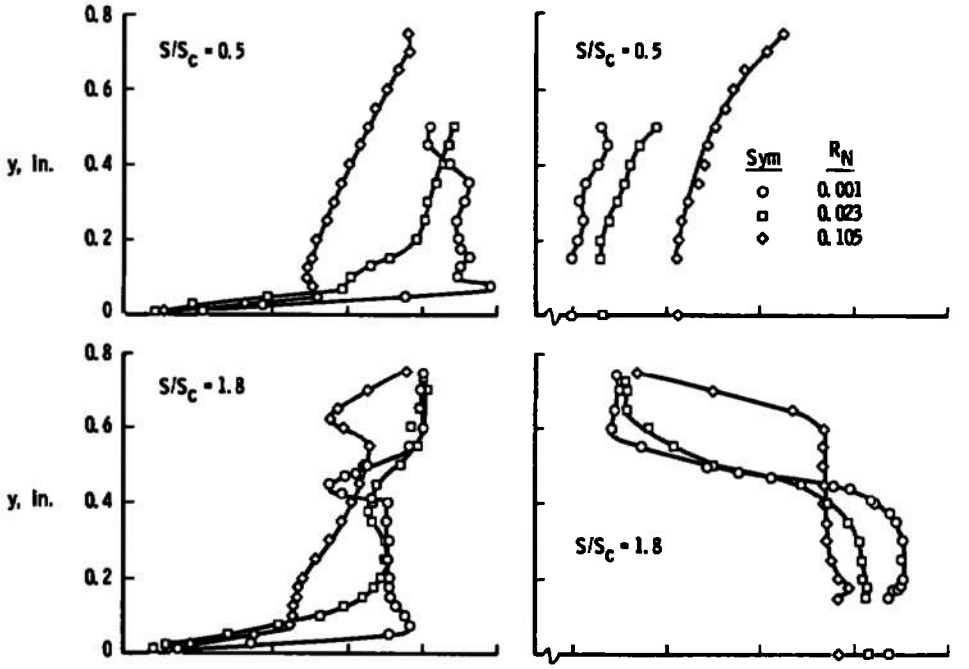

c. $Re_c = 0.25 \times 10^6$, $T_{wall}/T_{t_\infty} \approx 0.3$

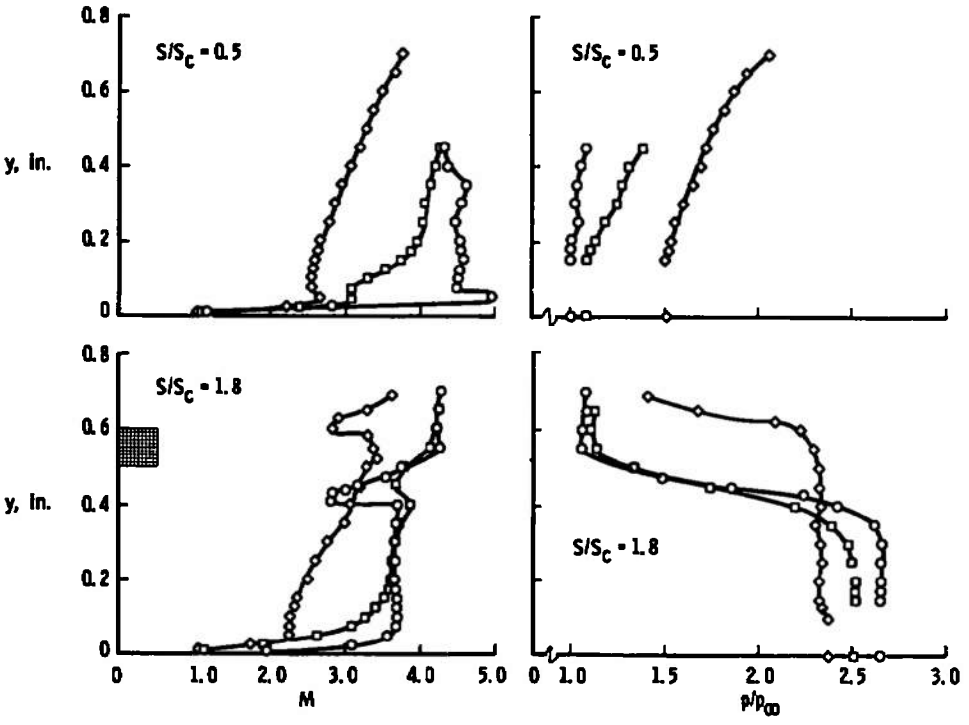

d. $Re_c = 1.0 \times 10^6$, $T_{wall}/T_{t_\infty} \approx 0.3$

Fig. 20 Concluded

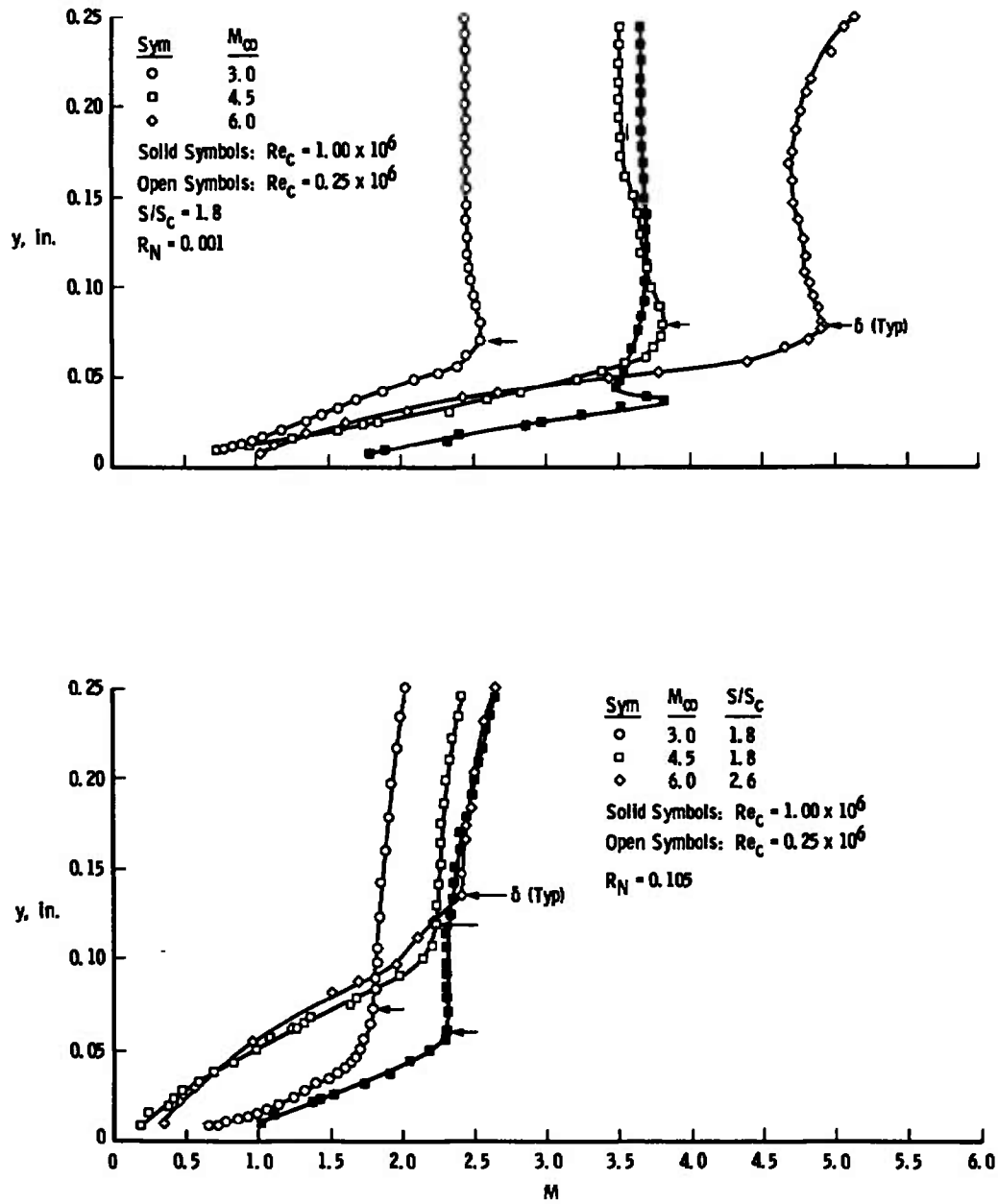

a. M versus y

Fig. 21 Effects of Mach Number on the Ramp Boundary-Layer Profiles, Adiabatic Wall

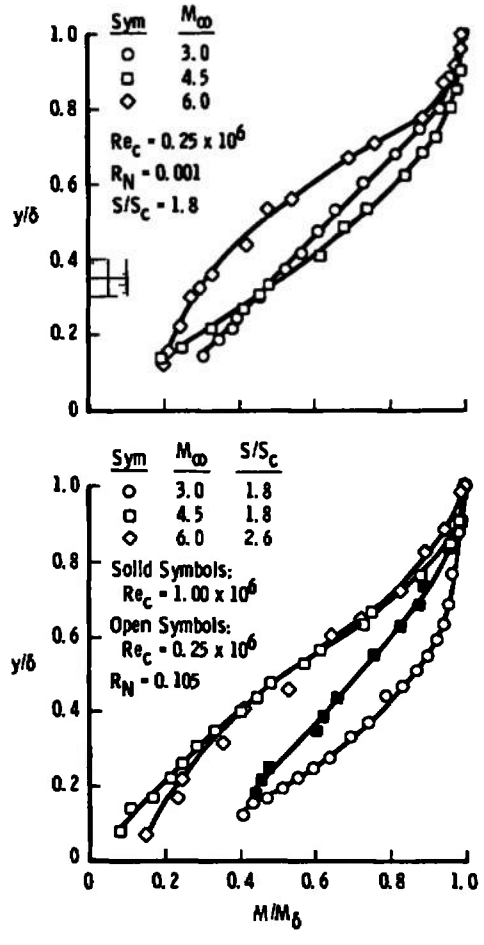

b. M/M_δ versus y/δ

Fig. 21 Concluded

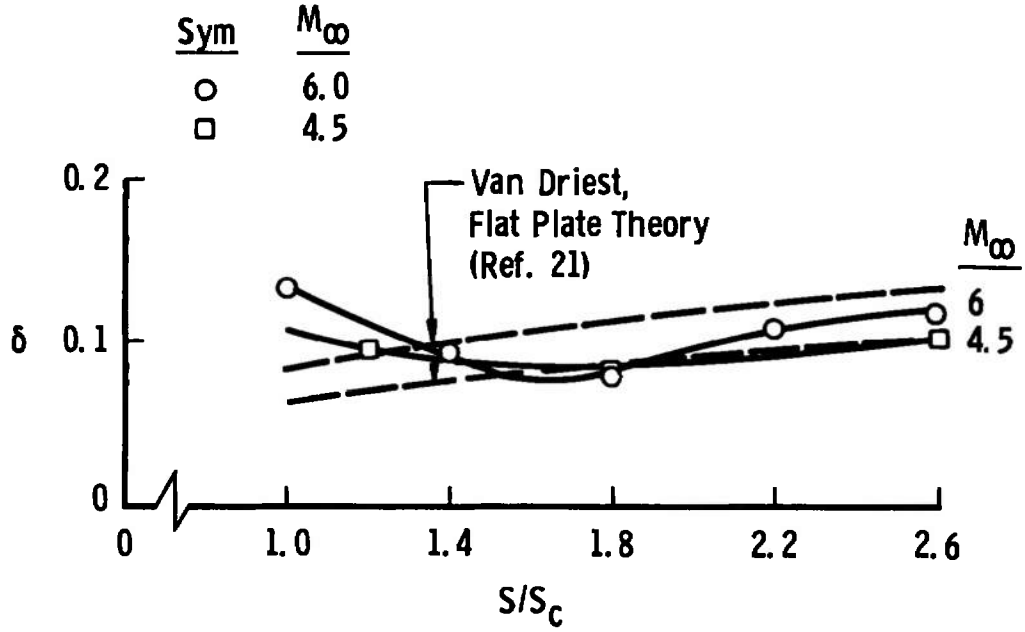

a. $Re_c = 0.25 \times 10^6$

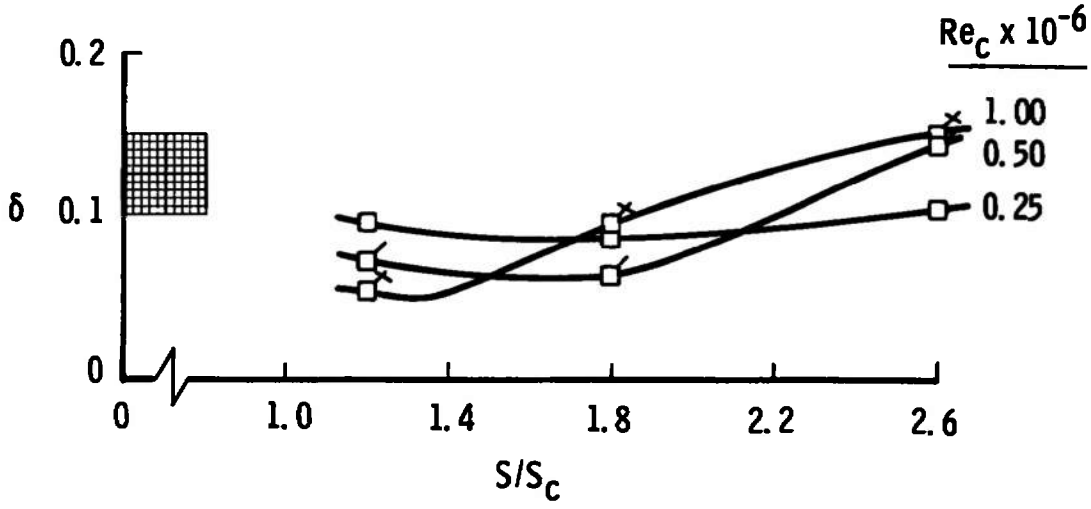

b. $M_\infty = 4.5$

Fig. 22 Effects of Mach Number and Reynolds Number on Ramp Boundary-Layer Thickness for Adiabatic Wall, $R_N = 0.001$

SECTION V
COMPARISON WITH CORRELATIONS AND INTEGRAL-MOMENT THEORY

5.1 INTEGRAL-MOMENT THEORY RESULTS

The integral-moment method (Ref. 22) of Lees, Reeves, and Klineberg (LRK) has been shown (Refs. 7 and 8) to estimate reasonably well the surface pressure distribution for ramp-induced laminar flow interactions at moderate Mach number ($4 \leqslant M_\infty \leqslant 6$) and at Reynolds numbers less than about 10^5 on sharp-leading-edge plates for adiabatic wall conditions. It was also applied in Ref. 22 to the cold wall case ($T_{wall}/T_{t,\infty} = 0.2$) at $M_\infty = 6$, and reasonable agreement with pressure data was again shown. However, application of this theory to nonadiabatic conditions is more difficult than for the adiabatic case since polynomial fits of the integral functions must be available for each wall temperature ratio desired. Furthermore, the iteration routine required to bridge the singularity downstream of reattachment is not as straightforward as for the simple adiabatic iteration. The use of finite-difference methods (Ref. 23) is obviously the best general approach to solutions of this problem. Since neither of these programs is available at this time, the subsequent comparisons of theory with the present experimental results will be restricted to the adiabatic wall case using the LRK integral-moment theory. Moreover, modifications of the integral-moment program made in an attempt to account for the influence of leading-edge blunting are described and the results compared with the present data.

In order to illustrate the influence of free-stream flow conditions on some characteristics of the subject interactions, selected theoretical results are presented for $R_N = 0$. In Fig. 23 the effect of Mach number is shown at constant Reynolds number, Re_c, which is based on the distance to the hinge line, S_c. Since this is the characteristic Reynolds number for the interaction, the parameters of interest here may be plotted versus the distance relative to this characteristic length, i.e., S/S_c. Thus, if the flat-plate length were doubled but the free-stream unit Reynolds number halved to hold Re_c constant, the interaction lengths would also be doubled—assuming that boundary-layer transition onset would still be sufficiently far removed from reattachment. It should be noted also that the pressure has been nondimensionalized by that at the beginning of the interaction but that it increases with Mach number because of the displacement-thickness-induced pressure perturbation. The trends shown have been conclusively confirmed experimentally at $6 \leqslant M_\infty \leqslant 10$ (Ref. 7) although there were discrepancies observed (a) in the magnitude of the upstream interaction extent (at $S/S_c < 1$) and (b) particularly in the maximum pressure gradient on the ramp (at $S/S_c > 1$). Of special interest in this figure is the relatively substantial downstream movement of separation with increasing Mach number whereas reattachment moves upstream much less in relation to the hinge line. Since the distance to transition onset in wind tunnels is known to increase with Mach number increase or unit Reynolds number decrease (Ref. 16), it is evident therefore that laminar flow reattachment should be more easily obtained by an increase in Mach number.

Reynolds number effects, which are illustrated in Fig. 24 at $M_\infty = 6$, are noted to be opposite to Mach number effects. That is, increasing the Reynolds number increases the upstream extent of the interaction, moves separation, s, upstream, and causes the reattachment location, r, to move downstream—toward transition, which is being moved upstream itself by the increase of unit Reynolds number. The characteristic small variation in the maximum pressure gradient on the ramp is useful in this form for detecting the onset of transition during flow reattachment in experimental results.

Three additional characteristics illustrated in these two figures are (1) the significant deviations in the boundary-layer thickness relative to that on a flat plate, (2) the conditions under which a pressure plateau upstream of the hinge line is predicted to exist, and (3) the pressure rise to reattachment. It is of particular significance to the heat-transfer-rate that the boundary-layer thickness at $S/S_c = 2$ is less than 60 percent of the flat-plate value. Assuming this to be true also for slight wall cooling and with similar enthalpy profiles, this thickness reduction would correspond to a significant (i.e., 167 percent) increase in heat-transfer rate. These calculations further indicate that a plateau forms when either decreasing Mach number or increasing Reynolds number sufficiently, both of which are conditions conducive to transitional flow reattachment. Obviously, however, the pressure plateau is not a fundamental characteristic of laminar reattaching flows. It is more characteristic of a laminar separation sufficiently far removed from the mechanism which induced it. Finally, these figures show that the pressure rise between the corner and reattachment location may vary from 50 to about 75 percent of that from the corner to the peak ramp value, being the greatest percentage when the separation is the largest.

The effect of increasing the ramp angle is to increase the upstream interaction size (Ref. 7) at a rate of change which increases with an increase in Reynolds number. At the free-stream conditions of interest here, it is very difficult to achieve laminar flow reattachment with ramp angles larger than about 10 deg (Ref. 18).

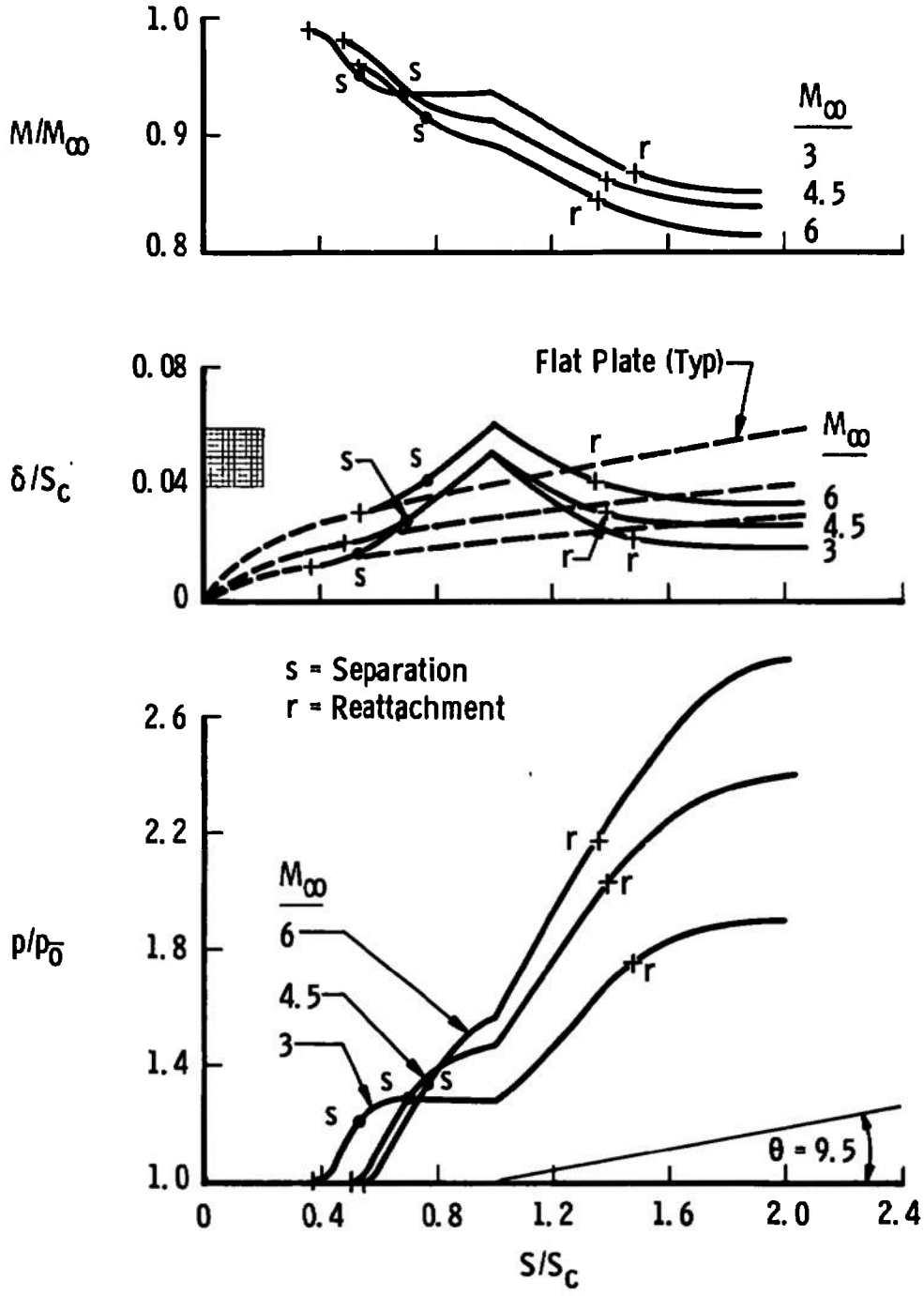

Fig. 23 Effects of Mach Number on Ramp-Induced Laminar Flow Interaction, Integral-Moment Theory for Adiabatic Flow, $Re_c = 0.25 \times 10^6$ and $R_N = 0$

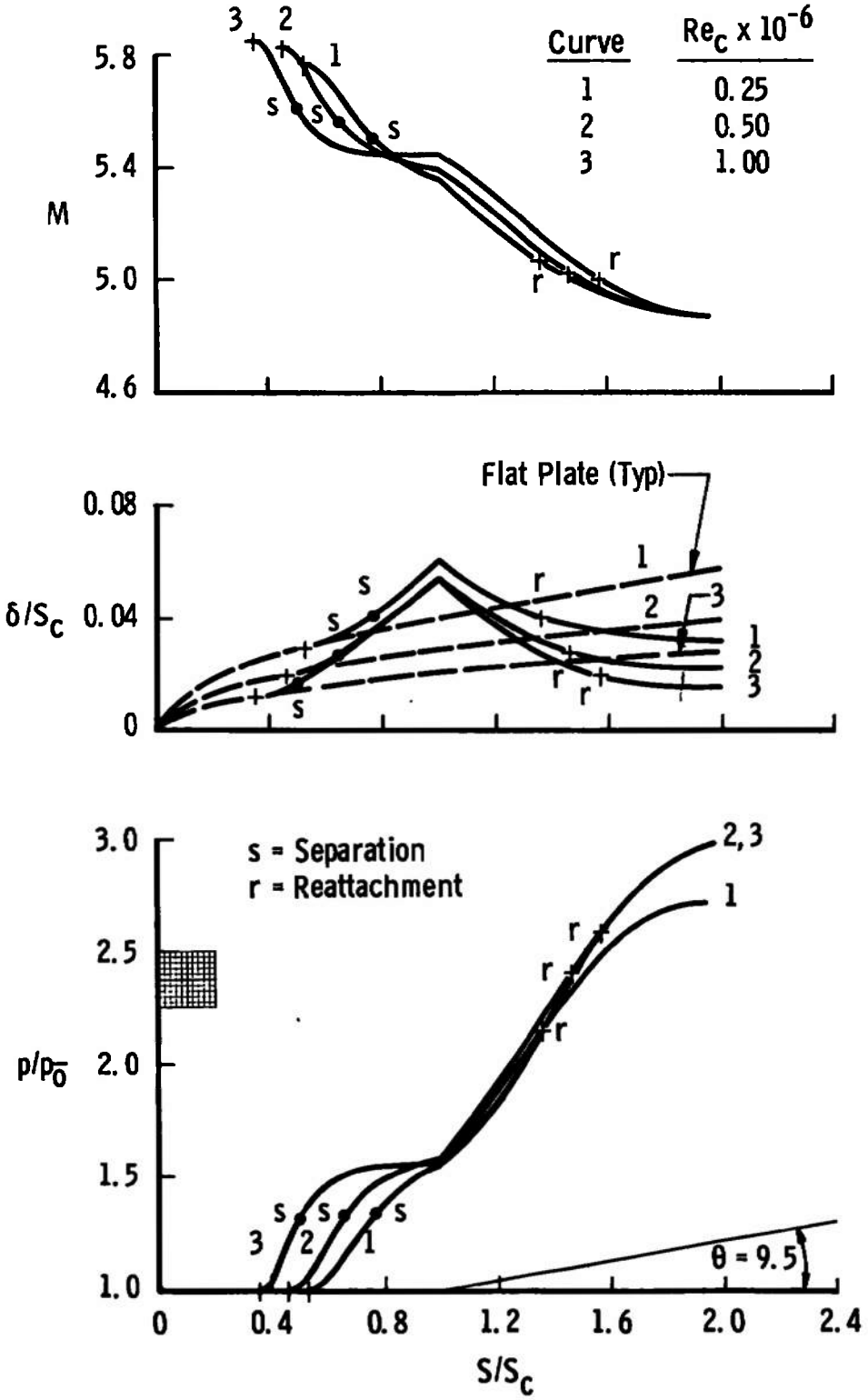

Fig. 24 Effects of Plate Reynolds Number on Ramp-Induced Laminar Flow Interaction, Integral-Moment Theory for Adiabatic Flow, $M_\infty = 6$ and $R_N = 0$

5.2 CORRELATIONS

5.2.1 Needham-Stollery Extent Correlation

Many attempts at correlating separation extent data have been made, but, in a recent evaluation of them, Hill (Ref. 24) was led to conclude that no satisfactory correlation exists, possibly because of the lack of consistency in the published data. One of the correlations he examined, and one which has been utilized often in other papers, is the one proposed by Needham and Stollery (Ref. 25). In order to eliminate the data inconsistency noted in Ref. 24, some results of integral-moment theory calculations have been cast in the correlation form of Ref. 25 and are presented in Fig. 25. It is evident that these coordinates do not correlate the calculations and that the Needham-Stollery correlation curve drastically underestimates the separation extent. This further confirms Hill's conclusion.

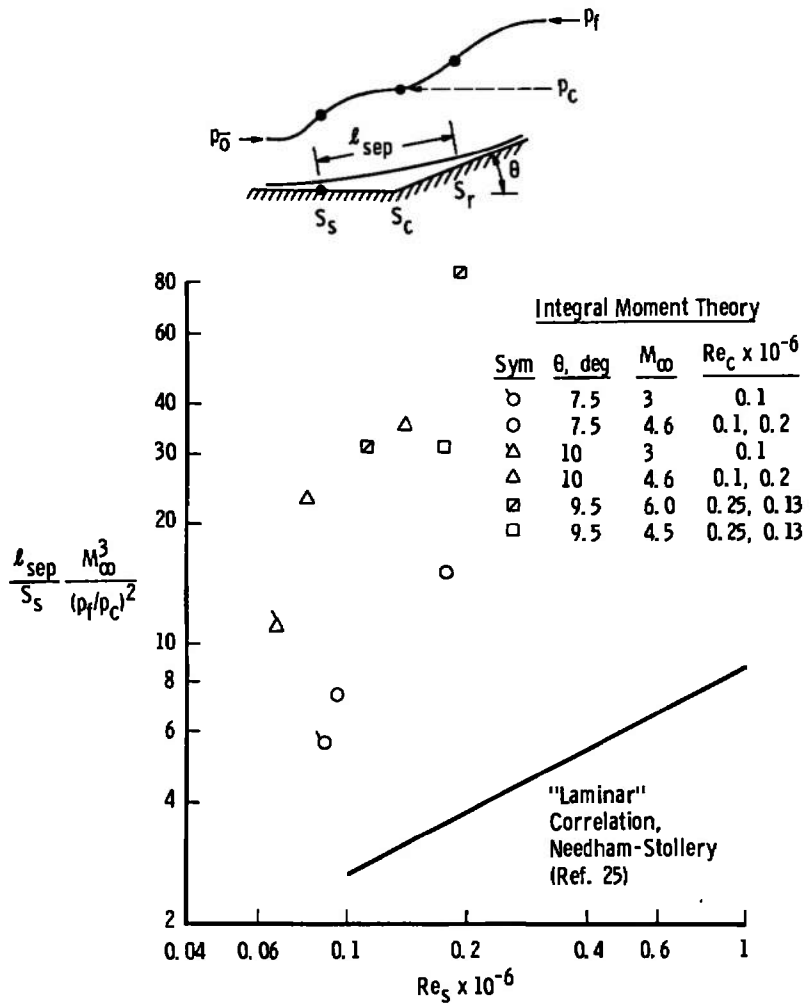

Fig. 25 Integral-Moment Theory Results for Separation Extent Presented in Needham-Stollery Correlation Form, Adiabatic Wall, $R_N = 0$

5.2.2 Sharp-Leading-Edge Plateau Pressure Correlation

The plateau pressure correlation of Ref. 24 is also compared with integral-moment theory results in order to examine the validity of the correlation when applied to totally self-consistent laminar reattaching flows. These results (Fig. 26) are presented in two ways to illustrate a vague definition existing in the literature. It is unclear which pressure (p_∞ or $p_{\bar{0}}$) should be used in the pressure coefficient. This question was first exposed in Ref. 7 by the comparisons of laminar data with a comparable plateau pressure correlation when $p_{\bar{0}}$ was used. It is evident in Fig. 26 that the correct form of the correlation requires the use of inviscid flat-plate pressure, p_∞ (open symbols), rather than the pressure at the start of the interaction, $p_{\bar{0}}$ (solid symbols).

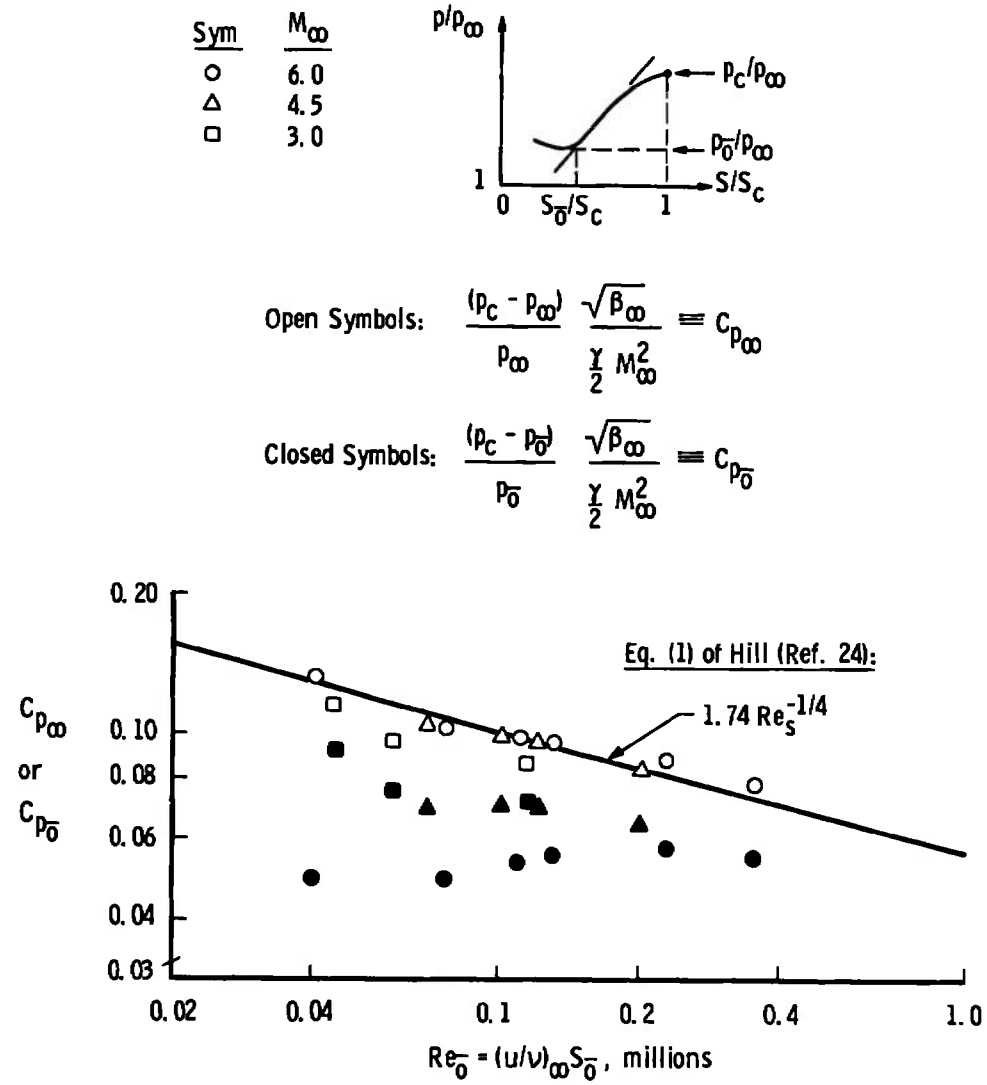

Fig. 26 Integral-Moment Theory Results for "Plateau" Pressure Presented in Chapman Correlation Form, Adiabatic Wall, $R_N = 0$

5.2.3 Blunt-Leading-Edge Plateau Pressure Correlation

Representative peak flat-plate (plateau) pressure data obtained in the present investigation have been put in the appropriate form and are compared to the correlation curve (Ref. 24) in Fig. 27 to show the effect of leading-edge blunting. The inviscid conditions used (subscript wo) were those corresponding to normal shock total pressure at M_∞ and the local inviscid pressure at the beginning of the interaction. These results compare rather well with the correlation curve, although it is suggested that both the exponent and the coefficient of the Reynolds number should be larger to fit these results. Considering the scatter in these results, which is characteristic of this type of data correlation, it hardly seems warranted to use more refined adjustments in the abscissa (e.g., as in Ref. 1).

5.2.4 Chapman-Curle Interaction Correlation

Correlation of the entire pressure distribution upstream of the hinge line has been shown in Refs. 8 and 7, within certain limits, to be feasible using scaling laws derived in Ref. 26. These so-called Chapman-Curle coordinates have been shown in Ref. 8 to account adequately for wall cooling effects, but for the present data which were converted to these coordinates and which are shown in Fig. 28 it would appear that the correlation of the cold wall data (solid symbols) is not so satisfactory. Data obtained with the blunt leading edges, which are also included in this figure, correlate as well as the sharp-leading-edge plate data. The most significant points of interest in this figure are the substantial band covered by the data examined and the large stretching of the abscissa caused by wall cooling. The quality of this correlation, like most correlations, is keenly sensitive to judicious choices of certain reference values. No attempt was made to improve these results since it is felt that the effort is difficult to justify when more consistent methods for predicting the pressure distribution, such as the integral-moment theory, are available.

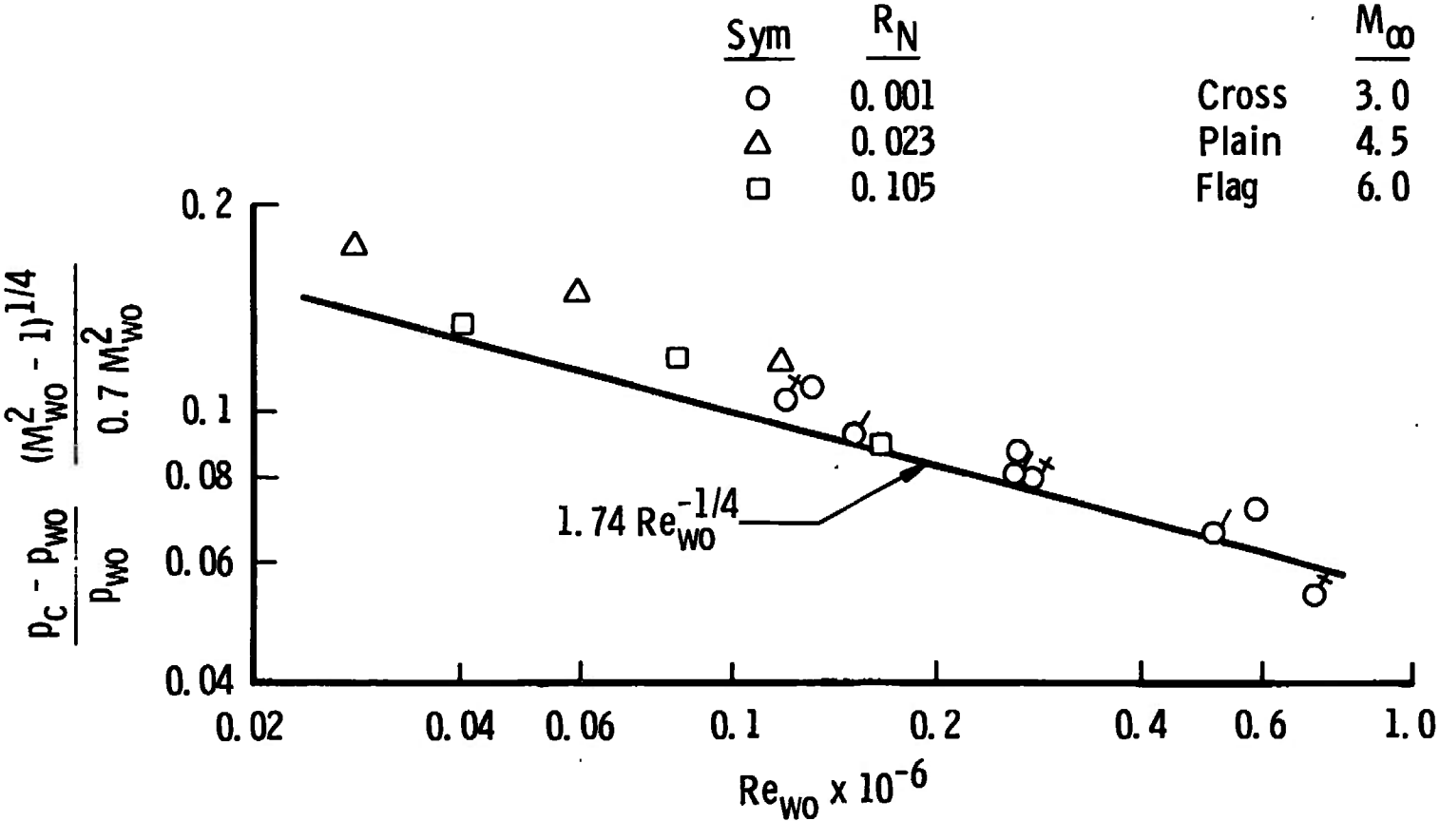

Fig. 27 Typical Peak Pressure Data Correlation for Blunt and Sharp Leading Edges, Adiabatic Wall

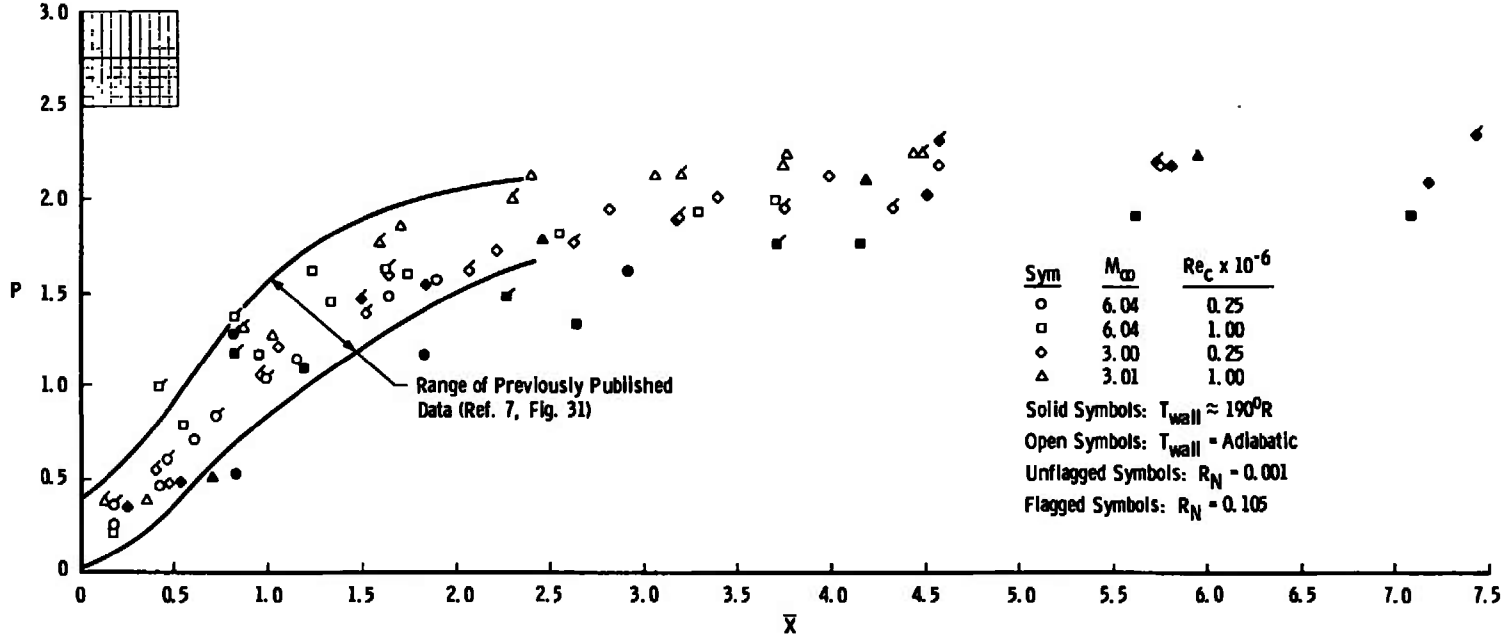

Fig. 28 Typical Correlation of Selected Present Results in Chapman-Curle Coordinates

5.2.5 Ramp Pressure Gradient Correlation

It would be useful if there were available some general criteria to evaluate the conditions at which transition onset may be expected for reattaching flows. In an attempt to find such a rule, the maximum pressure gradient measured on the ramp has been evaluated, since it is plain that transition is triggered earlier during reattachment by increases in the inviscid pressure rise (Ref. 18). The results which are presented in nondimensional form in Fig. 29a, for both the adiabatic and cold wall data, show that the parameter increased either with Reynolds number increase or with wall temperature decrease but that the effects of nose radius and Mach number were both somewhat mixed. In order to compensate for these mixed effects, a local pressure coefficient gradient was evaluated which was based on the conditions estimated to exist at the hinge line (S_c) after accounting for the total pressure loss across a normal shock at M_∞. These results, presented in Fig. 29b, as expected show a significant reordering of the data such that highest gradients are now observed at the lowest free-stream Mach number. The solid symbols on this figure indicate the conditions for which the reattachment was considered to be transitional on the basis of the various types of data previously or subsequently presented. This judgement was based on as many as possible of the various techniques for determining transition location; i.e., interaction length (Figs. 11 to 14), heat transfer (Figs. 32 and 33), boundary-layer surveys (Figs. 18 and 19), shadowgraphs (Figs. 3, 4, and 6b), and/or comparisons to theory. These results, Fig. 29b, although they do not preclude a value which is dependent on Mach number or Reynolds number, suggest that a range of critical values for the reattachment gradient (C_p'), dependent on wall temperature, could be specified. The adiabatic wall data at $M_\infty = 3$ suggest that the maximum value of C_p' for which laminar flow could be expected at the lowest Reynolds number is approximately 0.2. The adiabatic wall data at $Re_c = 0.5$ million and $M_\infty = 4.5$ suggest approximately the same value, whereas the data at $M_\infty = 6$ at the highest Reynolds number indicate that the critical value is greater than 0.15. Therefore a tentative specification for a critical value of C_p', independent of Mach number and Reynolds number, could be 0.20 for the adiabatic wall case and, by similar reasoning, 0.35 for the cold wall case. It would thus classify as transitional during flow reattachment all $M_\infty = 3$ data, except for the sharp leading edge, adiabatic wall, at minimum Re_c. All of the $M_\infty = 4.5$, $Re_c = 1.0$ million data would be classified transitional except the $R_N = 0.001$, $T_{wall}/T_{t_\infty} = 0.6$ condition. This exception is not unusual because the other data in this figure show that the reattachment pressure gradient was less with moderate cooling than with the ratios of $T_{wall}/T_{t_\infty} = 0.12$ or 0.3.

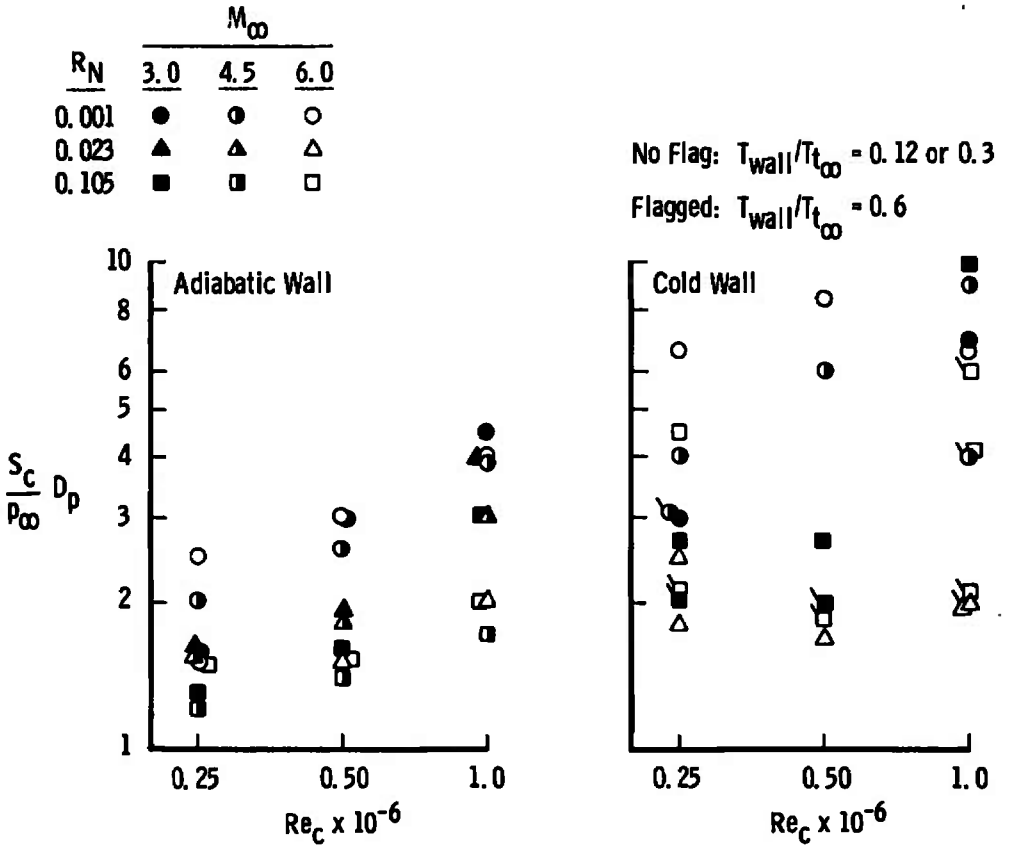

a. Pressure Ratio Form

Fig. 29 Variation of Maximum Pressure Gradient on Ramp with Reynolds Number for Adiabatic and Cold Wall Conditions

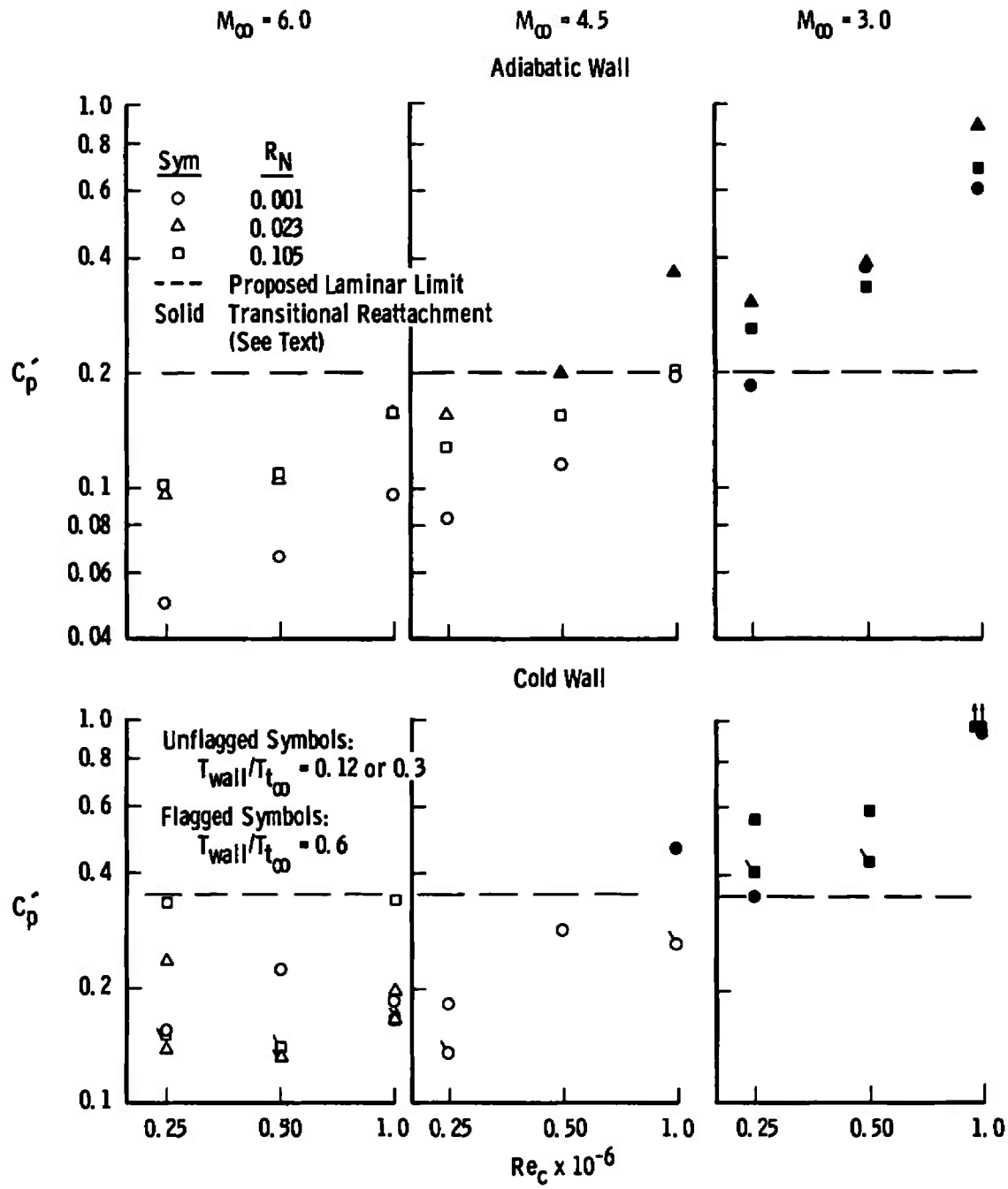

b. Pressure Coefficient Form
Fig. 29 Concluded

5.3 MODIFIED INTEGRAL-MOMENT THEORY RESULTS

Since the local flow conditions were so significantly modified by the leading-edge blunting investigated here, the LRK integral-moment theory used in Ref. 7 could not be expected to apply when $R_N >> 0$. In order to apply it, some simple modifications were made to relate the boundary conditions to realistic values. These changes involved matching locally (1) the theoretical inviscid pressure distribution at the beginning of the interaction and at some ramp station, chosen to be 1.8 S_c, (2) the inviscid Mach number at 1.8 S_c, (3) the displacement thickness calculated for the appropriate inviscid pressure distribution on a blunt plate and evaluated at the nominal onset of the interaction, and (4) the inviscid total pressure loss at the nominal boundary-layer edge at the interaction onset. From these the required initial conditions for Mach number, Reynolds number, and incompressible displacement thickness were computed, but it was assumed that the Blasius value adequately represented the initial velocity profile parameter.

Calculations of the longitudinal pressure distribution at $M_\infty = 4.5$ and 6 for all three nose radii are compared to the adiabatic wall, experimental results at the minimum and maximum Reynolds number in Fig. 30. The sharp-leading-edge data upstream of the hinge line which are in reasonable agreement with theory at $Re_c = 0.25$ million indicate that the flow reattachment was laminar in that case, but at Re_c of one million these comparisons in Fig. 30a indicate (because of the lack of significant change) that it was certainly transitional at $M_\infty = 4.5$ and was at least approaching the same condition at $M_\infty = 6$. Note in particular the differences in the ramp pressure gradient data at these conditions. Data for the moderately blunted leading edge in Fig. 30b indicate the same evidence of transition effects at $M_\infty = 4.5$ (i.e., at $Re_c = 1.0$ million) and rather good agreement with the modified theory at $Re_c = 0.25$ million, whereas at $M_\infty = 6$ the ramp pressure distribution was grossly overestimated by the theory. Orifice dam data (Appendix I) at $M_\infty = 4.5$ for $Re_c = 0.25$ million show excellent agreement with the calculations for separation, whereas reattachment was indicated to have been further aft than calculated but at a pressure nearer to predictions. Results for the bluntest ($R_N = 0.105$) leading edge, which are compared in Fig. 30c, show generally good agreement of the theory with the data. These results, especially those at $M_\infty = 4.5$, suggest that the lack of variation with Reynolds number in the measured upstream interaction extent was not necessarily a result of transitional flow reattachment. Orifice dam data for reattachment at $M_\infty = 4.5$ indicate it was downstream of the predicted location, but the agreement is closer than for $R_N = 0.023$ (Fig. 30b). Finally, typical results at $M_\infty = 3$, but at the lowest Reynolds number tested, are compared to predictions in Fig. 31; it is noted that agreement was obtained for the upstream interaction only with the sharp leading edge. Calculation results could not be obtained at much higher Reynolds numbers (at these low Mach numbers) because convergence of the initialization procedure could not be obtained. This usually occurs when the upstream extent gets too large (leading-edge separation and an unrealistic decay in pressure upstream of the hinge line).

The results of the comparisons shown in this section are considered to generally confirm Holden's (Ref. 3) interpretation of data obtained at much different free-stream Mach number. That is, for small bluntnesses the effects of local inviscid Mach number decrease at the onset of the interaction (Fig. 23) override the opposing influence of local inviscid Reynolds number decrease at the onset of the interaction (Fig. 24). For higher bluntness the Reynolds number decrease is the dominant factor.

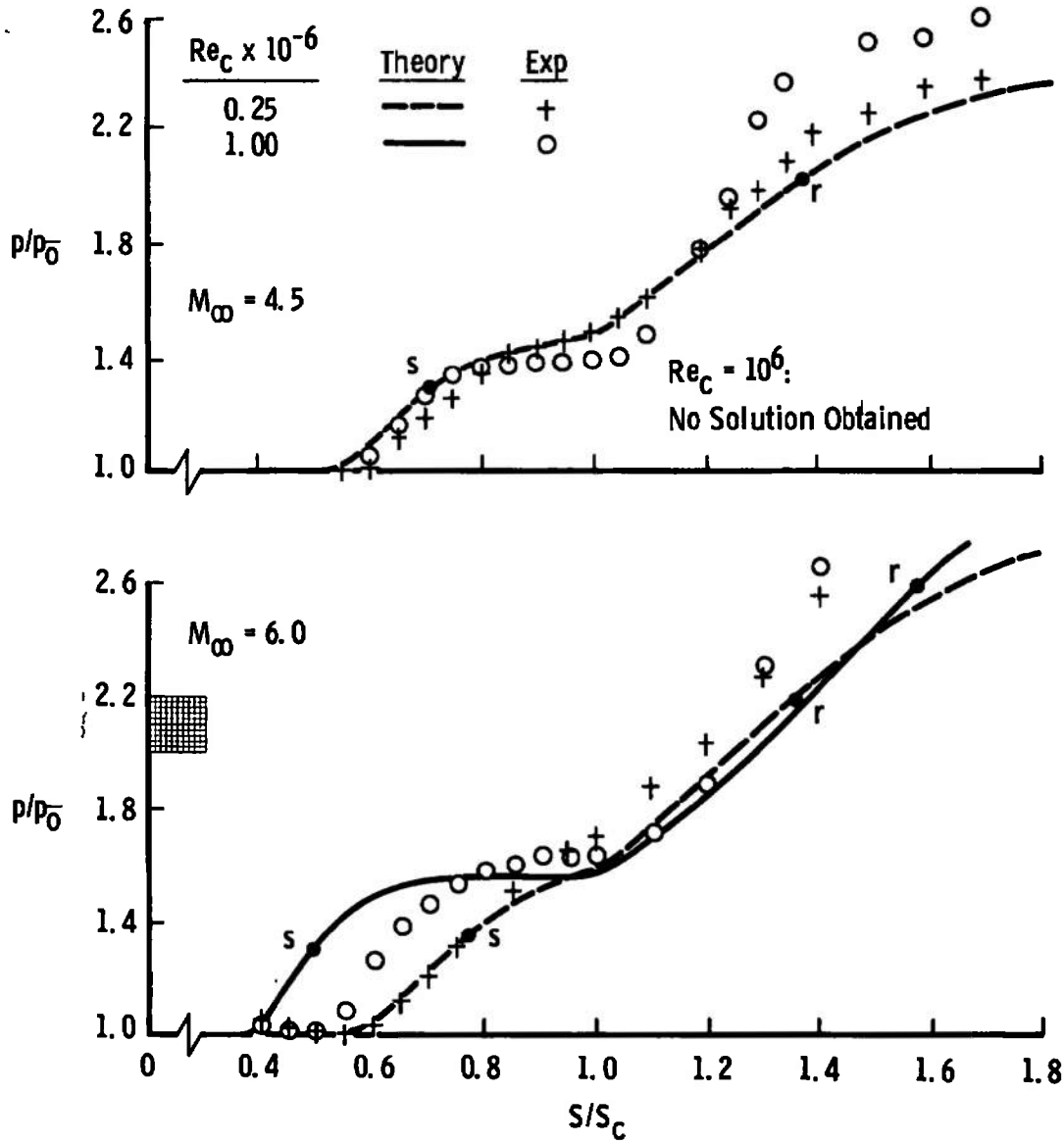

a. $R_N = 0.001$

Fig. 30 Comparison of Surface Pressure Data with Modified Integral-Moment Theory at Low and High Reynolds Number, Adiabatic Flow

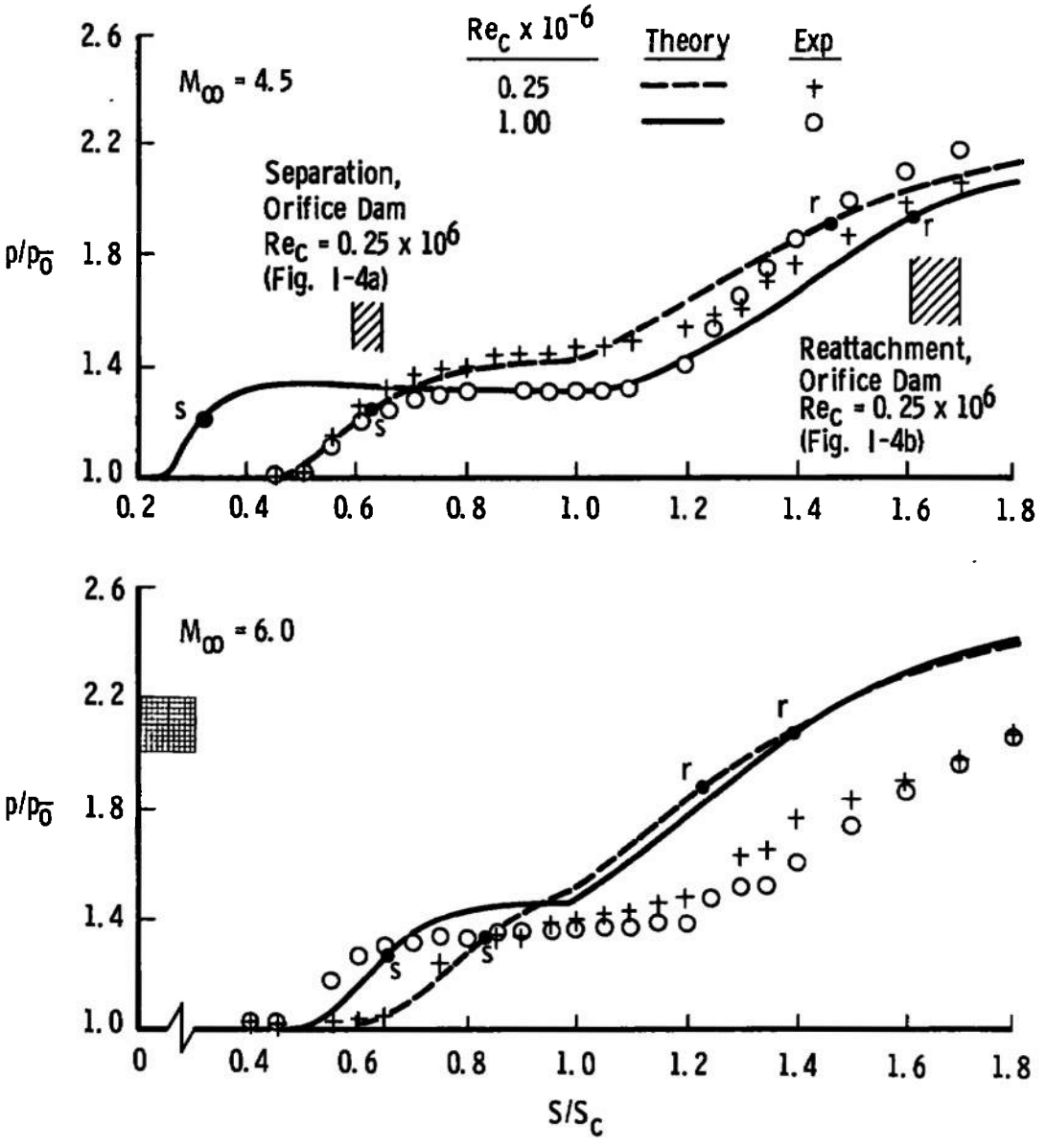

b. $R_N = 0.023$

Fig. 30 Continued

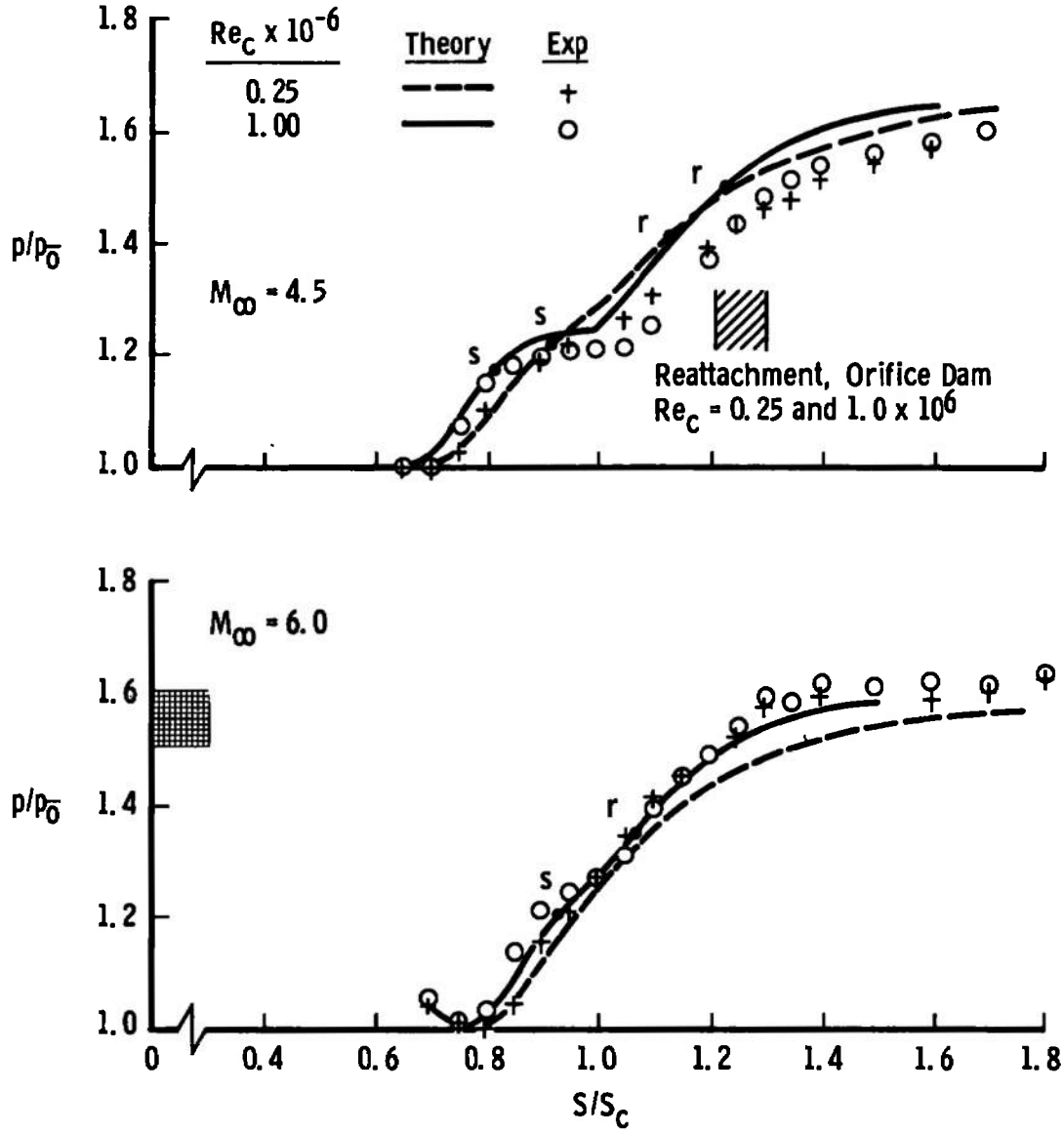

c. R_N = 0.105

Fig. 30 Concluded

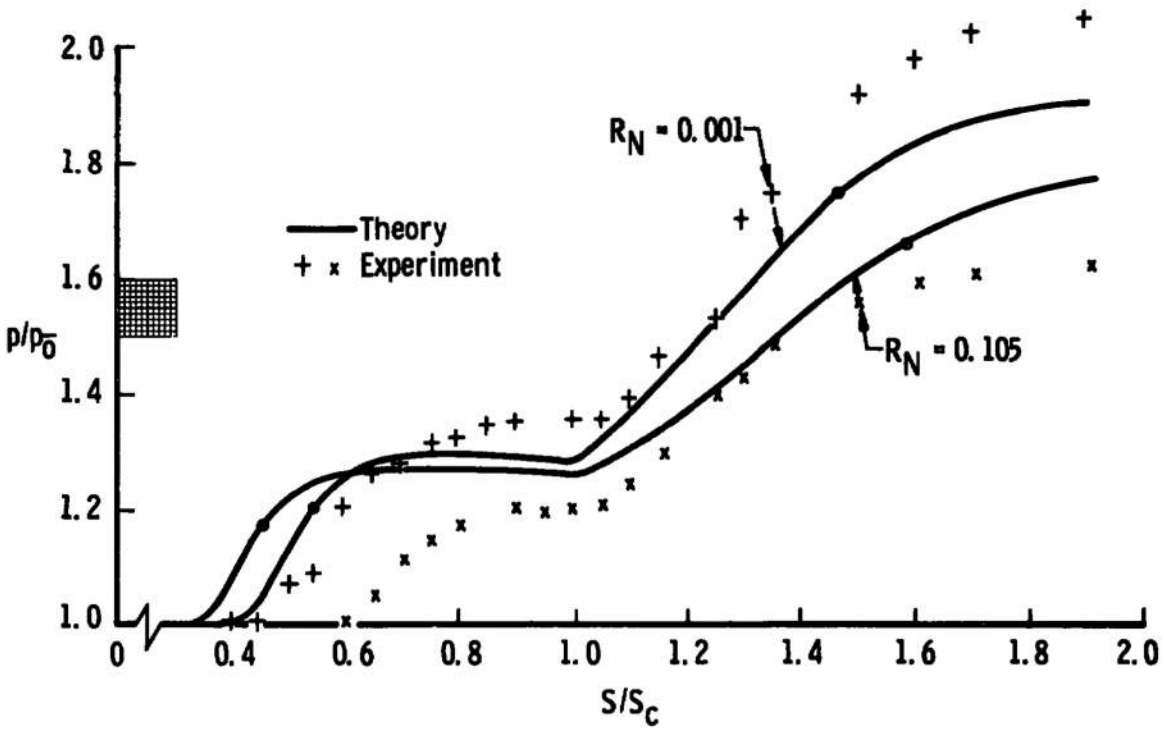

Fig. 31 Comparison of Surface Pressure Data with Modified Integral-Moment Theory at $M_\infty = 3$ and $Re_c = 0.25 \times 10^6$

5.4 COMPARISON OF HEAT-TRANSFER RESULTS WITH FLAT-PLATE THEORY

Only a brief examination of the heat-transfer data, presented originally in Figs. 15 and 16, is required to conclude that those results are less systematic than the surface pressure data. In order to sort out the effects of transition on the ramp heat transfer, the data in Stanton number form were compared with estimates based on the methods of Ref. 27, using the equations described in Appendix IV. Selected results are presented in Figs. 32 and 33 to illustrate the different characteristic effects observed, and they are presented in log-log coordinates so as to elucidate the laminar/turbulent Reynolds number trends.

The effects of Mach number and the plate Reynolds number (Re_c) for the sharp-leading-edge configuration at coldest wall conditions are shown in Fig. 32. The plate heat-transfer levels are noted to agree very well with laminar theory; the ramp levels, at sufficiently high length Reynolds number, tend toward the predicted turbulent heating levels. At $M_\infty = 3$ (Fig. 32a) turbulent rates were measured on the ramp, thus showing that transition was certainly very near to reattachment at even $Re_c = 0.25$ million. However, for $M_\infty = 4.5$ (Fig. 32b) the minimum Re_c data are observed to lie clearly between the predicted laminar and turbulent ramp levels but with a Reynolds number dependence which was essentially laminar. This illustrates the influence of the reduced boundary-layer thickness relative to that on a flat plate, as shown previously in Figs. 23 and 24, thus indicating that the interaction effects may persist for large distances. A similar result (Fig. 32c) was also obtained at $M_\infty = 6$ for minimum Re_c. By comparisons with Fig. 32c the combined effects of wall temperature increase and changes in leading-edge radius are shown in Fig. 33a for the same conditions (except for wall temperature) which gave the worst comparison on the ramp between modified LRK theory and pressure data (Fig. 30b). These were the only data obtained which show that the theoretical laminar levels in the ramp heating could be realized so close to reattachment. Results for the largest nose radius are shown in Fig. 33b at $M_\infty = 6$; here there is a slight overshoot in the data relative to the predicted laminar level, whereas at $M_\infty = 3$ (Fig. 33c) turbulent heating levels were attained on the ramp at all Reynolds numbers. It is noted that when the ramp heating rates were close to the predicted laminar level for a wedge, the measured rates at $S = 1.2\ S_c$ were equal to (Fig. 33b) or less than (Fig. 33a) the flat-plate rates, whereas at this location the rates were otherwise well above the flat-plate levels.

Incidentally, these two figures provide some quantitative data concerning the effects of nose blunting on transition onset at $M_\infty = 6$. Specifically, the data in Fig. 33a indicate that for $R_N = 0.023$ at $Re_c \leqslant 0.5$ million, $S_{to}/S_c \geqslant 2.6$, but at 1.0 million $S_{to}/S_c \geqslant 1.8$. Moreover for $R_N = 0.105$ (Fig. 33b) the data indicate that $S_{to}/S_c \geqslant 2.6$ for $Re_c \leqslant 1.0$ million. This result was also shown by the schlieren photographs in Fig. 4b for the adiabatic wall case. Thus it appears at least at $M_\infty = 6$ that increasing the nose radius delayed the onset of transition relative to that shown in Fig. 6a, but that at $M_\infty = 3$ it had no effect—for the cold wall case at least.

The consistent but definite scatter shown by the ramp data should be acknowledged, since it was observed to be surprisingly repeatable at fixed test conditions. Thus it is believed that it may have been caused by very slight misalignments observed between the heat-transfer gage and ramp surface.

The peak heating measured on the ramp as affected by Reynolds number, Mach number, nose bluntness, and the degree of cooling is summarized in Fig. 34 relative to that predicted on a wedge with a turbulent boundary layer (Appendix IV). These results show that the peak heating at maximum Reynolds number was never more than 125 percent of the predicted turbulent level, and at minimum Reynolds number it became as small as 40 percent of this predicted level at $M_\infty \geq 4.5$, in which cases it was laminar but not relaxed to the asymptotic wedge level.

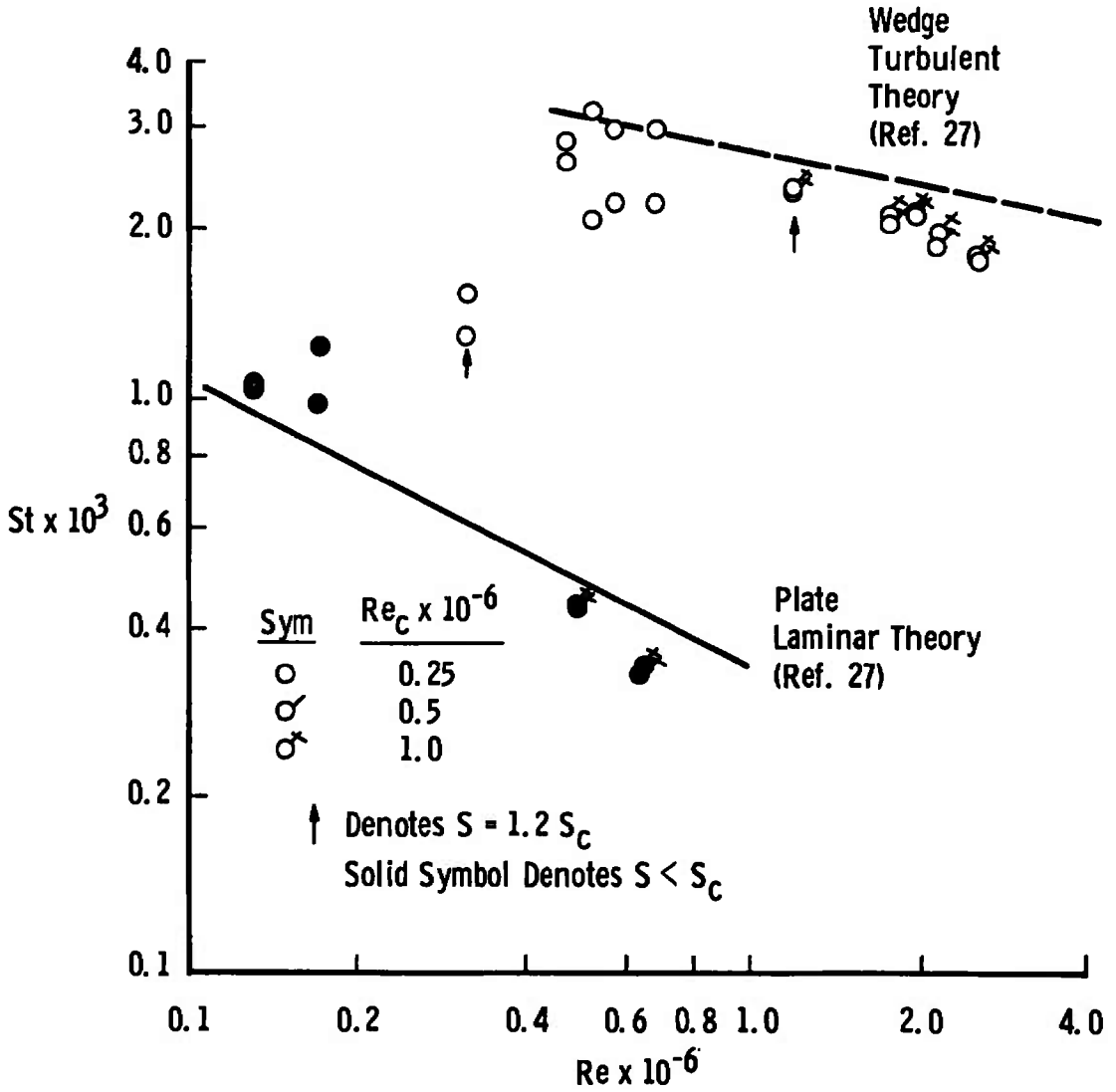

a. $M_\infty = 3$ ($T_{wall}/T_t \approx 0.3$)

Fig. 32 Comparisons of Stanton Number versus Reynolds Number with Theoretical Estimates for a Plate and Wedge, $R_N = 0.001$

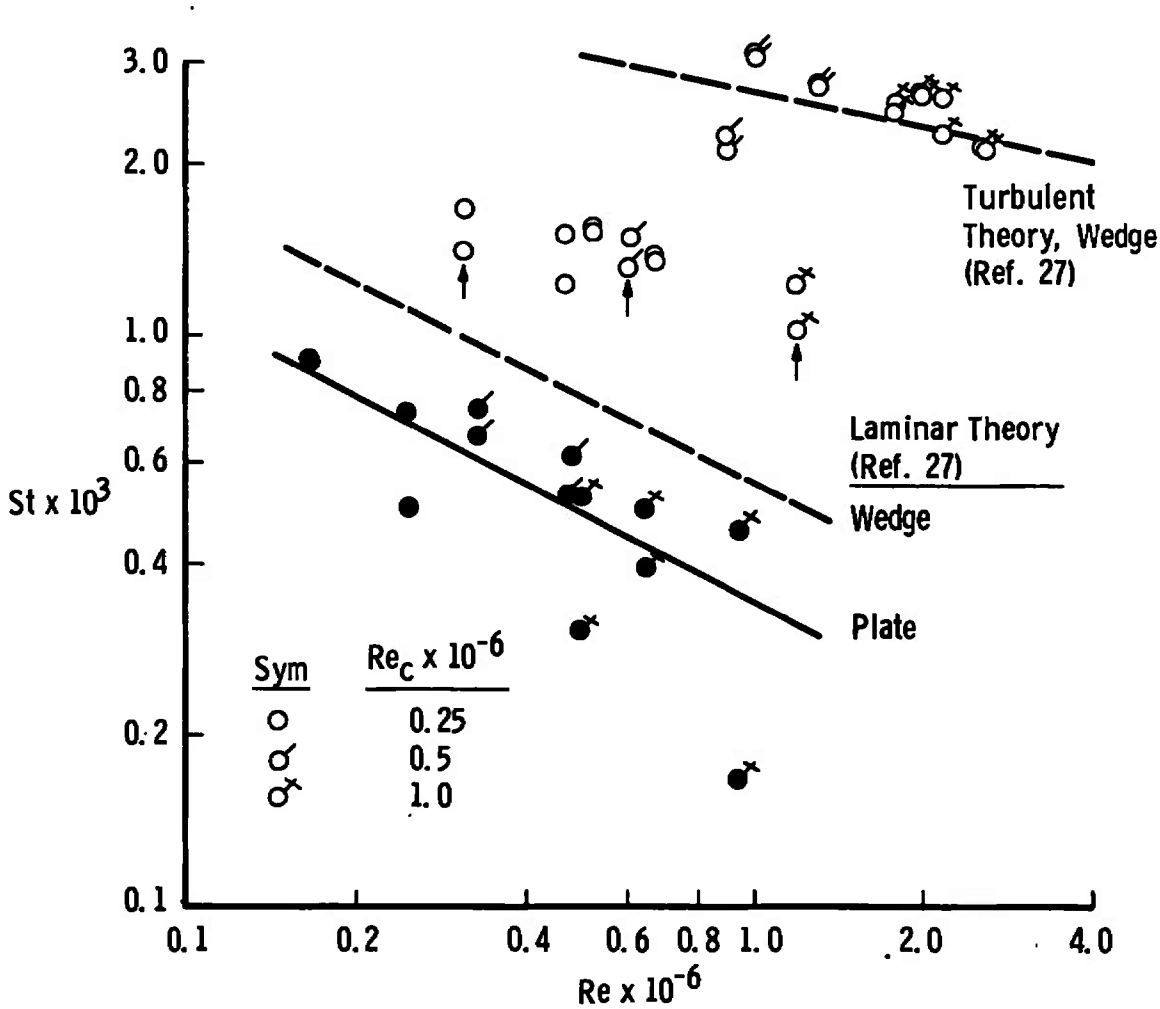

b. $M_\infty = 4.5$ ($T_{wall}/T_t \approx 0.3$)
Fig. 32 Continued

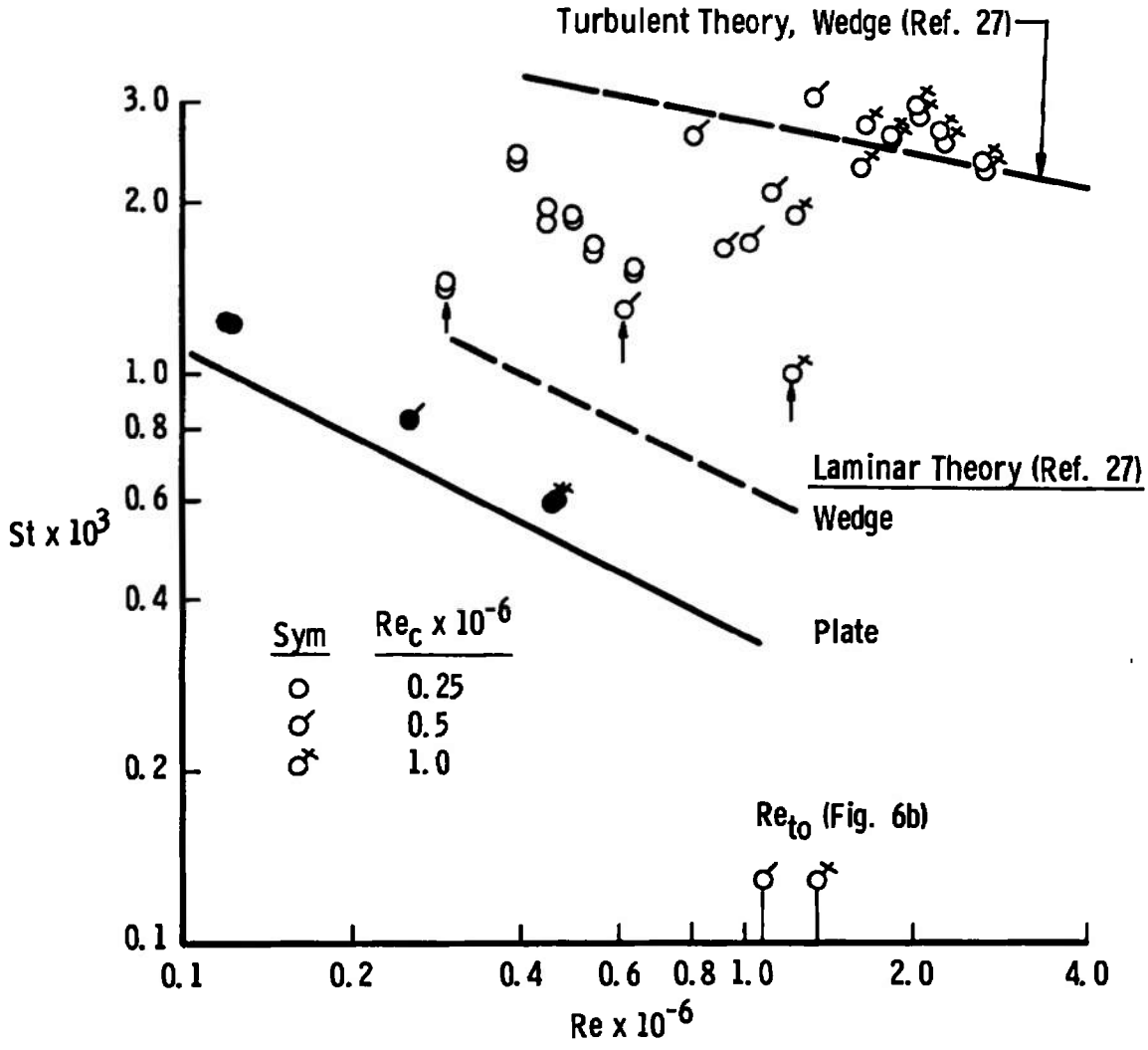

c. $M_\infty = 6.0$ ($T_{wall}/T_t \approx 0.1$)

Fig. 32 Concluded

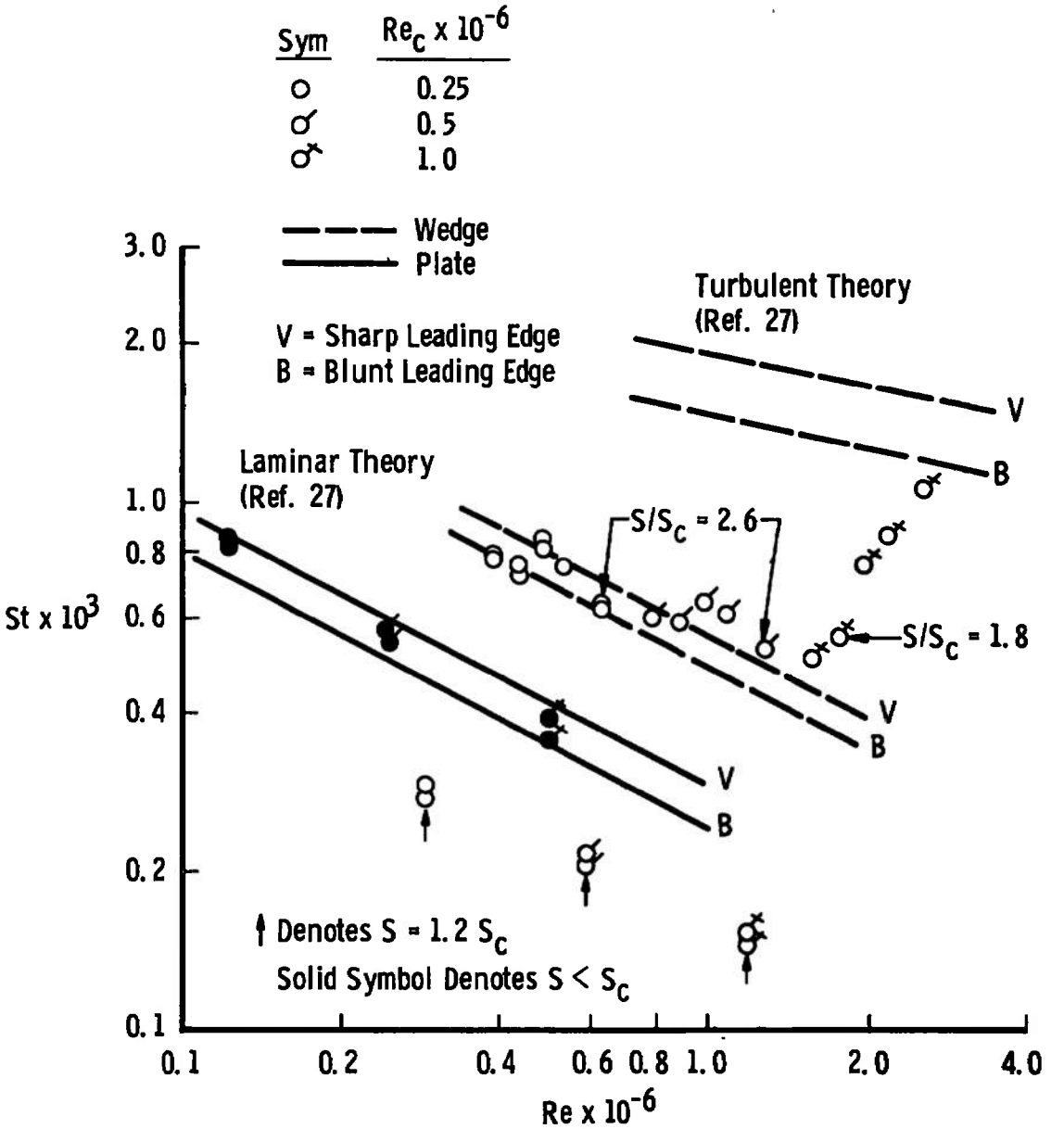

a. $M_\infty = 6$, $R_N = 0.023$ ($T_{wall}/T_t \approx 0.6$)

Fig. 33 Comparisons of Stanton Number versus Reynolds Number with Theoretical Estimates for a Plate and Wedge, Blunted Leading Edges

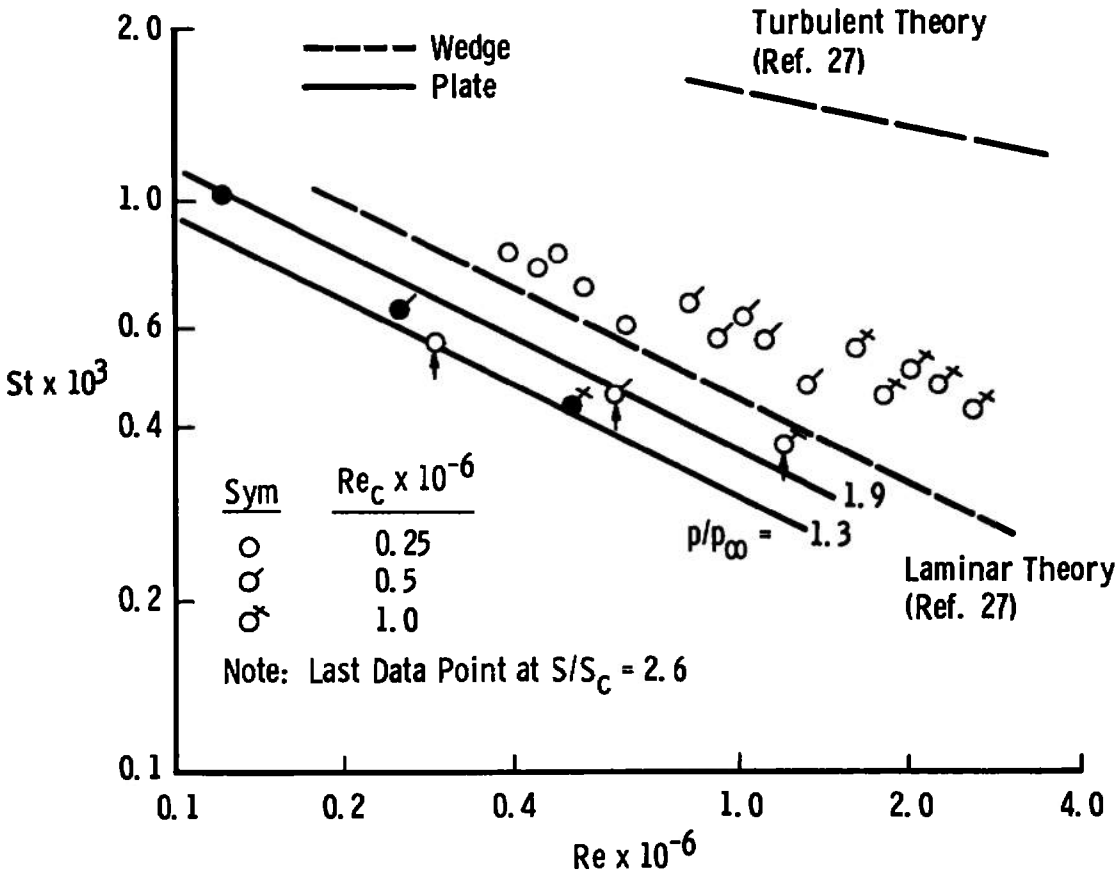

b. $M_\infty = 6$, $R_N = 0.105$ ($T_{wall}/T_t \approx 0.6$)
Fig. 33 Continued

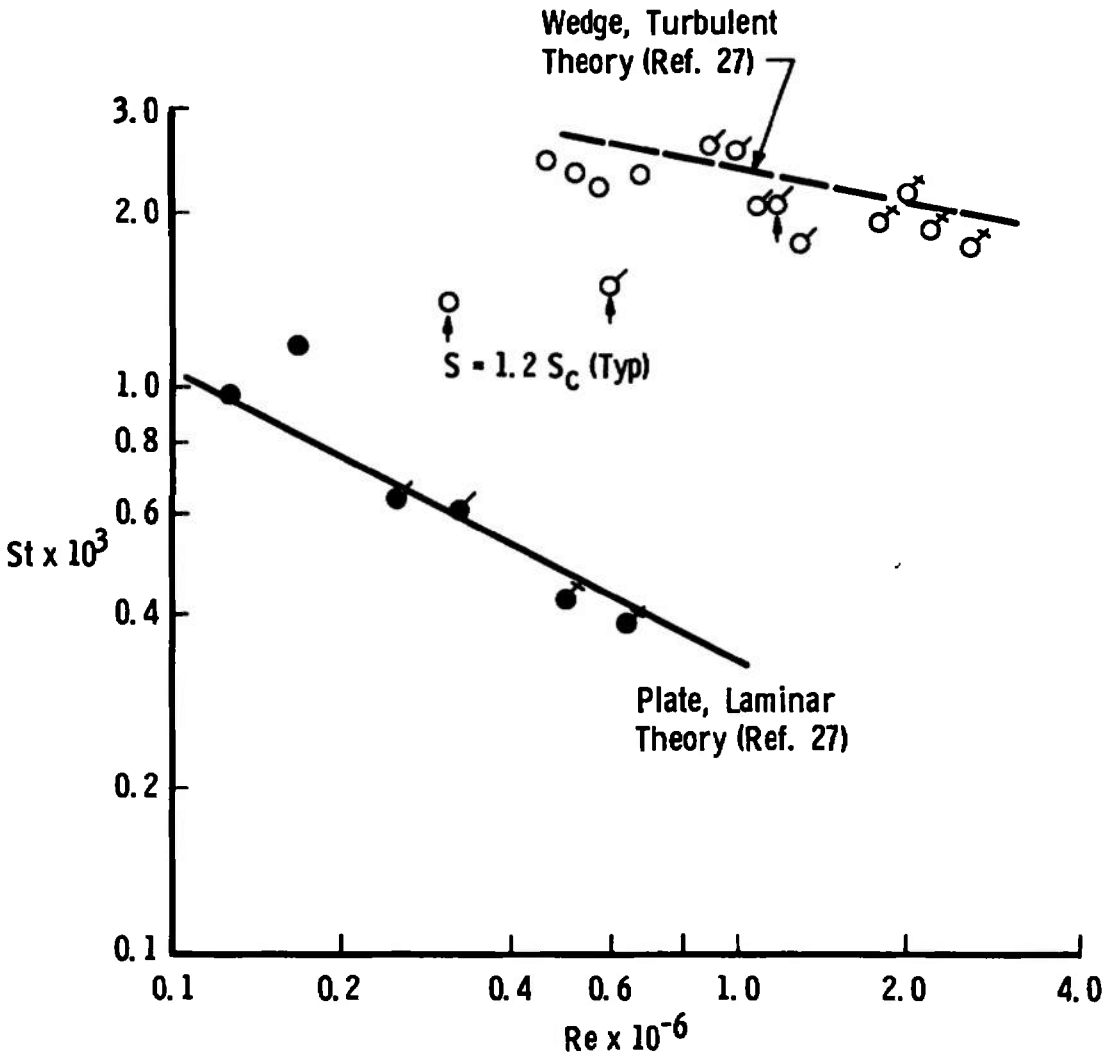

c. $M_\infty = 3$, $R_N = 0.105$ ($T_{wall}/T_t \approx 0.3$)

Fig. 33 Concluded

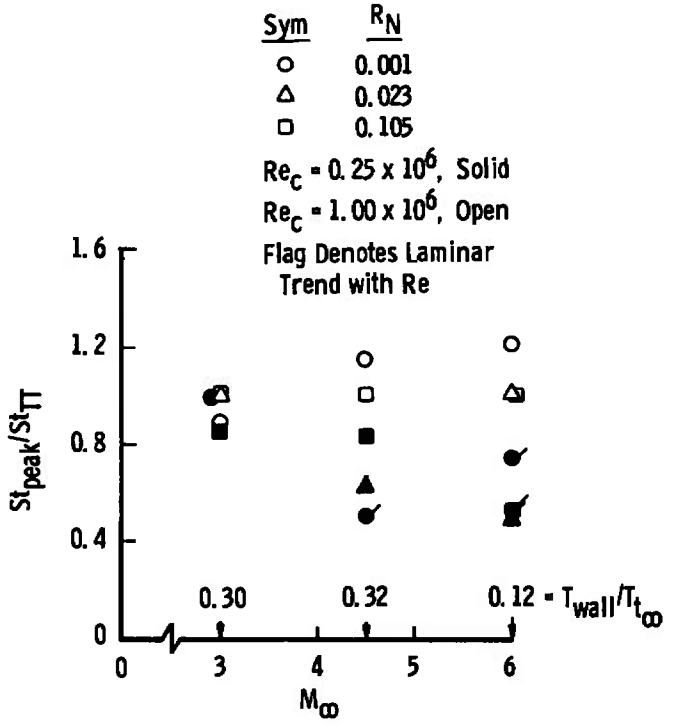

a. Maximum Cooling

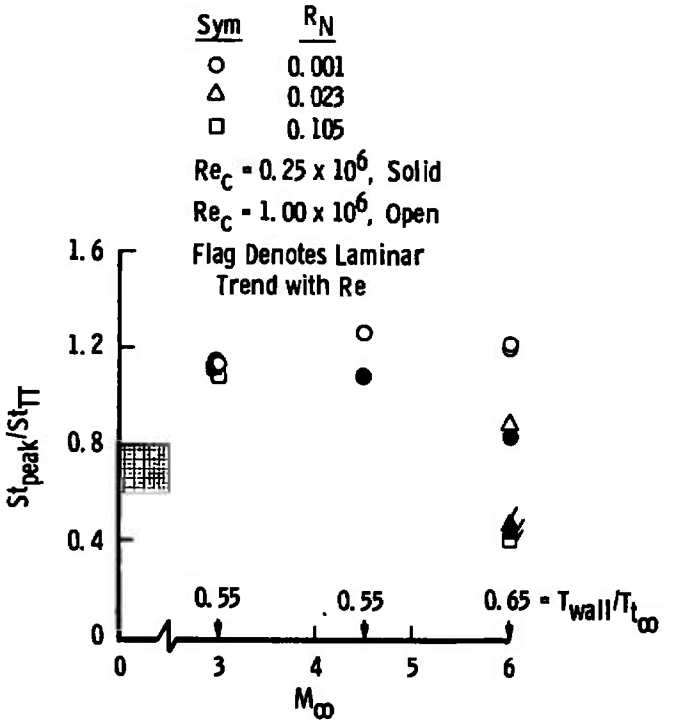

b. Moderate Cooling

Fig. 34 Ratio of Measured Peak Heating on Ramp to Theoretical Turbulent Heating on Wedge of Same Angle

SECTION VI
SUMMARY

Transition onset was indicated by the results in the many forms presented to occur so much earlier on the ramp at $M_\infty = 3$ than at $M_\infty = 6$ that laminar flow reattachment was probably obtained only at the minimum Reynolds number with the sharp leading edge and an adiabatic wall at $M_\infty = 3$. Moreover, an increase in leading-edge radius was found to delay transition onset only at $M_\infty \geq 4.5$, with the distance being the greatest at $M_\infty = 6$. The effects of wall cooling were somewhat mixed, in that at $M_\infty = 6$ when transition onset was well downstream of reattachment (minimum Re_c), increased cooling delayed the onset; however, when the onset was near to reattachment (maximum Re_c), increased cooling precipitated transition.

Surface pressure distributions show that small increases in leading-edge radius may have greater effects on the overall interaction than large radii. In fact, the upstream extent of the ramp-induced interaction was larger when $R_N = 0.023$ than with either $R_N = 0.001$ or 0.105, regardless of the proximity of transition to the reattachment zone. In addition, decreasing the wall temperature generally reduced the interaction extent to a significant degree when the reattachment was either transitional or laminar. A modification of the integral-moment theory was shown to predict correctly the reversal caused by nose blunting, as well as the general characteristics of the overall interaction for the adiabatic wall situation. Moreover, the small variation of upstream interaction extent found for a fourfold increase in plate Reynolds number at $M_\infty \geq 4.5$ indicates that leading-edge blunting may significantly alter the trends customarily associated with ramp-induced laminar reattaching flows. Significant viscous weak interaction was found upstream of the ramp-induced interaction with all nose radii at all Mach numbers. Examination of a nondimensional, maximum pressure gradient on the ramp suggested a critical value beyond which transition would occur at reattachment, and which was presumed to be independent of Mach number and Reynolds number, but dependent on the wall temperature ratio.

The maximum heat transfer on the ramp was found to be closely predicted for nearly all conditions investigated when using the appropriate local conditions on a wedge in turbulent flow. Local peak heating rates of up to about 125 percent of that predicted for turbulent wedge flow were generally obtained, whereas theoretical laminar heating rates on a wedge were indicated only at quite limited test conditions.

The use of ramp orifice dams to locate flow reversal at the separation and reattachment of a laminar boundary layer appears feasible.

Tabulated surface data are presented in Appendix V for $Re_c = 0.25$ million since flow reattachment was most likely laminar at this condition.

REFERENCES

1. Townsend, J. C. "Effects of Leading Edge Bluntness and Ramp Deflection Angle on Laminar Boundary-Layer Separation in Hypersonic Flow." NASA Tech Note D-3290, November 1965.

2. Holloway, P. F., Sterrett, J. R. and Creekmore, H. S. "An Investigation of Heat Transfer within Regions of Separated Flow at a Mach Number of 6.0." NASA TN D-3074, November 1965.

3. Holden, M. S. "Leading-Edge Bluntness and Boundary Layer Displacement Effects on Attached and Separated Laminar Boundary Layers in a Compression Corner." AIAA 6th Aerospace Sciences Meeting, Paper No. 68-68, January 1968.

4. Harvey, W. D. "Experimental Investigation of Laminar-Flow Separation on a Flat Plate Induced by Deflected Trailing-Edge Flap at Mach 19." NASA Tech Note D-4671, August 1968.

5. Gray, J. D. "Nose Bluntness Effects on Axisymmetric Laminar Reattaching Flows at Mach 19." AEDC-TR-67-16 (AD812442), April 1967.

6. Gadd, G. E. "An Experimental Investigation of Heat Transfer Effects on Boundary Layer Separation in Supersonic Flow." J. Fluid Mech. 2, 105 (1957).

7. Gray, J. D. and Rhudy, R. W. "Investigation of Flat-Plate Aspect Ratio Effects on Ramp-Induced, Adiabatic, Boundary-Layer Separation at Supersonic and Hypersonic Speeds." AEDC-TR-70-235 (AD719747), March 1971.

8. Lewis, J. E. "Experimental Investigation of Supersonic Laminar, Two-Dimensional Boundary-Layer Separation on a Compression Corner with and without Cooling." California Institute of Technology, Ph.D. Thesis, 1967.

9. Ferguson, Harold and Schaefer, John W. "Heat Transfer and Pressure Distribution on Cone-Cylinder-Flare Configuration with Boundary-Layer Separation." NASA TN D-1436, October 1962.

10. Gray, J. D. "Wall Cooling Effects on Axisymmetric Laminar Reattaching Flows at Hypersonic Speeds." AEDC-TR-68-135 (AD677589), November 1968.

11. Holden, M. "Separated Flow Studies at Hypersonic Speeds, Part II: Two-Dimensional Wedge Separated Flow Studies." CAL Report AF-1285-A-13(2), December 1964.

12. Needham, D. A. "Laminar Separation in Hypersonic Flow." University of London, Ph.D. Thesis, August 1965.

13. Bushnell, D. M. and Weinstein, L. M. "Correlation of Peak Heating for Reattachment of Separated Flows." Journal of Spacecraft and Rockets, Vol. 5, No. 9, September 1968, pp. 1111-1112.

14. Ginoux, J. J. "Supersonic Flow over Flaps with Uniform Heat Transfer." von Kármán Institute VKI TN 30, September 1966.

15. Thomke, G. J. and Roshko, A. "Incipient Separation of a Turbulent Boundary Layer at High Reynolds Number in Two-Dimensional Flow over a Compression Corner." DAC-59819, January 1969.

16. Pate, S. R. and Schueler, C. J. "An Investigation of Radiated Aerodynamic Noise Effects on Boundary-Layer Transition in Supersonic and Hypersonic Wind Tunnels." AIAA 3rd Aerodynamic Testing Conference, Paper No. 68-375, April 1968.

17. Brinich, P. F. and Sands, N. "Effect of Bluntness on Transition for a Cone and a Hollow Cylinder at Mach 3.1." NACA TN-3979, May 1957.

18. Gray, J. D. "Investigation of the Effect of Flare and Ramp Angle on the Upstream Influence of Laminar and Transitional Reattaching Flows from Mach 3 to 7." AEDC-TR-66-190 (AD645840), January 1967.

19. Roberts, M. L. "Transitional Flow Separation Upstream of a Compression Corner." Journal of Spacecraft and Rockets, Vol. 7, No. 9, September 1970, pp. 1113-1118.

20. Kendell, J. M. "An Experimental Investigation of Leading-Edge Shock-Wave-Boundary-Layer Interaction at Mach 5.8." JAS, Vol. 24, No. 1, January 1957, pp. 47-56.

21. Van Driest, E. R. "Investigation of Laminar Boundary Layer in Compressible Fluids Using the Crocco Method." NACA TN 2597, January 1952.

22. Klineberg, J. M. "Theory of Laminar Viscous-Inviscid Interactions in Supersonic Flow." Ph.D. Thesis, California Institute of Technology, 1968.

23. Reyhner, T. A. and Flügge-Lotz, I. "The Interaction of a Shock Wave with a Laminar Boundary Layer." Journal of Non-Linear Mechanics, Vol. 3, No. 2, June 1968, pp. 173-199.

24. Hill, William G., Jr. "A Comparison of Theory and Experiment for Laminar Separation Ahead of a Compression Corner at Supersonic and Low Hypersonic Speeds." Grumman Aerospace Corporation, Research Department Report RE-401, December 1970.

25. Needham, D. A. and Stollery, J. L. "Boundary Layer Separation in Hypersonic Flow." AIAA 4th Aerospace Sciences Meeting Paper No. 66-455, June 1966.

26. Curle, N. "Shock-Induced Separation of a Laminar Boundary Layer in Supersonic Flow Past a Convex Corner." Aero. Quarterly, Vol. XVI, February 1965, pp. 33-41.

27. Harms, R. J., Schmitt, C. M., Hanawalt, A. J., and Schmitt, D. A. "A Manual for Determining Aerodynamic Heating of High-Speed Aircraft." Vol. I, Report No. 7006-3352-0001, (AD 229434), June 1959.

APPENDIXES

APPENDIX I
APPLICATION OF THE ORIFICE DAM TECHNIQUE

This technique, which was developed by Roshko and Thomke (Ref. 15), relies on the differences to be expected in the pressure adjacent to the base of a wedge-shaped ramp orifice dam when the flow is up the slope (base pressure) rather than toward the vertical face (plateau pressure). Because its use has heretofore been restricted to turbulent flow, some doubt existed concerning its applicability to the determination of laminar flow reversal locations in general and to separation in particular. As stated previously, the orifice dams in the present investigation were used either singly or in a series, and either as a ramp or a step.

A typical installation of a series of ramp dams on the model ramp centerline is shown in Fig. I-1. As expected, it was found that precise alignment of the dam in yaw or in distance from the surface tap (within one dam height) was not required. Because of the effects of the leading-edge joint spanwise variation (Section 2.1), it was uncertain whether dam data could be obtained on the off-centerline orifice row which would correspond to those obtained on centerline. Data which show both the repeatability and spanwise differences obtained at $M_\infty = 4.5$. with no dams installed, are presented in Fig. I-2; absolute differences are clearly evident, but qualitatively the pressure distributions are similar within the repeatability band obtained.

Data obtained with a series of dams installed either as ramps or as steps are compared in Fig. I-3. It is noted in Fig. I-3a that for reattachment indication the dams had rather small influence on the measurements not adjacent to a dam. However, it is obvious that the steps had significantly more effect on the adjacent measurement than did the ramps. In addition, it appears that the ramp dam provided more consistent indications than the step dam, but this may have been a result of the large dam height. These ramp dam data are interpreted to indicate (because of (1) the drop in pressure, i.e. base pressure, downstream of the ramp dam at $S/S_c = 1.3$ and (2) the unperturbed pressure at $S/S_c = 1.2$) that the reattachment flow-reversal location was between $1.2 < S/S_c < 1.3$ for the conditions shown (see Fig. 30c in Section 5.3 for a comparison of this variation with theoretical estimates). These same dams, applied on the sharp plate for separation indication, gave the results shown in Fig. I-3b. Although these dams were located too far upstream to indicate separation, the results indicate that this dam size may significantly alter the overall interaction, probably by tripping the boundary layer. Note the decrease in the interaction length and the increase in the ramp pressure rise, especially at the high Reynolds number.

A reasonably good indication of the separation and reattachment locations was obtained with 0.030-in.-high ramp dams (Fig. I-4). It appears that the pressure rise at the ramp dam in reversed laminar flow (acts as a step dam with respect to the local flow) may be very small, and that the indication of the approach to reversal must come from the decaying base pressure effect (Fig. I-4a). The data in Fig. I-4b indicate that a series of dams upset the overall interaction when used to locate separation but did not when used only for reattachment determination.

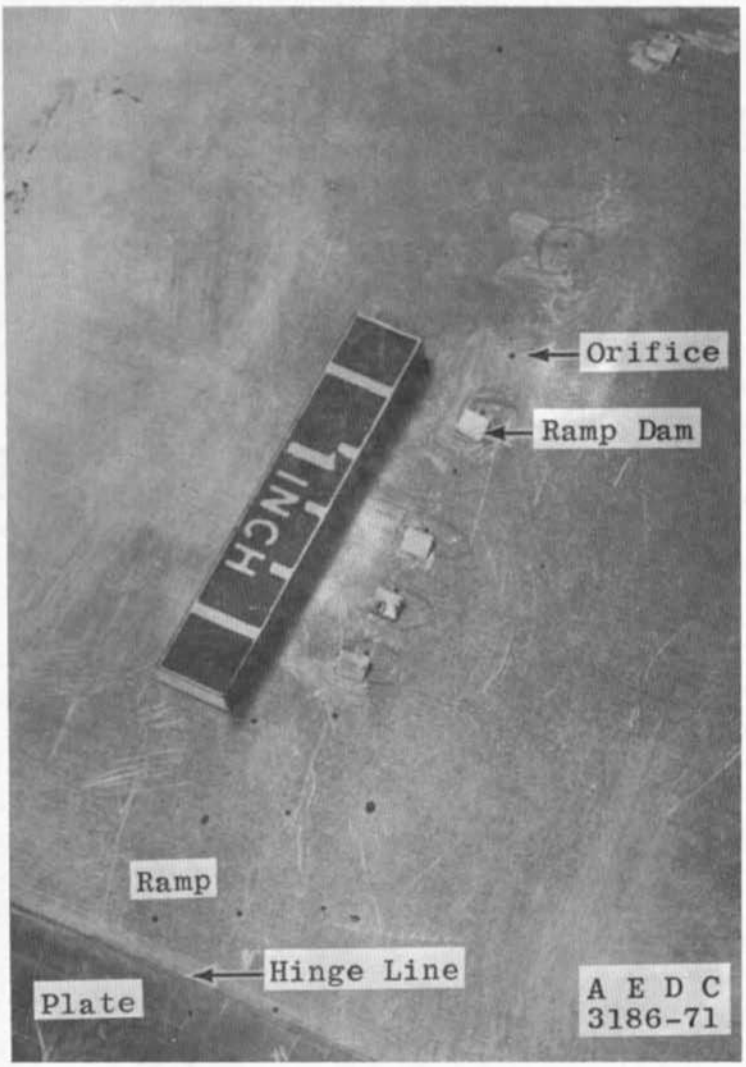

Fig. I-1 Typical Orifice Dam (Ramp) Installation on the Centerline of the Model Ramp

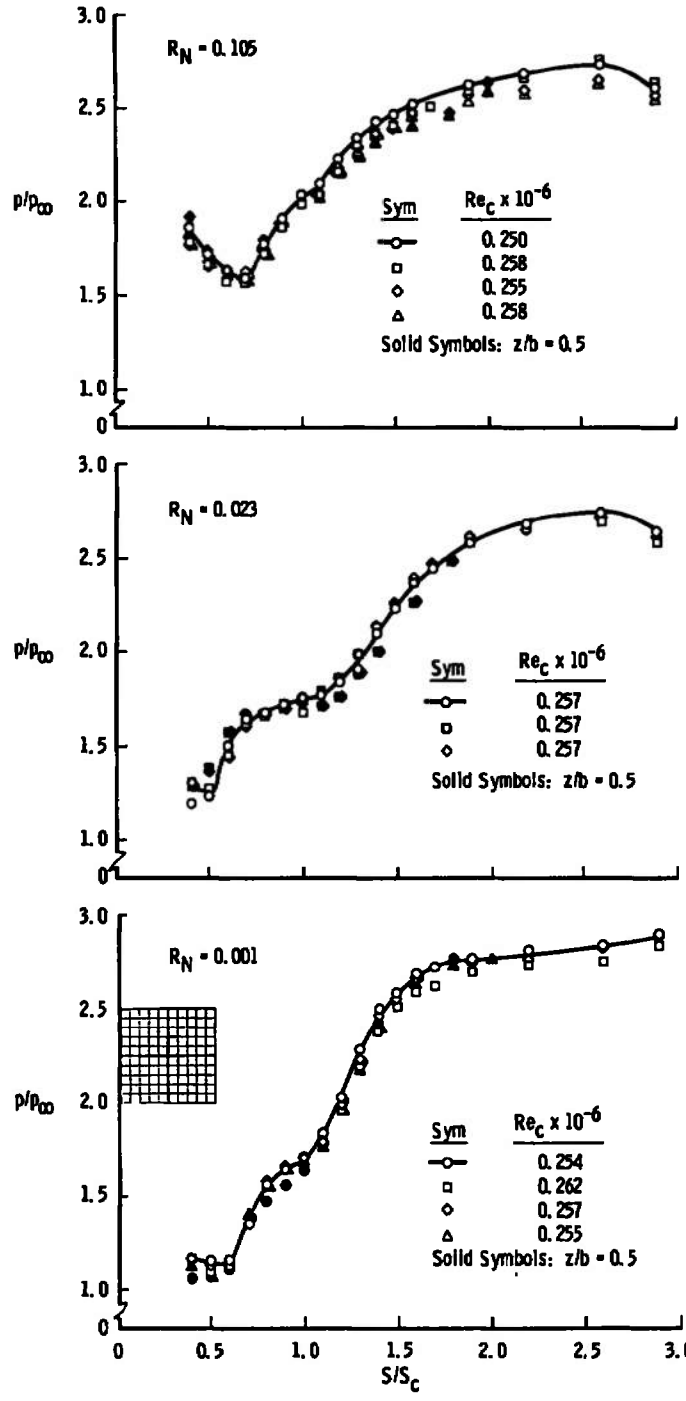

a. $T_{wall}/T_{t_\infty} \approx 0.9$

Fig. I-2 Repeatability of Data and Spanwise Variation at M_∞ = 4.5

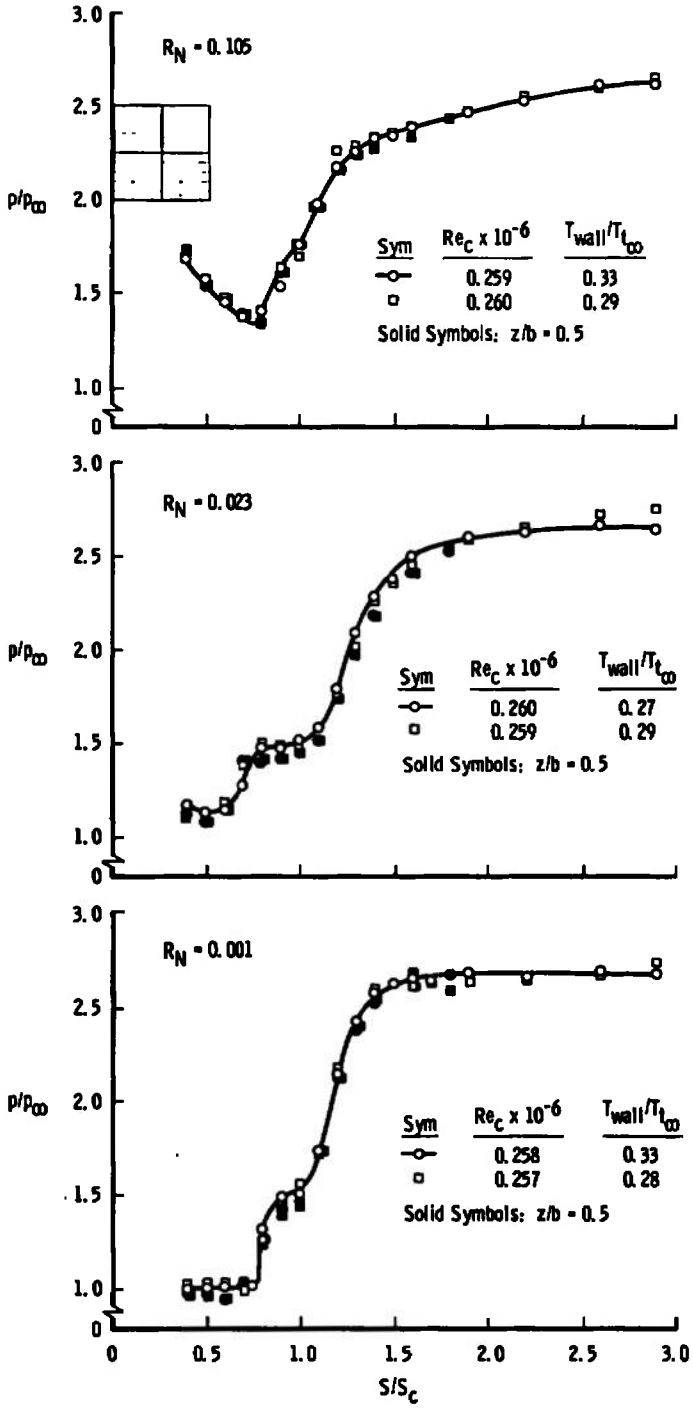

b. $T_{wall}/T_{t_\infty} \approx 0.3$

Fig. I-2 Concluded

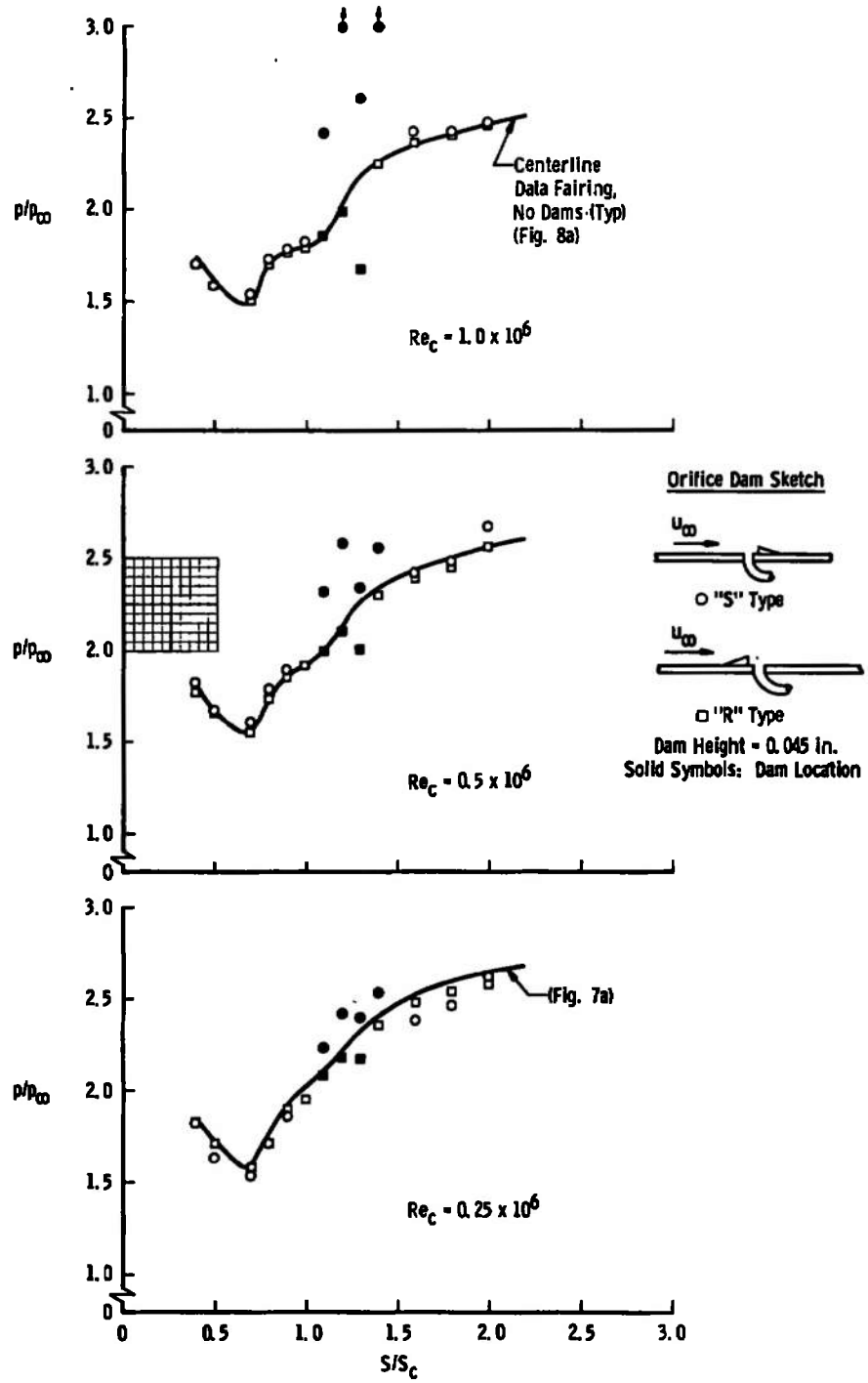

a. Reattachment Indication for $R_N = 0.105$

Fig. I-3 Comparison of Step- and Ramp-Dam Indications, z/b = 0.5 and $T_{wall}/T_{t_\infty} \approx 0.9$

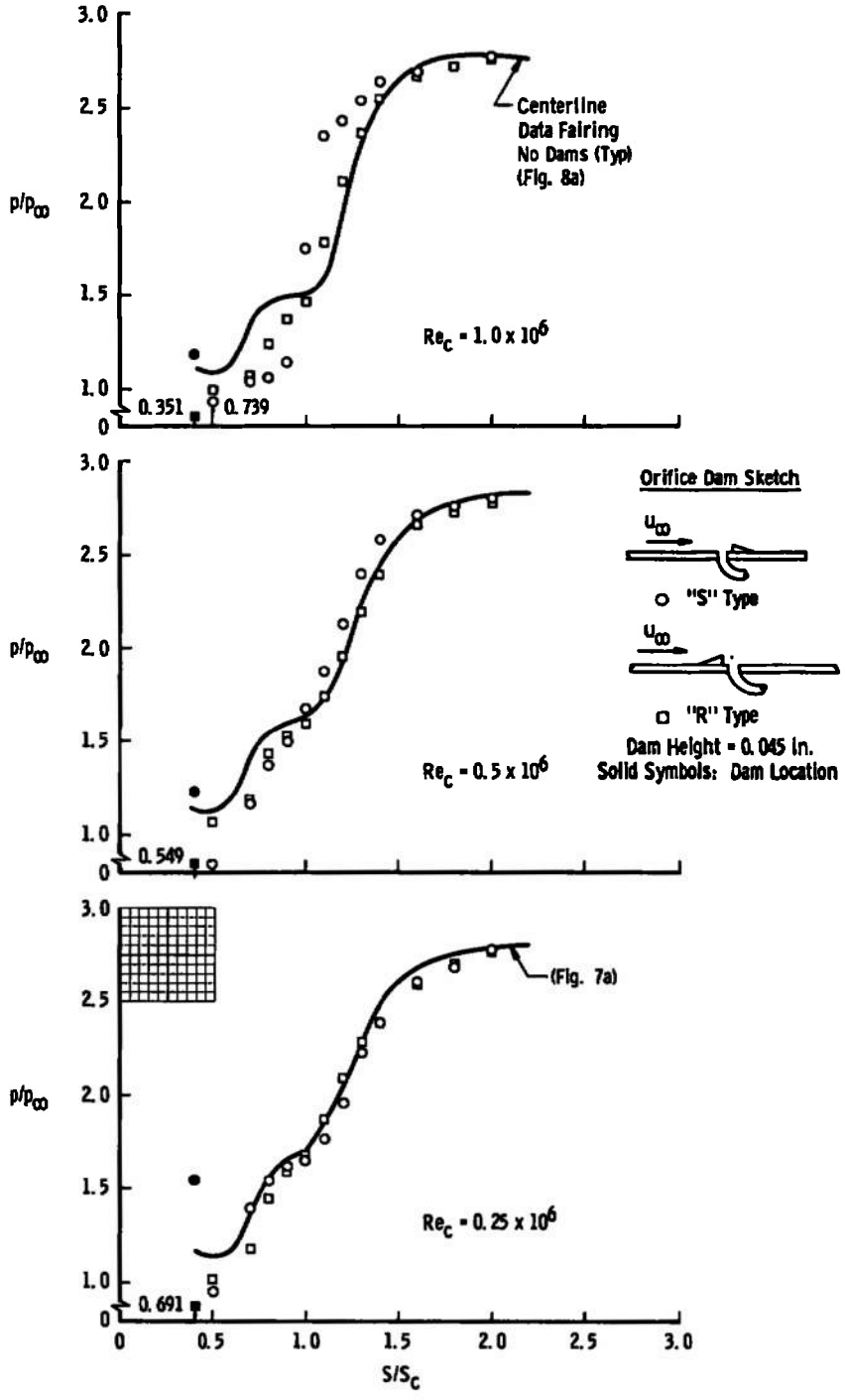

b. Separation Indication for R_N = 0.001

Fig. I-3 Concluded

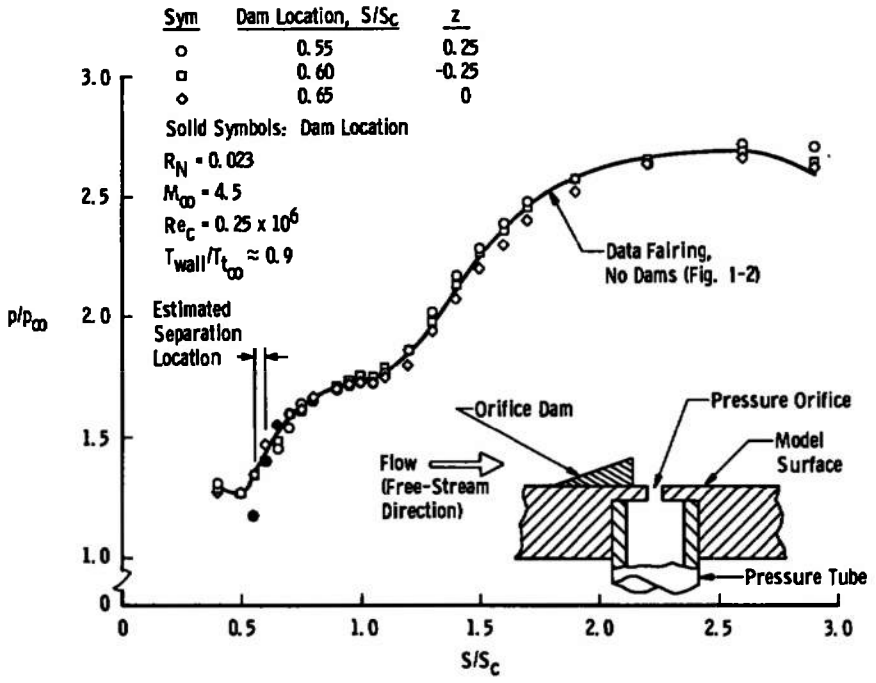

a. Separation Location, Single Dam Application

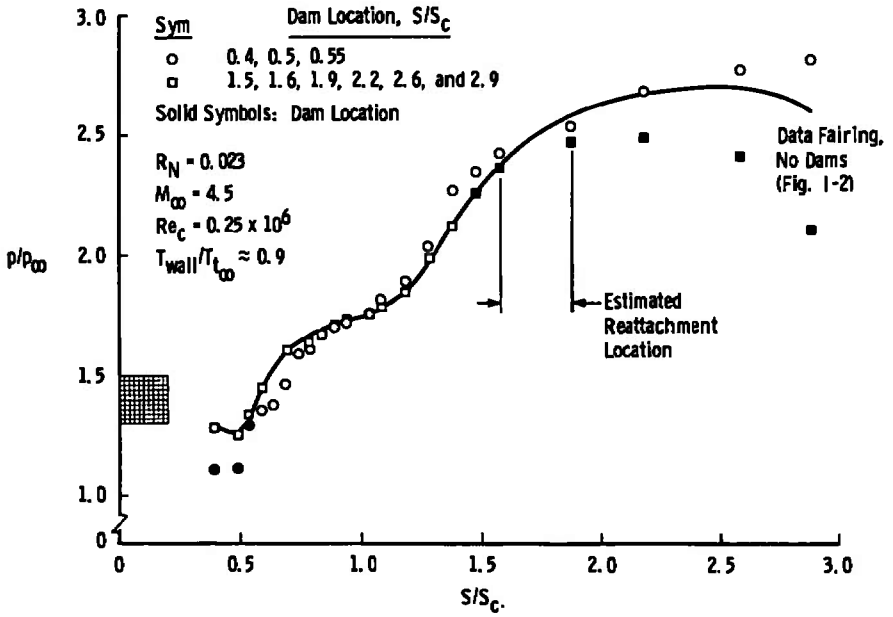

b. Reattachment Location, Series of Dams

Fig. I-4 Effect of Orifice Dams on Surface Pressure Distribution, z/b = 0

APPENDIX II
CORRECTION PROCEDURE FOR DISK STATIC PRESSURE PROBE

The use of the 0.25-in.-diam disk static pressure probe required a special data reduction program in order to obtain a true value of the local static pressure (p). Because the center of the orifice in the disk was, in general, approximately 0.15 in. above the model surface when the pitot probe was touching, the measured model surface pressure (p_m) was used to calculate the local Rayleigh Mach number (M) out to this point. In order to compensate for any yaw misalignment of the disk with the flow, an angle correction factor was calculated to make the disk probe measurement closest to the wall, after correction for a flat-plate viscous interaction ($\bar{\chi}_d$), be equal to the model surface pressure. This angle correction factor, K, was calculated by assuming a linear relation between the pressure perturbation and the product of the misalignment and the local Mach number, using the equation

$$K = \left[\frac{p_d/p_m}{(1 + 0.45\,\bar{\chi}_d)} - 1\right]\frac{1}{M} \qquad \text{(II-1)}$$

The local flow conditions were then calculated for the succeeding data points by use of the measured disk and pitot pressures, and an interation to correct for the yaw misalignment and viscous interaction simultaneously, using

$$p_d/p = (1 + 0.45\,\bar{\chi}_d)\,(1 + KM) \qquad \text{(II-2)}$$

APPENDIX III
TEST SUMMARY TABLES

TABLE I
SURFACE DATA SUMMARY

Nominal Mach No.	Nominal T_{wall}/T_{t_∞}	R_N = 0.001 in.	R_N = 0.023	R_N = 0.105
6.0	0.9	x + *	x + *	x + *
	0.6	x + *	x + *	x + *
	0.4	x + *		
	0.1	x + *	x + *	x + *
4.5	0.9	x + *	x + *	x + *
	0.6	x + *		x *
	0.3	x + *	x *	x *
3.0	0.9	x + *	x + *	x + *
	0.6	x + *	+ *	x + *
	0.3	+ *	+ *	x + *

Sym.	Nominal $Re_c \times 10^{-6}$
x	0.25
+	0.5
*	1.0

TABLE II
SURVEY DATA SUMMARY

Nominal Mach No.	Nominal T_{wall}/T_{t_∞}	Survey Station, S	R_N = 0.001	R_N = 0.023	R_N = 0.105
6.0	0.9	6.5	x +	x + *	x + *
		5.5	x		
		4.5	x		
		3.5	x		
		2.5	x		
	0.6	6.5	x *		x + *
	0.1	6.5			+ *
4.5	0.9	6.5	x + *	x + *	x + *
		4.5	x + *	x + *	x + *
		3.0	x + *	x + *	x + *
		1.25	x + *	x + *	x + *
	0.6	5.5		*	*
		4.5	x + *		
		1.25	x *		x *
	0.3	5.5		+ *	+ *
		4.5	x + *	x *	x *
		1.25	x *	x *	x *
3.0	0.9	5.5	*		x + *
		4.5	x	x	x
	0.6	5.5	+ *		x + *
	0.3	5.5	+ *		x + *

Sym.	Nominal $Re_c \times 10^{-6}$
x	0.25
+	0.5
*	1.0

TABLE III
OPERATING CONDITIONS

Nominal Conditions			
M_∞	p_{t_∞}	T_{t_∞}	$(u/\nu)_\infty \times 10^{-6}$
6.04	265	850	0.4
6.04	133	850	0.2
6.04	66	850	0.1
4.52	78	600	0.4
4.51	39	600	0.2
4.50	20	600	0.1
3.01	37	600	0.4
3.01	18	600	0.2
3.00	9	600	0.1

APPENDIX IV
THEORETICAL HEAT-TRANSFER ESTIMATES

The Stanton number was predicted, using the equations (derived in Ref. 27) which are based on solutions by Van Driest, and is as follows. By definition the Stanton number is

$$St = \frac{h\,(T_{ad} - T_{wall})}{\rho_\infty u_\infty (H_t - H_{wall})} \qquad \text{(IV-1)}$$

and where

$$h = k(144\, p_w u_w)^n\, (S)^{(n-1)}\, (T')^{-m} \qquad \text{(IV-2)}$$

$$T' = (T_{wall} + T_w)/2 + 0.22r\,(T_{ad} - T_w) \qquad \text{(IV-3)}$$

$$T_{ad} = T_w + r\,(T_{t,\infty} - T_w) \qquad \text{(IV-4)}$$

$$H_t - H_{wall} = 0.2235\,(T_{t,\infty} - T_{wall}) + 0.135 \times 10^{-4}\,(T^2_{t,\infty} - T^2_{wall}) \qquad \text{(IV-5)}$$

where the constants are

Boundary Layer	k x 10^3	r*	n	m
Laminar	2.675	0.85	0.5	0.040
Turbulent	9.560	0.90	0.8	0.576

*Note: Here r denotes the recovery factor.

The local conditions p_w, u_w, and T_w for the sharp-leading-edge configuration were free-stream values on the flat plate and on the ramp those corresponding to an isentropic compression through 9.5 deg. For the blunt-leading-edge configurations, the local plate conditions were those appropriate to the local inviscid static pressure and a total pressure equal to that for normal shock at free-stream conditions, whereas on the ramp the static pressure was that for an oblique shock compression through 9.5 deg at free-stream Mach number.

APPENDIX V
TABULATED SURFACE DATA

R_N = 0.001

M_∞ = 6.04

Re_c = 0.25 x 10^6

	T_{wall}/T_{t_∞} = 0.91	T_{wall}/T_{t_∞} = 0.64		T_{wall}/T_{t_∞} = 0.17	
S/S_c	p/p_∞	p/p_∞	St_∞ x 10^3	p/p_∞	St_∞ x 10^3
0.40	1.24	1.25		1.05	
0.45	1.21	1.20		1.00	
0.50	1.22	1.24	0.805	1.14	1.22
0.55	1.19	1.22		1.00	
0.60	1.21	1.22		1.05	
0.65	1.32	1.22		1.00	
0.70	1.43			1.15	
0.75	1.56	1.35		1.00	
0.80	1.77	1.53		0.98	
0.85	1.78	1.69		1.00	
0.90	1.97	1.85		1.20	
0.95	1.95	1.86		1.47	
1.00	2.01	1.99		1.63	
1.05				1.95	
1.10	2.21	2.22		2.40	
1.15				2.73	
1.20	2.40	2.54	0.664	2.88	1.44
1.25				3.16	
1.30	2.71	2.92		3.39	
1.35				3.32	
1.40	3.04	3.28		3.41	
1.50				3.42	
1.60	3.37	3.59	1.43	3.44	2.43
1.70				3.33	
1.80	3.59	3.72	1.40	3.39	1.94
1.90					
2.00	3.61	3.81	1.70	3.34	1.90
2.20	3.77	3.85	1.65	3.45	1.68
2.40	3.73				
2.60	3.71	3.88	1.79	3.53	1.53
2.80				3.61	
2.90		3.96		3.56	
2.95				3.62	

R_N = 0.023

M_∞ = 6.04

Re_c = 0.25 x 10^6

	T_{wall}/T_{t_∞} = 0.84	T_{wall}/T_{t_∞} = 0.66		T_{wall}/T_{t_∞} = 0.14	
S/S_c	p/p_∞	p/p_∞	St_∞ x 10^3	p/p_∞	St_∞ x 10^3
0.40	1.54	1.38		1.25	
0.45	1.48	1.39		1.18	
0.50	1.50	1.36	0.871	1.21	1.02
0.55	1.53	1.29		1.19	
0.60	1.56	1.33		1.18	
0.65	1.56	1.53		1.06	
0.70	1.84	1.56			
0.75	1.86	1.60		1.04	
0.80	1.86	1.79		1.09	
0.85	2.01			0.10	
0.90	1.99	1.80		1.08	
0.95	2.07	1.78		1.40	
1.00	2.05	1.83		1.52	
1.05	2.13	1.91		1.75	
1.10	2.15	1.99		1.96	
1.15	2.20	2.05		2.11	
1.20	2.22	2.06		2.22	0.866
1.25	2.44	2.26			
1.30	2.46	2.33		2.55	
1.35	2.47	2.38		2.60	
1.40	2.67	2.55		2.73	
1.50	2.77	2.61		2.82	
1.60	2.87	2.82	0.805	2.96	1.51
1.70	2.97	2.91		3.00	
1.80	3.09	3.04	0.774	3.09	
1.90	3.26	3.08		3.20	
2.00	3.31	3.25	0.826	3.15	1.06
2.20	3.41	3.32	0.767	3.30	1.19
2.40					
2.60	3.61	3.41	0.657	3.38	1.12
2.80	3.55	3.45			
2.90	3.40	3.39		3.50	
2.95	3.15	3.11		3.45	

R_N = 0.105

M_∞ = 6.04

Re_c = 0.25 x 10^6

	T_{wall}/T_{t_∞} = 0.91	T_{wall}/T_{t_∞} = 0.62		T_{wall}/T_{t_∞} = 0.15	
S/S_c	p/p_∞	p/p_∞	St_∞ x 10^3	p/p_∞	St_∞ x 10^3
0.40	2.50	2.42		2.34	
0.45		2.31		2.19	
0.50		2.27	1.04	2.17	1.20
0.55	2.35	2.13		2.00	
0.60	2.27	2.08		1.98	
0.65	2.13	2.02		1.89	
0.70	2.17	2.03			
0.75	2.11	1.88		1.77	
0.80	2.07	1.87		1.72	4.39
0.85	2.26	1.95		1.68	
0.90	2.33	2.14		1.67	
0.95	2.47	2.23		2.08	
1.00	2.54	2.37		2.22	
1.05	2.64	2.49		2.54	
1.10	2.76	2.63		2.77	
1.15	2.81	2.70		2.79	
1.20		2.74	0.596	2.79	0.913
1.25		2.83			
1.30	3.06	2.92		2.89	
1.35	2.98	2.85		2.83	
1.40	3.06	2.96		2.88	
1.50	3.14	2.83		2.81	
1.60	3.11	2.96	0.836	2.86	1.18
1.70	3.09	2.98		2.82	
1.80	3.18	3.02	0.736	2.92	
1.90	3.31	3.11		3.04	
2.00	3.26	3.08	0.785	2.95	0.879
2.20	3.36	3.18	0.708	3.08	0.927
2.40				3.26	
2.60	3.53	3.35	0.612	3.22	0.903
2.80	3.66	3.33		3.30	
2.90	3.28	3.22		3.32	
2.95	3.01	3.00		3.26	

R_N = 0.001

M_∞ = 4.50

Re_c = 0.25 x 10^6

	T_{wall}/T_{t_∞} = 0.89	T_{wall}/T_{t_∞} = 0.55		T_{wall}/T_{t_∞} = 0.32	
S/S_c	p/p_∞	p/p_∞	St_∞ x 10^3	p/p_∞	St_∞ x 10^3
0.40	1.17	1.11		1.01	
0.45					
0.50	1.16	1.06	1.12	1.01	
0.55	1.14	1.07		0.99	
0.60	1.16	1.06		1.03	
0.65	1.28	1.05	1.07	1.02	0.929
0.70	1.35	1.05		0.96	
0.75	1.42	1.16		1.02	
0.80	1.57	1.41		1.33	
0.85	1.63	1.50		1.44	
0.90	1.64	1.55		1.49	
0.95	1.66	1.59	0.270	1.51	0.743
1.00	1.71	1.61		1.51	
1.05	1.78	1.69		1.59	
1.10	1.84	1.82		1.74	
1.15					
1.20	2.03	2.15	1.22	2.15	1.68
1.25	2.20	2.33			
1.30	2.28	2.44		2.43	
1.35	2.38	2.53		2.53	
1.40	2.50	2.59		2.58	
1.50	2.58	2.65		2.63	
1.60	2.69	2.70		2.66	
1.70	2.72	2.73		2.65	
1.80			1.27		1.51
1.90	2.77	2.76		2.69	
2.00			1.79		1.58
2.20	2.81	2.76	2.56	2.67	
2.40					
2.60	2.84	2.78	1.79	2.70	1.41
2.80					
2.90	2.90	2.65		2.68	
2.95					

R_N = 0.023

M_∞ = 4.5

Re_c = 0.25 x 10^6

	T_{wall}/T_{t_∞} = 0.91	T_{wall}/T_{t_∞} = 0.27	
S/S_c	p/p_∞	p/p_∞	St_∞ x 10^3
0.40	1.19	1.18	
0.45	1.15		
0.50	1.22	1.14	1.01
0.55	1.38	1.13	
0.60	1.50	1.15	
0.65	1.58		0.870
0.70	1.64	1.28	
0.75	1.65	1.40	
0.80	1.67	1.48	
0.85	1.71	1.50	
0.90	1.72	1.48	
0.95	1.72	1.49	0.782
1.00	1.75	1.53	
1.05	1.76	1.53	
1.10	1.77	1.59	
1.15			
1.20	1.84	1.80	1.72
1.25	1.89	2.06	
1.30	1.90	2.10	
1.35	2.03	2.16	
1.40	2.10	2.29	
1.50	2.23	2.39	
1.60	2.36	2.51	
1.70	2.45		
1.80			1.26
1.90	2.58	2.61	
2.00			1.50
2.20	2.68	2.63	
2.40			
2.60	2.74	2.67	1.44
2.80			
2.90	2.63	2.64	
2.95			

R_N = 0.105

M_∞ = 4.5

Re_c = 0.25 x 10^6

	T_{wall}/T_{t_∞} = 0.91	T_{wall}/T_{t_∞} = 0.54		T_{wall}/T_{t_∞} = 0.32	
S/S_c	p/p_∞	p/p_∞	St_∞ x 10^3	p/p_∞	St_∞ x 10^3
0.40	1.86	1.75		1.68	
0.45					
0.50	1.72	1.66	1.24	1.58	1.10
0.55	1.67	1.58		1.53	
0.60	1.63	1.53		1.47	
0.65	1.60	1.47	1.10	1.44	1.02
0.70	1.59	1.45		1.38	
0.75	1.64	1.40		1.32	
0.80	1.77	1.52		1.41	
0.85		1.63		1.50	
0.90	1.91	1.74		1.64	
0.95	1.95	1.81		1.72	
1.00	2.03	1.84		1.77	
1.05	2.02	1.92		1.85	
1.10	2.09	2.04		1.99	
1.15					
1.20	2.22	2.21	3.01	2.18	2.19
1.25	2.78	2.29			
1.30	2.33	2.33		2.27	
1.35	2.37	2.34		2.28	
1.40	2.42	2.40		2.33	
1.50	2.46	2.41		2.34	
1.60	2.52	2.44		2.39	
1.70					
1.80			2.19		1.28
1.90	2.62	2.55		2.47	
2.00			1.32		1.24
2.20	2.68	2.61	1.13	2.53	
2.40					
2.60	2.73	2.72	1.09	2.62	1.13
2.80					
2.90	2.60	2.61		2.62	
2.95					

R_N = 0.001

M_∞ = 3.00

Re_c = 0.25 x 10^6

	T_{wall}/T_{t_∞} = 0.93	T_{wall}/T_{t_∞} = 0.57		T_{wall}/T_{t_∞} = 0.3	
S/S_c	p/p_∞	p/p_∞	St_∞ x 10^3	p/p_∞	St_∞ x 10^3
0.40	1.04	1.05			
0.45	1.05	1.07		1.01	
0.50	1.11	1.03	0.897	1.01	1.04
0.55	1.13	1.08		1.04	
0.60	1.25	1.11		1.01	
0.65	1.31	1.25	0.457		
0.70	1.33	1.29		1.08	
0.75	1.37	1.35		1.24	
0.80	1.38	1.37		1.29	
0.85	1.41	1.38		1.30	
0.90	1.41	1.39		1.33	
0.95	1.39	1.37		1.31	
1.00	1.41	1.38		1.34	
1.05	1.41	1.39		1.37	
1.10	1.46	1.44		1.44	
1.15	1.53	1.56			
1.20			0.799		1.56
1.25		1.69		1.79	
1.30	1.78	1.88		2.00	
1.35	1.83	1.95		2.04	
1.40		1.99		1.91	
1.50	2.00	2.05		2.11	
1.60	2.07	2.10		2.10	
1.70	2.11	2.12			
1.80			2.89		2.65
1.90	2.14	2.16			
2.00			2.28		3.29
2.20	2.14	2.18	3.03	2.31	3.03
2.40					
2.60	2.15	2.13	3.05	2.31	3.04
2.80					
2.90	2.12	2.16		2.17	
2.95					

R_N = 0.023

M_∞ = 3.00

Re_c = 0.25 x 10^6

T_{wall}/T_{t_∞} = 0.9

S/S_c	p/p_∞
0.40	1.13
0.45	1.13
0.50	1.26
0.55	1.31
0.60	1.35
0.65	1.37
0.70	1.38
0.75	1.39
0.80	1.39
0.85	1.42
0.90	1.41
0.95	1.40
1.00	1.41
1.05	1.41
1.10	1.43
1.15	1.44
1.20	
1.25	1.50
1.30	1.59
1.35	1.69
1.40	1.80
1.50	1.86
1.60	1.97
1.70	2.04
1.80	
1.90	2.11
2.00	
2.20	2.14
2.40	
2.60	2.13
2.80	
2.90	2.15
2.95	

R_N = 0.105

M_∞ = 3.00

Re_c = 0.25 x 10^6

	T_{wall}/T_{t_∞} = 0.9	T_{wall}/T_{t_∞} = 0.57		T_{wall}/T_{t_∞} = 0.32	
S/S_c	p/p_∞	p/p_∞	St_∞ x 10^3	p/p_∞	St_∞ x 10^3
0.40	1.27	1.24		1.23	
0.45	1.25	1.25		1.23	
0.50	1.26	1.22	0.850	1.23	0.969
0.55	1.24	1.24		1.21	
0.60	1.23	1.21		1.18	
0.65	1.30	1.19	0.911	1.17	
0.70	1.37	1.25		1.15	
0.75	1.41	1.38		1.19	
0.80	1.44	1.41		1.32	
0.85	1.49	1.43		1.42	
0.90	1.49	1.45		1.41	
0.95	1.47	1.42		1.39	
1.00	1.48	1.44		1.42	
1.05	1.48	1.46		1.46	
1.10	1.54	1.51		1.63	
1.15	1.60	1.61		1.71	
1.20			0.965		1.41
1.25	1.72	1.82		1.89	
1.30	1.76	1.85		1.88	
1.35	1.83	1.92		1.93	
1.40					
1.50	1.93	1.97		1.96	
1.60	1.97	1.99		1.99	
1.70	1.98	2.01		2.00	
1.80					2.47
1.90	2.01	2.04		2.03	
2.00			1.44		2.35
2.20	2.03	2.06	1.63		2.19
2.40					
2.60	2.05	2.09	2.26	2.04	2.35
2.80					
2.90	2.07	2.07		2.03	
2.95					

DOCUMENT CONTROL DATA - R & D

(Security classification of title, body of abstract and indexing annotation must be entered when the overall report is classified)

1 ORIGINATING ACTIVITY *(Corporate author)*
Arnold Engineering Development Center
Arnold Air Force Station, Tennessee 37389

2a. REPORT SECURITY CLASSIFICATION
UNCLASSIFIED

2b. GROUP
N/A

3 REPORT TITLE
EFFECTS OF WALL COOLING AND LEADING-EDGE BLUNTING ON RAMP-INDUCED, LAMINAR FLOW SEPARATIONS AT MACH NUMBERS FROM 3 THROUGH 6

4 DESCRIPTIVE NOTES *(Type of report and inclusive dates)*
Final Report - November 30, 1970, to April 16, 1971.

5 AUTHOR(S) *(First name, middle initial, last name)*
J. Don Gray and R. W. Rhudy, ARO, Inc.

6 REPORT DATE
March 1972

7a. TOTAL NO OF PAGES
118

7b. NO OF REFS
27

8a. CONTRACT OR GRANT NO.

b. PROJECT NO.

c. Program Element 62201F

d.

9a. ORIGINATOR'S REPORT NUMBER(S)
AEDC-TR-71-274

9b. OTHER REPORT NO(S) *(Any other numbers that may be assigned this report)*
ARO-VKF-TR-71-199

10. DISTRIBUTION STATEMENT
Approved for public release; distribution unlimited.

11. SUPPLEMENTARY NOTES
Available in DDC.

12 SPONSORING MILITARY ACTIVITY
Air Force Flight Dynamics Laboratory(FDCC), Wright-Patterson AFB, OH 45433.

13. ABSTRACT

The effects of wall cooling and nose bluntness on laminar and transitional reattaching flows induced by a 9.5-degree ramp were investigated at Mach numbers from 3 through 6 by measuring the longitudinal surface pressure and heat-transfer rate distributions, as well as the flow-field pressures, at several longitudinal stations. Reynolds number based on flat-plate length was varied from 0.25 to 1.0 million. Although transitional reattachment generally prevailed at all but the minimum Reynolds number at $M_\infty = 3$, an increase in leading-edge radius was found to delay transition onset at $M_\infty \geq 4.5$. When transition was well downstream of reattachment, increased cooling delayed the onset; however, the opposite was true when transition was near reattachment. The trend in the change in interaction length with Reynolds number increase indicated laminar reattachment at all test Reynolds numbers at $M_\infty = 6$ and transitional at the two higher Reynolds numbers at $M_\infty = 3.0$.

DD FORM 1 NOV 65 1473

14. KEY WORDS	LINK A		LINK B		LINK C	
	ROLE	WT	ROLE	WT	ROLE	W
wind tunnels						
boundary layer separation						
laminar flow						
supersonic flow						
ramps						
flaps						
leading edges						
bluntness						
pressure measurements						
heat transfer data						
flow field surveys						
boundary layer transition						
liquid cooling						
cooling systems						

AFSC
Arnold AFS Tenn